The Configuration Space of Parallel Mechanisms

Nir Shvalb

The Configuration Space of Parallel Mechanisms

Research thesis

Submitted in Partial Fulfilment of the
Requirement for the degree of
Doctor of Philosophy

Nir Shvalb

Submitted to Senate of
the Technion - Israel Institute of Technology

Haifa, Israel, Nov 2006, Kislev 5776

Acknowledgments

The Research Thesis Was Done Under The Supervision of Prof. Moshe Shoham in the Department of mechanical Engineering - The Technion and Dr. David Blanc from the Department of mathematics - Haifa University.

Contents

List of Notations

Notations for chapter 1.

$(L, \mathbf{x})$ The lengths of n concatenated rods together with a fixed end 3

$(\mathcal{L}, \mathcal{X})$ The set of lengthes and fixed ends of an arachnoid mechanism 3

$\mathbf{v}$ Link vector 3

$\wp^{(i)}$ Parenthesized superscript i designates the i-th branch 3

$\wp_j$ Subscript j designates the j-th link number 3

W A branch work space 4

$\mathcal{W}$ The work space of an arachnoid mechanism 4

$\mathbf{y}$ The arachnoid mechanism common endpoint 4

V A branch configuration 4

$\mathcal{V}$ An arachnoid mechanism configuration 4

$\mathcal{C}$ The Configuration space 8

$T\mathcal{C}$ The tangent bundle of the configuration space manifold space 7

$\mathbf{S}^i$ The i-th sphere 8

$\mathbf{T}^i$ The i-th torus $\underbrace{\mathbf{S}^1 \times \ldots \times \mathbf{S}^1}_{i}$ 8

Notations for chapter 2.

A Root junction or thorax of the Manipulator M 19

M_j Leg j of M with foot fixed at o_j and other end free, $j = 1, ..., k$ 19

n_j Number of links in M_j 19

$l_{j,i}$ Length of link i of M_j; $i = 1, ..., n_j$ 19

$\theta_{j,i}$ Angle of link i relative to link $i-1$ 19

$\tilde{M}_j(p)$ Leg j of M with foot fixed at o_j and other end fixed at p 20

$\tilde{M}(p)$ Manipulator with A fixed at p 20

L_j Sum of lengths of links of $\tilde{M}_j(p)$ 23

$L_{j,0}$ Sum of lengths of links of M_j 23

$\mathcal{L}_j(p)$ A set of long links of $\tilde{M}_j(p)$ 23

$|\mathcal{L}_j^*(p)|$ Number of long links of $\tilde{M}_j(p)$ 23

W_A Workspace of A 20

${}^dU_i$ Cell of dimension d of W_A 25

$\gamma = p(t)$ Curve in the plane of M 27

f Kinematic map of A 21

f_j Kinematic map of endpoint of M_j 21

Σ Critical set of f in W_A 21

Σ_j Critical set of f_j 21

$\tilde{\mathcal{C}}(p)$ configuration space of $\tilde{M}(p)$ 21

$\mathcal{C}_j$ configuration space of M_j 21

$\tilde{\mathcal{C}}_j(p)$ configuration space of $\tilde{M}_j(p)$ 21

Notations for chapter 3.

V A branch configuration 47

$\mathbf{p}^{(i)}$ The i-th vertex of the polygonal moving platform 48

$g^{(i,j)}$ The edge length $\|\mathbf{p}^{(i)} - \mathbf{p}^{(j)}\|$ 48

$\text{Line}^{(i)}$ A line with direction vector equal to the aligned direction vector $\mathbf{v}^{(i)}$ 48

$\wp^{(i)}$ Parenthesized superscript i designates the i-th branch 50

$\wp_j$ Subscript j designates the j-th link number 50

N The number of links $\sum_{i=1}^{k} n^{(i)}$ in a polygonal mechanism 50

$\mathbf{a}^{(i,j)}$ The vector of the moving platform edge connecting vertices i and j. ..52

$(\mathcal{L}, \mathcal{X}, \mathcal{P})$ A polygonal mechanism which consists of set of lengths, fixed ends of the branches and the polygonal platform. 53

$\mathcal{C}(k)$ the configuration space of the omitted k-th branch 53

$\hat{\mathcal{C}}$ The configuration space of the triangular mechanism obtained by omitting the last branch 53

Notations for chapter 4.

$\$_{j,k}$ A unit screw describing the movement of each spherical joint in the k-th direction 77

$\theta_{j,k}$ The input coordinate for the $\$_{j,k}^{(i)}$ screw 77

$\$_p$ The instantaneous twist of the end-effector 77

List of Figures

Abstract

We study the configuration space of some parallel mechanism that are in use. starting with the configuration spaces of arachnoid mechanisms which consist of k branches each of which has an arbitrary number of links and a fixed initial point, while all branches end at one common end-point. We show that generically, the configuration spaces of such mechanisms are manifolds, and determine the conditions for the exceptional cases. The configuration space of planar arachnoid mechanisms having k branches, each with two links is fully characterized for both the non-singular and the singular cases.

Applying these results we study the motion planning problem for such planar manipulators. A topological analysis is used to understand the global structure of the configuration space so that motion planning problem can be solved exactly. The worst-case complexity of our algorithm is $O(k^3N^3)$, where N is the maximum number of links in a leg. Examples illustrating our method are given.

Next we study the configuration space $\mathcal{C}$ of a parallel polygonal mechanism, having a moving polygonal platform, and a flexible leg (consisting of concatenated rods) attached to each vertex, with the other end fixed in $\mathbb{R}^d$. We give necessary conditions for the existence of uncertainty singularities; and show that generically $\mathcal{C}$ is a smooth manifold. In the planar case, we construct an explicit Morse function on $\mathcal{C}$, and show how geometric information about the mechanism can be used to identify the critical points. Finally we describe how topological singularities give rise to instantaneous kinematic and explicit example is provided.

Methods and preliminaries

We now introduce some definitions, theorems and methods which are in extensive use in this dissertation.

Smooth Manifolds: An n-dimensional *manifold* is a *topological space* which "near" each of its points is locally like $\mathbb{R}^n$ i.e. there is a neighborhood which is topologically "the same" as an open unit ball in $\mathbb{R}^n$. Formally, two additional properties are needed to form a manifold, being *Hausdorff* and *Second Countable* (see for example [C]).

A differential manifold $\mathcal{M}$ is a manifold for which overlapping *charts* "relate smoothly" to each other, where a chart $\alpha : U \to \mathbb{R}^n$ is a continuous injection from an open subset U of $\mathcal{M}$ to $\mathbb{R}^n$.

A manifold is *connected* if, roughly speaking, it is all in one piece.

A *submanifold* is a subset of a manifold which is itself a manifold, but has smaller dimension. For example, the equator of a sphere is a submanifold.

If $\mathcal{M}$ is an orientable surface, its genus $g(\mathcal{M})$ is the number of "handles" it possesses. Furthermore, any orientable surface is a sphere, or the *connected sum* of n tori. We say the sphere has genus 0, and that the connected sum of n tori has genus n. Also, $g(\mathcal{M}) = 1 - \chi(\mathcal{M})/2$ where $\chi(\mathcal{M})$ is the Euler characteristic of $\mathcal{M}$.

Smooth Mappings and Singularity: The following enabled us to prove smoothness of generic arachnoid mechanism, and used also in finding necessary conditions for uncertainty singularities in polygonal mechanisms:

Let $f : \mathcal{N}^n \to \mathcal{M}^m$ be a smooth map on smooth manifolds. A critical point of f is a point $x \in \mathcal{N}$ such that the differential df considered as a linear transformation of real vector spaces has rank $< m$. A critical value of f is the image $f(x)$ of a critical

point. A regular value of f is a point which is not the image of any critical point.

Theorem 0.0.1. *(Regular value theorem) Let $f : \mathcal{N}^n \to \mathcal{M}^m$ be a smooth mapping. if y is a regular value of f then $f^{-1}(y)$ is a smooth $n - m$ manifold.*

The notion of objects *intersecting transversally* is fundamental to singularity theory. The simplest situation to look at is two subspaces of a vector space V: We say that they intersect transversally when their vector sum is V, formally:

Definition 0.0.2. Let $f : \mathcal{N} \to \mathcal{M}$ be a smooth mapping, and let Q be a smooth submanifold of $\mathcal{M}$. f and Q are said to intersect transversally (denoted $f \pitchfork Q$) iff for all $x \in \mathcal{N}$ with $y = f(x) \in Q$ we have $d_x f(T_x\mathcal{N}) + T_y Q = T_y\mathcal{M}$.

where $T_x\mathcal{M}$ is the space spanned by the set of all vectors tangent to $\mathcal{M}$ at point $x \in \mathcal{M}$, and $d_x f$ the jacobian of the map f calculated at point x. The next proposition (see also [63, pp31]) provides us a tool for examining uncertainty singularities in the special case where the regular value theorem fail.

Proposition 0.0.3. *Let $f : \mathcal{N} \to \mathcal{M}$ be a smooth mapping, and let Q be a smooth submanifold of $\mathcal{M}$ with $f \pitchfork Q$: then $f^{-1}(Q)$ is a smooth submanifold of $\mathcal{N}$, having the same codimension as Q or is empty.*

Introduction

Generally speaking a *configuration* is a set of independent parameters uniquely specifying the position of each of its mechanical components relative to a fixed frame of reference. A *configuration space* of a given mechanism is therefore the totality of all its admissible positions in the Euclidean space. For example, a simple n-linked branch mechanism with revolute joints have the n-torus $\mathbb{T}^n$ as its configuration space.

Obviously knowing the configuration space is a powerful tool for motion planning problems, singularities characterization and global understanding of a system. Main research have been set on the configuration spaces of a type of mechanism called *polygonal linkage*, which is simply a concatenation of links and hinged joints forming a closed chain in $\mathbb{R}^2$ and $\mathbb{R}^3$. A substantial amount of mathematical literature on polygonal linkage's configuration space has has been written using various methods like computation of Euler characteristics, homology groups and handle-body surgery;

Worth special note is the work of J. C. Hausmann, and A. Knutson [6] who determine the cohomology rings for these spaces and the co-work of R.J. Milgram and J. Trinkle [14] who presented full surgery analysis for the same kind of mechanism. The results of [11], provide a good review of previous work and some interesting results on the structure of these configuration spaces.

However, to the best of the author's knowledge configuration spaces of more common parallel mechanisms, i.e. mechanisms with multiple branches having a *tree* topology or a spider like mechanisms where all branches are attached in one rigid platform (*polygonal mechanism*) or one point (*Arachnoid mechanism*), have never been dealt with before. Such mechanisms are of great importance in the "real life" due to their

accuracy and stiffness properties.

In this dissertation we deal with mechanisms which are constructed by rigid rods and spherical (rotational) joints, called *graph mechanisms*, which mathematically speaking are simply graphs $(G(v,e),\mathcal{L})$ having s ets of vertices and edges such that $e(G) = v(g) \times v(g)$ and a set of fixed lengths $\mathcal{L}$.

The configuration space is sometimes non-accurately defined in literature. Here we define the configuration space as the quotient $\mathcal{C} = \mathcal{R}(G)/\Lambda$ where

$$\mathcal{R}(G) = \{\mathbf{x}_i \in \mathbb{R}^{v(G)} | i \in v(G), \|\mathbf{x}_i - \mathbf{x}_j\| = \mathcal{L}(i,j)\}$$

and Λ is the group of isometries of translations and rotations in $\mathbb{R}^2$, or in $\mathbb{R}^3$. Thus Λ "fixes" the the mechanism to a fixed frame. The difference between these two definitions for the configuration space can be realized in the following: A subgraph H of graph G is a graph such that $v(H) \subset v(G)$ and $e(H) \subset e(G)$, which leads to the definition:

Definition 0.0.4. A *sub-mechanism* $(H, \mathcal{L}|_H) \subset (G,\mathcal{L})$ is a subgraph H of G together with the restricted length subset $\mathcal{L}|_H$, and we denote such a sub-mechanism simply by H. A *branch* is a sub-mechanism such that all vertices in H have valence 1 or 2.

In light of these definitions one can define a feasible configuration of a parallel mechanism on condition that all of its branches "agree" upon one (or more) branch configuration. One could claim that for arachnoid mechanisms the configuration space is simply the fibered product of the configuration space of its branches, but then he would be wrong. Alternatively we know that:

Theorem 0.0.5. *Given a mechanism* $(G,\mathcal{L})$ *with a set* $H_1, H_2, H \subset G$ *of its sub-mechanisms such that* $H_1 \cap H_2 = H$ *then* $\mathcal{R}(\mathcal{L})$ *is the pullback of the the natural projections:*

$$\mathcal{R}(H_1) \xrightarrow{\pi_{H_1}} \mathcal{R}(H) \xleftarrow{\pi_{H_2}} \mathcal{R}(H_2).$$

Note that this does not extend to the configuration space $\mathcal{C}$ since the induced projections $\{\mathcal{R}(H_i)/\Lambda \to \mathcal{R}(H)/\Lambda\}$ are determined up to isometry Λ and thus do not determine a unique point (A proof for this theorem and a detailed discussion can be found in the Appendix 6).

We first analyze a simple class of mechanism called *arachnoid* which consists of multiple branches each having arbitrary number of links a fixed initial point, and all end at a common point (this type of mechanism resembles some parallel robots which are in practical use [1]: parallel manipulators, walking robots, and dexterous manipulation). It is shown (see Chapter 1) that generically, the configuration spaces of such mechanisms are manifolds, and the conditions for the exceptional cases are then determined. We analyze the configuration space of planar arachnoid mechanisms having k branches, each with two links. Such mechanisms have a 2 dimensional configuration space which enables a full classification. The non-manifold cases where singularities emerges are calculated.

As mentioned above, knowing the configuration space often enables problems solving, like the existence of continuous motion planners (Farber cf. [3]) or the motion planning problem (Note that this kind of approach completely discards the nature of the mechanism in issue). Due to the computational complexity and difficulty of implementing general exact motion planning algorithms, such as Canny's [39], today sample-base algorithms, such as Kavraki's [40] dominate motion planning research. However, there are important classes of problems for which these algorithms do not perform well. These arise in systems whose configuration space cannot effectively be represented as a set of parameters with simple bounds, but rather is most naturally represented as a variety of co-dimension one or greater embedded in a higher-dimensional ambient space [42]. Examples of these systems include manipulators with one or multiple closed loops, whose configuration space is defined by loop closure constraints. The *Random Loop Generator* method [22, 23] improves the

sampling techniques through estimating the regions of sampling parameters. However, its efficiency relies on the accuracy of the estimation, which is often case-variant. Moreover, it ignores the global structure of configuration space and may fail to sample globally important regions. For which specialized exact methods have not been developed. This provides motivation to try to develop effective exact algorithms. For most mechanisms configuration space is of dimension greater than two which makes them impossible to be fully characterized. Yet, global properties like connectivity and smoothness are attainable. Recent advances (especially connectivity analysis methods) in the understanding of the global structure of configuration space of single-loop closed chains [15, 27] allow us (Chapter 2 here) to develop a polynomial-time exact algorithm for arachnoid manipulators (which actually can be extended to any planar mechanism with an arbitrary tree topology).

Next we focus attention on parallel robots (in any dimension) comprised of arbitrary number of branches each having arbitrary number of links concatenated by rotational joints and attached to a moving platform, which we shall refer to as *polygonal mechanisms*, these are the mathematical parallel of most parallel mechanisms which are increasingly in use. Still their configuration space had never been analyzed. We examine closely the case of parallel robots singularity called uncertainty singularity which is simply a topological singularity of the configuration space:

Kinematic singularities of parallel mechanisms have been studied extensively in the literature (cf. [52], and the example of open kinematic chains in [53, 54]). On the other hand, the configuration space of such a mechanism may have topological singularities. Our goal here is to try to relate these two kinds of singularity, for that certain class of mechanisms.

Choosing appropriate local coordinates for a given mechanism, we try to endow its configuration space with the structure of a differentiable manifold. The points where this cannot be done constitute the *topological singularities* of the mechanism. We shall be concerned only with *uncertainty singularities* (where the *instantaneous mobility* is greater than the *full cycle mobility* – cf. [52]); In such a position the

mechanism as a whole gains an additional degree of freedom. Such points may sometimes separate configuration space into distinct regions, allowing transition between different operating modes. (An extensive examination of such remarkable transitions in a special case (a *constraint* singularity for 3-URU parallel mechanism with three degrees of freedom) is given in [55]). In Chapter 3 we give a necessary geometric condition for uncertainty singularities in said mechanisms, and explain how such topological singularities give rise to instantaneous kinematic singularities in Chapter 4. Finally, the occurrence of an uncertainty singularity is illustrated visually in an explicit example.

Chapter 1

Arachnoid mechanisms

A paper published in *Forum Mathematica* Vol 17/6 (Nov '05), 1033-1042.
Co-authors: David Blanc and Moshe Shoham.

The configuration spaces of arachnoid mechanisms are analyzed in this paper. These mechanisms consist of k branches each of which has an arbitrary number of links and a fixed initial point, while all branches end at one common end-point. It is shown that generically, the configuration spaces of such mechanisms are manifolds, and the conditions for the exceptional cases are determined. The configuration space of planar arachnoid mechanisms having k branches, each with two links is analyzed for both the non-singular and the singular cases.

1.1 Introduction

Mechanisms and robots consist of links and joints, the actuation of which causes them to move. The type of a mechanism is described by an abstract graph which corresponds to its links and joints, and a specific embedding of this graph in the plane or in 3-space is called a *configuration* of the mechanism. The collection of all such embeddings forms a topological space, called the *configuration space* of the mechanism. For example, the configuration space of a planar mechanism with revolute

joints consisting of n rods arranged serially is the n-torus.

In recent years, there has been interest among mathematicians in the study of such spaces, which are of importance in motion planning – that is, moving a mechanism from one given position to another, taking into account various constraints (see for example [15]). The topological properties of the configuration space provide insight into practical questions in planning such motions (see [3]) and analysis of some mechanical singularities (see [16], and [17]).

The main focus had been set on the configuration spaces of a type of mechanism called *polygonal linkage*, which is simply a concatenation of links and hinged joints forming a closed chain. A substantial amount of mathematical literature on polygonal linkage's configuration space has accumulated: Kamiyama , Tezuka and Toma studied Euler characteristics in [10], and homology groups in [12, 13]; Trinkle and Milgram constructed a handle-body surgery in [14]; and in [8], Holcomb studied a special parallel graph mechanism called multi-polygonal linkages, which are three free branches identified at their initial and terminal vertices.

In this paper we analyze a type of mechanism called *arachnoid* which, to the best of our knowledge, has never been dealt with in the literature. This kind of mechanism consists of multiple branches each of which has an arbitrary number of links and a fixed initial point, while all branches end at a common end-point (this type of mechanism resembles some parallel robots which are in practical use). It is shown that generically, the configuration spaces of such mechanisms are manifolds, and the conditions for the exceptional cases are then determined. The configuration space of planar arachnoid mechanisms having k branches, each with two links is fully analyzed, while for the non-manifold cases we analyze the singular configurations.

We now introduce some notation and terminology to describe such mechanism types, and in particular the arachnoid mechanisms which are the subject of this note:

Definition 1.1.1. For a mechanism M in $\mathbb{R}^d$, a *branch* $(L, \mathbf{x})$ of multiplicity n is a sequence $L = (\ell_1, \ldots, \ell_n)$ of n positive numbers, together with a point $\mathbf{x} \in \mathbb{R}^d$. We think of L as the lengths of n concatenated rods, having revolute (i.e., rotational)

joints at the meeting point of every two consecutive rods, and at the fixed initial point $\mathbf{x}$, called the *base point* of the branch.

A *branch configuration* $V = (\mathbf{v}_1, \ldots, \mathbf{v}_n)$ for a branch $(L, \mathbf{x})$ then consists of n vectors in $\mathbb{R}^d$ with the given norms $\|\mathbf{v}_i\| = \ell_i$ $(i = 1, \ldots n)$.

Since the configuration space of a branch $(L, \mathbf{x})$ is independent of the order of the set $\ell_1, .., \ell_n$ (up to homeomorphism), we can (and shall) assume $\ell_1, .., \ell_n$ to be in descending order.

Definition 1.1.2. An *arachnoid mechanism* consists of k branches

$$(\mathcal{L}, \mathcal{X}) = ((L^{(1)}, \mathbf{x}^{(1)}), \ldots (L^{(k)}, \mathbf{x}^{(k)}))$$

with multiplicities $n^{(1)}, ..., n^{(k)}$. We think of this as a linkage of branches connected by a single revolute joint at their common end point (whose location is not fixed).

An arachnoid mechanism configuration for $(\mathcal{L}, \mathcal{X})$ thus consists of a set

$$\mathcal{V} = (V^{(1)}, .., V^{(k)})$$

of branch confiurations for $\mathcal{L}$ having a common *end point* $\mathbf{y} = \mathbf{x}^{(i)} + \sum_{j=1}^{n^{(i)}} \mathbf{v}_j^{(i)}$ $(i = 1, .., k)$.

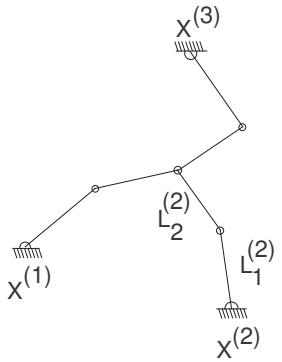

Figure 1.1.1: An arachnoid mechanism with $k = 3$, multiplicities 2.

Definition 1.1.3. For an arachnoid mechanism $(\mathcal{L}, \mathcal{X})$:

1. A branch configuration $\mathcal{V} = (\mathbf{v}_1, \ldots, \mathbf{v}_n)$ is *aligned* (with direction $\mathbf{w}$) if each vector $\mathbf{v}_1, \ldots, \mathbf{v}_n$ is a scalar multiple of $\mathbf{w}$.

2. A configuration $\mathcal{V} = (V^{(1)}, .., V^{(k)})$ of $(\mathcal{L}, \mathcal{X})$ is called a *t-node* if it has t aligned branch configurations with directions $\mathbf{w}_{i_1}, \ldots, \mathbf{w}_{i_t}$ respectively, which are linearly dependent; otherwise $\mathcal{V}$ is called *generic*.

Definition 1.1.4. The collection $\mathcal{C} = \mathcal{C}(\mathcal{L}, \mathcal{X})$ of all configurations $\mathcal{V}$ for $(\mathcal{L}, \mathcal{X})$ is called its *configuration space*. It is topologized as a subspace of the appropriate Euclidean space. The space of all such common endpoints $\mathbf{y}$ will be called the *work space* $\mathcal{W} = \mathcal{W}(\mathcal{L}, \mathcal{X})$ for $(\mathcal{L}, \mathcal{X})$. The *work map* $\Phi : \mathcal{C} \to \mathcal{W}$ assigns to each configuration $\mathcal{V}$ its common endpoint $\mathbf{y}$.

Organization. In section 3.2 we show that the configuration space of a generic arachnoid mechanism $(\mathcal{L}, \mathcal{X})$ is a manifold. In section 3.3 we study planar arachnoid mechanisms for which each branch has 2 joints, and give an explicit formula for the toplogical type of $\mathcal{C} = \mathcal{C}(\mathcal{L}, Xc)$ in the generic case. Finally, in section 1.4, we analyze the singularities of $\mathcal{C}$ for such planar arachnoid mechanisms in the non-manifold case.

1.2 Generic arachnoid mechanisms in $\mathbb{R}^d$

First, we show that, generically, the configuration space of an arachnoid mechanism is a manifold:

Theorem 1.2.1. *Let $(\mathcal{L}, \mathcal{X})$ be an arachnoid mechanism in $\mathbb{R}^d$ with k branches of multiplicities $n^{(1)}, ..., n^{(k)}$, respectively. If all configurations of $(\mathcal{L}, \mathcal{X})$ are generic, then its configuration space $\mathcal{C}$ is a smooth closed orientable manifold of dimension $d(N - k + 1) - N$, where $N = \sum_{i=1}^{k} n^{(i)}$.*

Proof. We can identify $\mathcal{C} = \mathcal{C}(\mathcal{L}, \mathcal{X})$ as the pre-image of a certain function $G : \mathbb{R}^{d(N-k+1)} \to \mathbb{R}^N$, where G is defined as follows:

For each $n \geq 1$ let $g_n : (\mathbb{R}^d)^n \to \mathbb{R}^{n-1}$ be defined

$$g_n(\mathbf{v}_1, \ldots, \mathbf{v}_n) := (|\mathbf{v}_2 - \mathbf{v}_1|^2, \ldots, |\mathbf{v}_n - \mathbf{v}_{n-1}|^2),$$

where $|\mathbf{u}| := (\sum_{i=1}^d t_i^2)^{1/2}$ is the length of a vector $\mathbf{u} = (t_1, \ldots, t_d) \in \mathbb{R}^d$. Now for each branch $L^{(i)} = (\ell_1^{(i)}, .., \ell_{n^{(i)}}^{(i)})$ of $\mathcal{L}$, let $(\mathbf{v}_1^{(i)}, \ldots, \mathbf{v}_{n^{(i)}}^{(i)})$ be position vectors of the ends of the $n^{(i)}$ links of a branch configuration, where $\mathbf{v}_0^{(i)} = \mathbf{x}^{(i)}$ (the given base point for this branch). Since in an arachnoid mechanism all branches end at the same point $\mathbf{u} \in \mathbb{R}^d$, we have $\mathbf{v}_{n^{(i)}}^{(i)} = \mathbf{u}$ for all $1 \leq i \leq k$. Thus we have $N - k + 1$ different vectors $\{\mathbf{v}_1^{(i)}, \ldots, \mathbf{v}_{n^{(i)}}^{(i)}\}_{i=1}^k$, and we define

$$G(\mathbf{v}_1^{(1)}, \ldots, \mathbf{v}_{n^{(k)}}^{(k)}) := (g_{n_1}(\mathbf{v}_0^{(1)}, \ldots, \mathbf{v}_{n_1}^{(1)}), g_{n_2}(\mathbf{v}_0^{(2)}, \ldots, \mathbf{v}_{n_2}^{(2)}), \ldots g_{n_k}(\mathbf{v}_0^{(k)}, \ldots, \mathbf{v}_{n_k}^{(k)})),$$

so that $\mathcal{C} = G^{-1}(\vec{\ell})$ for $\vec{\ell} := (\ell_1^{(1)})^2, .., (\ell_{n^{(1)}}^{(1)})^2, \ldots (\ell_1^{(k)})^2, .., (\ell_{n^{(k)}}^{(k)})^2)$. By the Regular Value Theorem (see [50, I, Thm. 3.2]), $\mathcal{C}$ will be a smooth manifold if $\vec{\ell}$ is a regular value of G – that is, dG has maximal rank.

Note that (after applying elementary row and column operations), dG has the following $N \times dN$ Jacobian matrix:

$$dG = 2 \begin{pmatrix} A^{(1)} & B^{(1)} & & 0 & \\ A^{(2)} & & B^{(2)} & & \\ \vdots & & & \ddots & \\ A^{(k)} & 0 & & & B^{(k)} \end{pmatrix}$$

where each $(n^{(i)} \times d)$-block $A^{(i)}$ is:

$$A^{(i)} = \begin{pmatrix} \mathbf{v}_{n^{(i)}}^{(i)} - \mathbf{v}_{n^{(i)}-1}^{(i)} \\ 0 \\ \vdots \\ 0 \end{pmatrix}$$

and $B^{(i)}$ is:

$$\begin{pmatrix} \mathbf{v}^{(i)}_{n^{(i)}-1} - \mathbf{v}^{(i)}_{n^{(i)}} & 0 & 0 & \dots & 0 & 0 \\ \mathbf{v}^{(i)}_{n^{(i)}-1} - \mathbf{v}^{(i)}_{n^{(i)}-2} & \mathbf{v}^{(i)}_{n^{(i)}-2} - \mathbf{v}^{(i)}_{n^{(i)}-1} & 0 & \dots & 0 & 0 \\ 0 & \mathbf{v}^{(i)}_{n^{(i)}-2} - \mathbf{v}^{(i)}_{n^{(i)}-3} & \mathbf{v}^{(i)}_{n^{(i)}-3} - \mathbf{v}^{(i)}_{n^{(i)}-2} & \dots & 0 & 0 \\ 0 & 0 & 0 & \dots & 0 & 0 \\ \vdots & \vdots & \vdots & \ddots & \vdots & \vdots \\ 0 & 0 & 0 & \dots & \mathbf{v}^{(i)}_2 - \mathbf{v}^{(i)}_1 & \mathbf{v}^{(i)}_1 - \mathbf{v}^{(i)}_2 \\ 0 & 0 & 0 & \dots & 0 & \mathbf{v}^{(i)}_1 - \mathbf{v}^{(i)}_0 \end{pmatrix}$$

an $n^{(i)} \times d(n^{(i)} - 1)$ matrix which can be thought of as the Jacobian matrix for a corresponding closed $n^{(i)}$-branch. Note that $\mathrm{Rank}(B^{(i)}) \leq n^{(i)}$, and $B^{(i)}$ has less than full rank only when all vectors $\mathbf{v}^{(i)}_{n^{(j)}-1} - \mathbf{v}^{(i)}_{n^{(j)}}$ are collinear for $1 \leq j \leq n^{(i)}$ – so that the i-th branch is aligned. In this case $\mathrm{Rank}(B^{(i)}) = n^{(i)} - 1$, and the non-zero row $\mathbf{w}^{(i)} := \mathbf{v}^{(i)}_{n^{(i)}} - \mathbf{v}^{(i)}_{n^{(i)}-1}$ of $A^{(i)}$ is precisely the direction of the branch.

We can thus divide the matrix dG horizontally into two blocks: (A, B), where

$$A := \begin{pmatrix} A^{(1)} \\ \vdots \\ A^{(k)} \end{pmatrix} \quad \text{and} \quad B := \begin{pmatrix} B^{(1)} & & 0 \\ & B^{(2)} & \\ & & \ddots \\ 0 & & B^{(k)} \end{pmatrix},$$

and the rank of dG is then given by:

$$\mathrm{Rank}(A, B) = \mathrm{Rank}(A) + \mathrm{Rank}(B) - \dim(\mathrm{Col}(A) \cap \mathrm{Col}(B)). \tag{1.2.1}$$

Denote by I the set of all indices i for which the $i^{(th)}$ branch is aligned, so that $\mathrm{Rank}(B) = N - |I|$. Thus if $I = \emptyset$, then dG has maximal rank. If $|I| \neq 0$, let A_I be the sub-matrix of A consisting of the blocks $A^{(i)}$ with $i \in I$. Its rows are therefore spanned by the directions $\{\mathbf{w}^{(i)}\}_{i \in I}$ of the aligned branches. Observe that $\mathrm{Rank}(A) - \mathrm{Rank}(A_I)$ is the dimension of the subspace of $\mathrm{Col}(A)$ consisting

of columns whose entries vanish in the rows indexed by $i \in I$. Since the blocks of B indexed by $i \notin I$ have full rank, we see that

$$\dim(\mathrm{Col}(A) \cap \mathrm{Col}(B)) \;\leq\; \mathrm{Rank}(A) - \mathrm{Rank}(A_I)$$

(in fact, equality holds). By (1.2.1):

$$\mathrm{Rank}(dG) \geq \mathrm{Rank}(A_I) + \mathrm{Rank}(B) = N - |I| + \mathrm{Rank}(A_I),$$

which means that dG has full rank unless $|I| > \mathrm{Rank}(A_I)$. The latter implies that the directions of the aligned branches are linearly dependent – that is, we have a k-node configuration.

Note that $\mathcal{C} = G^{-1}(\vec{\ell})$ is in fact orientable when dG has maximal rank, since in that case it induces an isomorphism between the normal bundle ν to $\mathcal{C}$ in $\mathbb{R}^{d(N-k+1)}$ at any point and the "normal bundle" to $\{\ell\} \hookrightarrow \mathbb{R}^N$. Thus ν (the complement to the tangent bundle $T\mathcal{C}$ in $\mathbb{R}^{d(N-k+1)}$) is orientable, so $T\mathcal{C}$ is, too. Finally, $\mathcal{C}$ is compact since it is a closed subset of the free configuration space, which is a N-torus. □

Remark 1.2.2. For an arachnoid mechanism in $\mathbb{R}^3$, the matrix dG will be singular for a 2-node configuration (two aligned branches along one line); a 3-node configuration (three aligned branches contained in one plane); or a 4-node configuration (four aligned branches).

1.3 Planar mechanisms

¿From now on we restrict attention to arachnoid mechanisms $(\mathcal{L}, \mathcal{X})$ in the ¿plane (that is, $d = 2$).

1.3.1 The work space

In this case, each vector v_j in a branch configuration V (of multiplicity n) is determined by its argument θ_j (since $\|v_j\| = \ell_j$), and V can thus be identified with a

point $(\theta_1, .., \theta_n)$ in the n-torus

$$\mathbf{T}^n = \underbrace{\mathbf{S}^1 \times \ldots \times \mathbf{S}^1}_{n}.$$

Thus if $\nu = n^{(1)} + \ldots + n^{(k)}$, then $\mathcal{C}(\mathcal{L}, \mathcal{X}) \subseteq \mathbf{T}^\nu = \prod_{i=1}^k \mathbf{T}^{n^{(i)}}$.

Given such an arachnoid mechanism, we can describe the work space $\mathcal{W}$ as follows: for any branch $L = (\ell_1, \ldots, \ell_n)$, let $\beta(L)_{\min}$ denote the minimal value of $|\sum_{j=1}^n \varepsilon_j \ell_j|$, where $\varepsilon_j = \pm 1$ for each $1 \leq j \leq n$; and let $\beta(L)_{\max} := \sum_{j=1}^n \ell_j$ (the maximal value). The work space $W = \mathcal{W}(L, \mathbf{x})$ for the branch L with base point $\mathbf{x}$ (without any constraint on the end point) is then an annulus bounded by circles of radius $\beta(L)_{\min}$ and $\beta(L)_{\max}$, respectively.

If $\mathcal{L} = (L^{(1)}, ..., L^{(k)})$, with multiplicities $n^{(1)}, ..., n^{(k)}$, and $\mathcal{X} = (\mathbf{x}^{(1)}, ..., \mathbf{x}^{(k)})$, the work space for $(\mathcal{L}, \mathcal{X})$ is $\mathcal{W} = \bigcap_{i=1}^k W^{(i)}$, where $W^{(i)} = W(L^{(i)}, \mathbf{x}^{(i)})$. Each component of $\mathcal{W}$ is a curvilinear polygon P (not necessarily convex), whose edges $\mathrm{Edge}(P)$ are arcs of the annuli boundary circles $\partial W^{(i)}$, and whose vertices $\mathrm{Vertex}(P)$ are intersection points of such arcs.

1.3.2 The configuration space

The configuration space for any branch $L = (\ell_1, \ldots, \ell_n)$ and base-point $\mathbf{x}$ is an n-torus $\mathbf{T}^n$, with work map $\phi : \mathbf{T}^n \to W$.

Note that the fiber $\phi^{-1}(z)$ over any point $z \in \operatorname{Int} W$ is the configuration space for the *closed* chain with links $\ell_0, \ell_1, \ldots, \ell_n$, where $\ell_0 := z - \mathbf{x}$. This configuration space has been analyzed in [9]. On the other hand, if z is on the boundary of the annulus W, then $\phi^{-1}(z)$ is evidently discrete, and in fact consists of a single point (unless it is on the inner circle, and $\beta(L)_{\min}$ can be written as $|\sum_{j=1}^n \varepsilon_j \ell_j|$ in more than one way).

If $\mathcal{L} = (L^{(1)}, ..., L^{(k)})$, with multiplicities $n^{(1)}, ..., n^{(k)}$, and $\mathcal{X} = (\mathbf{x}^{(1)}, ..., \mathbf{x}^{(k)})$, its configuration space is the pullback

$$\mathcal{C}(\mathcal{L}, \mathcal{X}) \;=\; \{(\tau_1, \ldots, \tau_k) \in \prod_{i=1}^k \mathbf{T}^{n^{(i)}} \mid \phi_1(\tau_1) = \ldots = \phi_k(\tau_k) \in \mathcal{W}\}.$$

1.3.3 Example

Consider an arachnoid mechanism consisting of three branches, each of multiplicity 2, as in Figure 1.1.1.

The workspace for each free branch is an annulus; let us assume that the three annuli intersect in the shaded lens-shaped component P in Figure 1.3.1.

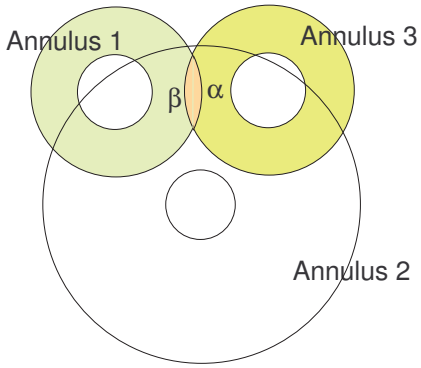

Figure 1.3.1: Polygonal intersection

Now consider an interior point $y \in \mathrm{Int}(P)$: in the corresponding configurations in the fiber $\Phi^{-1}(y)$, each of the three branches can be in one of two positions (branch configurations), usually termed "elbow up" ($\mathbf{u}$) and "elbow down " ($\mathbf{d}$), so for each branch we have a copy of $\mathbf{S}^0 = \{\mathbf{u}, \mathbf{d}\}$. Thus the fiber consists of eight points $\mathbf{uuu}, \mathbf{uud}, \ldots, \mathbf{ddd}$, thought of as the product $\mathbf{S}^0 \times \mathbf{S}^0 \times \mathbf{S}^0$. Thus $\Phi^{-1}(\mathrm{Int}(P)$ is simply an eight-fold cover of the interior of the lens.

On the other hand, if y is on the edge α of P, which is in the outer boundary of the first annulus, the first branch is completely extended, identifying its $\mathbf{u}$ and $\mathbf{d}$ positions, thus collapsing the first $\mathbf{S}^0$ to a single point, and generally identifying the copy of α in $\mathcal{C}$ indexed by $\mathbf{u} * *$ with the copy indexed by $\mathbf{d} * *$, for $** \in \{\mathbf{uu}, \mathbf{ud}, \mathbf{du}, \mathbf{dd}\}$.

Similarly, the copy of β in $\mathcal{C}$ indexed by $* * \mathbf{u}$ is identified with that indexed by $* * \mathbf{d}$. Therefore, the fiber of $y \in \alpha \cap \beta$ consists of two points. Note that the second $\mathbf{S}^0$-factor never collapses, so $\mathcal{C}$ is of the form $\mathbf{S}^0 \times \mathcal{M}$ – i.e., $\mathcal{C}$ has two components,

each isomorphic to $\mathcal{M}$.

To evaluate the Euler characteristic of $\mathcal{M}$, note that it is obtained from four 2-gons (the lens-shaped intersection in $\mathcal{W}$) by identifying their 8 edges pairwise (as explained above), identifying the "top" vertex in all the 2-gons to a single point, and similarly for the "bottom" vertex. Thus $\chi(\mathcal{M}) := V - E + F = 4 - 4 + 2 = 2$, so $\mathcal{M}$ is a 2-sphere, and $\mathcal{C} \cong \mathbf{S}^2 \sqcup \mathbf{S}^2$.

1.3.4 Invariants of annulus arrangements

An annulus (i.e., pair of concentric circles) in the plane is determined by $(\mathbf{x}, \beta_{\min}, \beta_{\max})$, where $\mathbf{x} \in \mathbb{R}^2$ is the center and $0 < \beta_{\min} < \beta_{\max}$ are the radii. Consider a system

$$\langle (\mathbf{x}^{(1)}, \beta(1)_{\min}, \beta(1)_{\max}); \ldots ; (\mathbf{x}^{(k)}, \beta(k)_{\min}, \beta(k)_{\max}) \rangle$$

of k such pairs (with distinct centers), and let $\mathcal{W}$ denote the intersection of all the corresponding anulli; this may have several connected components $V_1, \ldots, V_t$. What we have in mind, of course, is the collection of boundary circles for the work space of branches of an arachnoid mechanism.

The boundary ∂V of each component V of $\mathcal{W}$ is a curvilinear planar polygon, not necessarily connected; let $\alpha := \alpha(V)$ denote the number of components of ∂V contained in the interior of its convex hull $\mathrm{conv}(V)$. We set

$$\gamma := \gamma(V) = \begin{cases} 1 & \text{if } \mathrm{conv}(V) \text{ is a disc} \\ 0 & \text{otherwise.} \end{cases}$$

be wholely contained in the interior of some of the annuli; denote the number of such annuli by $\beta := \beta(V)$ $(0 \le \beta(V) \le k)$, and let the *c-invariant* of V be $c(V) := 2^\beta$. Finally, the *g-invariant* of V is:

$$g(V) := 1 - 2^{k-\beta-3}(|\,\mathrm{Vertex}(V)| - 2|\,\mathrm{Edge}(V)| + 4 + 2\gamma - 4\alpha).$$

Theorem 1.3.5. *Let $(\mathcal{L}, \mathcal{X})$ be a planar arachnoid mechanism with k branches, each of multiplicity 2, and assume that the configuration space $\mathcal{C} = \mathcal{C}(\mathcal{L}, \mathcal{X})$ has no*

node configrations; then $\mathcal{C}$ *decomposes as the disjoint union of the pre-image under* Φ *of the components of the workspace* $\mathcal{W}$*, and for each such component* V*,* $\Phi^{-1}(V)$ *consists of* $c(V)$ *closed orientable surfaces of genus* $g(V)$*.*

A special case of this Theorem appears in [2].

Proof. As in example 1.3.3 above, $\Phi^{-1}(V)$ is obtained from the 2^k curvilinear polygonal "tiles" (i.e., copies of V, corresponding to the "elbow up/elbow down" position of each branch), by identifications of those edges which correspond to the $k-\beta$ "relevant" branches. Since we know from Theorem 1.2.1 that (each component of) $\mathcal{C}$ is a closed orientable 2-manifold, its type (genus) is determined by the Euler characteristic, which may be computed by calculating how many identifications we have for each vertex or edge of $\Phi^{-1}(V)$.

To orient $\Phi^{-1}(V)$, choose an orientation for some (fixed) tile H_0. Every other tile H of $\Phi^{-1}(V)$ differs from H_0 in exactly τ of the k possible "elbow up/elbow down" positions, and we reverse its orientation (relative to that of H_0) if and only if τ is odd. □

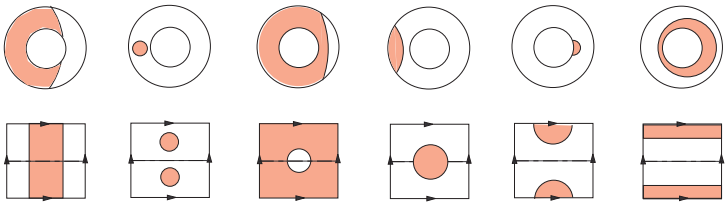

Figure 1.3.2: Work and configuration space intersections of two branches

Remark 1.3.6. As noted in §1.3.1, the workspace $\mathcal{W}$ was obtained by repeatedly intersecting annuli, which are the workspaces of the individual branches. If we concentrate on the annulus A of the first branch, say, then generically the annuli for each of the remaining branches will interesect with A in one of the six shaded patterns V in the first row of Figure 1.3.2. In each case we obtain a certain subset $\phi^{-1}(V)$ of the

2-torus $\mathbf{T}^2$ which is the configuration space for the first branch, where $\phi : \mathbf{T}^2 \to A$ is the work map for the first branch.

Note that when we further intersect V with a third annulus, the pattern may be more complicated; in particular, three-fold intersections need not be connected, as illustrated by Figure 1.3.3, which shows the subset of the 2-torus associated with the workspace of Figure 1.1.1 (without indicating the identifications).

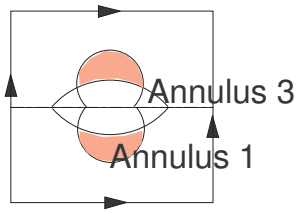

Figure 1.3.3: Subset of $\mathbf{T}^2$

1.4 Singular configuration spaces

While the analysis of the configuration space $\mathcal{C} = \mathcal{C}(\mathcal{L}, \mathcal{X})$ of a mechanism in the non-manifold case is in general difficult, for a planar arachnoid mechanism with branch multiplicity 2 the description of Theorem 1.3.5 can actually be extended to singular points, corresponding to the node configurations.

Proposition 1.4.1. *Let $(\mathcal{L}, \mathcal{X})$ be a planar arachnoid mechanism with k branches, each of multiplicity 2, and let $\mathcal{V}$ be a node configuration in $\mathcal{C} = \mathcal{C}(\mathcal{L}, \mathcal{X})$. Then $\mathcal{V}$ has an open neighborhood in $\mathcal{C}$ which is a wedge of $2^{q-\varepsilon}$ 2-dimensional discs with common center $\mathcal{V}$, where q is the number of aligned branches, $\varepsilon = 1$ if the aligned branches have a common direction, and $\varepsilon = 2$ otherwise.*

Proof. Let $v := \Phi(\mathcal{V})$ be the common end-point of the k-branches in $\mathcal{V}$, and let U be an small disc containing v in the workspace $\mathcal{W}$. Since v is necessarily in the

boundary of a curvilnear polygonal component of $\mathcal{W}$, then P, the boundary of U near v, consists of arcs of the boundary circles of the annuli.

1. When all of the q aligned branches have a common direction, the centers of the corresponding annuli must be collinear, and P is an arc e of a single boundary circle of such an annulus. Note that $\Phi^{-1}(\mathrm{Int}(U))$ intersects the component of $\mathcal{V}$ in 2^q disjoint discs, which are identified pairwise along $\Phi^{-1}(e)$ so as to yield 2^{q-1} discs whose only common point is $\mathcal{V} \in \Phi^{-1}(v)$.

2. Otherwise, P must consist of two arcs $e_1,\ e_2$ of distinct boundary circles (whose centers are not collinear with v). Again $\Phi^{-1}(\mathrm{Int}(U))$ intersects the component of $\mathcal{V}$ in 2^q disjoint discs, but now every four of them (corresponding to the four "elbow up/elbow down" positions of the two branches associated to e_1 and e_2, respectively) are identified in $\Phi^{-1}(U) \subset \mathcal{C}$ along $\Phi^{-1}(e_1)$ and $\Phi^{-1}(e_2)$, forming the four quadrants of a new disc – where again $\mathcal{V}$ is the only point in common. This yields a total of 2^{q-1} discs. □

Chapter 2

Motion Planning for a Class of Planar Closed-Chain Manipulators

Accepted to *International Journal of Robotic Research*, 2006.
Co-authors: Guanfeng Liu, Jeff Trinkle and Moshe Shoham.
Presented in *IEEE International Conference on Robotics and Automation*, 2006.

We study the motion planning problem for planar *star-shaped* manipulators. These manipulators are formed by joining k "legs" to a common point (like the thorax of an insect) and then fixing the "feet" to the ground. The result is a planar parallel manipulator with $k-1$ independent closed loops. A topological analysis is used to understand the global structure the configuration space so that planning problem can be solved exactly. The worst-case complexity of our algorithm is $O(k^3N^3)$, where N is the maximum number of links in a leg. Examples illustrating our method are given.

2.1 Introduction

The canonical robot motion planning problem is known as the "piano movers'" problem. In this problem, one is given initial and goal configurations of a "piano" (a rigid body that is free to move in an environment with fixed rigid obstacles) and geometric

models of the piano and obstacles. The goal is to find a continuous motion of the piano connecting the initial and goal configurations. Lozano-Perez studied this problem in configuration space, or configuration space, a space in which a configuration of the piano maps to a point, a motion maps to a continuous curve, and the obstacles map to the C-obstacle, *i.e.,* the set corresponding to overlap between the piano and an obstacle [20]. The dimension of configuration space is equal to the number of degrees of freedom of the system. The free space, or C-free, is what remains after removing the C-obstacle from configuration space. In configuration space, the motion planning problem becomes a path planning problem. That is, one must construct a continuous path connecting the initial and goal configurations that lies entirely within C-free. Theoretical results for the piano movers' problem were first obtained by Schwartz, Sharir, and Hopcroft [32, 30]. They found that the problem is PSPACE hard, and proposed an algorithm based on Collins' decomposition to find a path. Since the worst-case running time of Collins' decomposition algorithm is doubly exponential in the dimension of configuration space, it is impractical.

The more complex generalized movers' problem, is the problem in which there are multiple rigid bodies moving simultaneously in a workspace. The bodies are the links of one or more robots, and thus may be required to obey constraints corresponding to their kinematic structures and joint limits. Given the importance of motion planning problem in robotics, researchers worked to find more efficient algorithms despite the depressing complexity results found earlier. The most efficient exact method known is Canny's algorithm, which has time complexity that is only singly exponential in the dimension of configuration space[39]. He also made the important observation that this bound is worst-case optimal, since the worst-case number of components in configuration space is exponential in its dimension. Canny's algorithm is very difficult to implement - to date no full implementation exists.

In the 1990's, the intractability of exact motion planning for general problems stimulated a paradigm shift to randomized methods. The method of Barraquand and Latombe combined potential field methods with random walk [28]. In essence,

a potential field method defines an artificial potential field on configuration space such that the goal configuration is the global minimum of the potential function and no saddle points or other local minima exist. When the function has this property, motion planning can be done by any gradient following algorithm. An important class of such functions are navigation functions [19, 24, 26]. Ideally, the potential function will be a function of the goal configuration, and the global minimum property will hold for all possible goal configurations. Since such potential functions can be difficult to design, Barraquand and Latombe suggested the use of random walks to escape local minima [28]. This modification yielded a method that is practically effective and probabilistically complete.

When possibly many motion planning queries must be handled for a single static environment, a different type of randomized method has been found to be more efficient than rerunning the Barraquand-Latombe algorithm for each query. The probabilistic roadmap method (PRM) of Kavraki *et. al* [40], is an easy-to-implement randomized version of Canny's [39].

Because PRMs have been successful in solving problems in configuration spaces with dimension approaching 100, many researchers have worked to make the method more efficient (*e.g.,* [34, 35, 36]) and to modify it to solve more challenging types of problems, such as those with closed kinematic loops, nonholonomic constraints, dynamics, and intermittent contact (*e.g.,* [42, 33, 18, 37, 38, 31]).

In this paper, we are particularly interested in planar *star-shaped manipulators*. These manipulators are formed by joining k planar "legs" to a common point (like the thorax of an insect) and then fixing the "feet" to the ground. The result is a planar parallel manipulator with $k-1$ independent closed loops. They are important because they arise in parallel manipulators, walking robots, and dexterous manipulation, and motion plans are difficult to obtain using PRMs. In such systems, configuration space is often most naturally viewed as a lower-dimensional space embedded in an ambient space (typically the joint space). The embedding results from equality constraints corresponding to kinematic loop closure. In such settings, it is difficult to obtain an

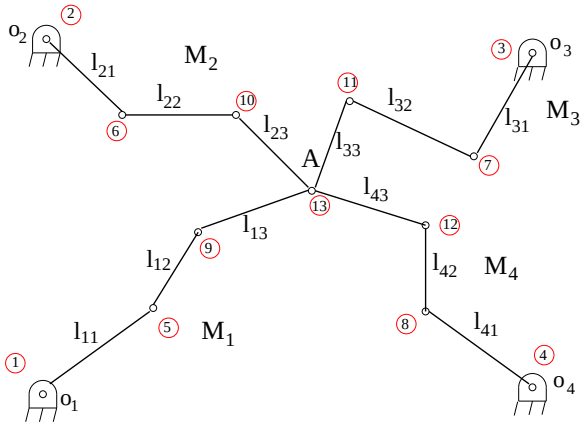

Figure 2.1.1: Star-shaped manipulator with $k = 4$.

explicit description of configuration space with minimal number of parameters and a suitable metric to guide sample generation. These problems make it difficult to construct a roadmap with the requisite properties, and hence difficult to solve motion planning problems for systems with kinematic loops using PRMs. The RLG (random loop generator) method [22, 23] improves the sampling techniques through estimating the regions of sampling parameters. However, its efficiency relies on the accuracy of the estimation, which often varies case by case. Moreover, it ignores the global structure of configuration space, and may fail to sample globally important regions. The difficulties associated with applying randomized motion planning methods to manipulators with closed chains and the availability of new results in topology [13, 11, 14, 27] have recently led to renewed interest in exact planning algorithms. Trinkle and Milgram derived some topological properties of the configuration spaces (the number of components and the structures of the components) of single-loop closed chains with spherical joints in a workspace *without* obstacles [15, 14]. These properties drove the design of a complete, polynomial-time motion planning algorithm that works roughly as follows.

1. Choose a subset $\mathcal{A}$ of the links that can be positioned arbitrarily, and yet the remaining links can close the loop;

2. Move the links in $\mathcal{A}$ to their goal orientations along an arbitrary path while maintaining loop closure;

3. Permanently fix the orientations of the links in $\mathcal{A}$;

4. Repeat until all link orientations are fixed.

The main result that guided the algorithm's design is Theorem 2 in [14]. In generic cases, the configuration space is the union of manifolds that are products of spheres and intervals. The joint coordinates corresponding to the spheres are those that can contribute to the subset $\mathcal{A}$ mentioned above and the structure of the configuration space suggests a local parametrization for each step.

Here, the previous methods for configuration space connectivity analysis are extended to planar star-shaped manipulators with revolute joints. These manipulators have a common junction point and k ($k > 0$) legs connecting the junction to the fixed base. Following a topological analysis of the global structure of configuration space (i.e., the structure of the inverse kinematics of the manipulator), the motion planning problem is solved completely in polynomial time. Furthermore since we consider only a point end-effector, the direct kinematics is straightforward while the inverse kinematics is more complex. Thus, while for most parallel mechanisms using configuration space as a mean for path planning should be carefully considered, here our approach is natural.

Note that this paper is aimed at possibly more complex macromolecules with non-covalent bonds (not just manipulators) for which the number of legs and links in each leg may be very large [21]. So such a polynomial-complex algorithm would play a key role in several issues in structural biology, such as structure prediction in protein folding and binding, and study of protein mobility in folded states. In these applications, we are interested in the robot motion planning problem without considering the control and sensor issues.

The main contributions of this paper are two folds. First, we establish the global

connectivity of the configuration space of star-shaped manipulators via a combination of the cell decomposition of workspace and the structure of the configuration space at points in all cells. Although the results seem obvious, the proof detail is highly non-trivial. Second, the global connectivity result of configuration space only suggests an exponential algorithm for path existence, which makes the motion planning formidable for macromolecules with very large number of links. In this paper we propose novel techniques for path existence that avoids the exponential complexity. This paper is organized as follows. In Section 2.2, kinematics and singularities

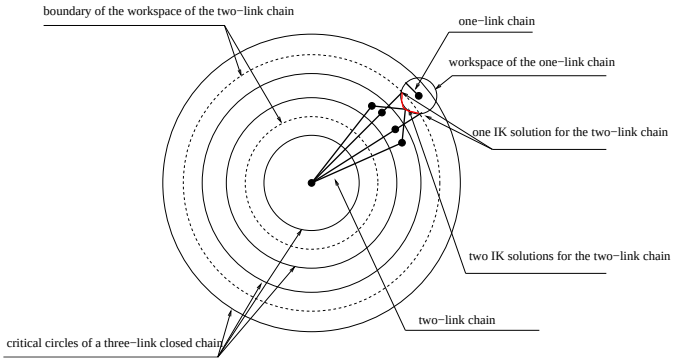

Figure 2.1.2: Inverse kinematics of a three-link serial chain.

of the manipulator are analyzed. In Section 2.3, necessary and sufficient conditions for configuration space connectivity and path existence are derived, based on which a complete polynomial-time algorithm is developed in Section 2.4. Section 2.5 addresses path optimization and robustness issues. Section 2.6 shows simulation results that tests the effectiveness of our algorithm. Finally 2.8 ends this paper with a brief conclusion.

2.2 Preliminaries

A star-shaped manipulator is composed of k serial chains with all revolute joints (see Fig. 2.1.1). Leg M_j is composed of n_j links of lengths $l_{j,i}, i = 1, ..., n_j$ and joint angles $\theta_{j,i}, i = 1, ..., n_j$. At one end (the foot), M_j is connected to ground by a revolute joint

fixed at the point o_j. At the other end, it is connected by another revolute joint to a junction point denoted by A. Note that when k is one, a star-shaped manipulator is an open serial chain. When k is two, it is a single-loop closed chain.

Assuming that the foot of M_j is fixed at o_j, let $f_j(\Theta_j) = p$ denote the kinematic map of M_j, where $\Theta_j = (\theta_{j,1}, \cdots, \theta_{j,n_j})$ is the tuple of joint angles, and p is the location of the endpoint of the leg (the thorax end). When M_j is detached from the junction A, the image of its joint space is the reachable set of positions of the free end of the leg, called the workspace W_j. In the absence of joint limits, the workspace W_j is an annulus if and only if there exists one link with length strictly greater than the sum of all the other link lengths. Otherwise it is a disk. Clearly, the workspace W_A of A when all the legs are connected to A is given by:

$$W_A = \bigcap_{j=1}^{k} W_j. \tag{2.2.1}$$

In our study of $\mathcal{C}$, it will be convenient to refer to several other configuration spaces. The configuration space of leg M_j when detached from the rest of the manipulator will be denoted by $\mathcal{C}_j$. When the endpoint is fixed at the point p, leg j will be denoted by $\tilde{M}_j(p)$, where the tilde is used to emphasize the fact that the endpoint has been fixed. Note that $\tilde{M}_j(p)$ is a single-loop planar closed chain, about which much is known (see [15]), including global structural properties of its configuration space, denoted by $\tilde{\mathcal{C}}_j(p) = f_j^{-1}(p)$. When the junction A of a star-shaped manipulator is fixed at point p, its configuration space will be denoted by $\tilde{\mathcal{C}}(p)$. Since collisions are ignored, the motions of the legs are independent, and therefore the configuration space of the manipulator (with fixed junction) is the product of the configuration spaces of the legs with all endpoints fixed at p:

$$\left.\begin{aligned} \tilde{\mathcal{C}}(p) &= \tilde{\mathcal{C}}_1(p) \times \cdots \times \tilde{\mathcal{C}}_k(p) \\ &= f_1^{-1}(p) \times \cdots \times f_k^{-1}(p) \\ &= f^{-1}(p) \end{aligned}\right\} \tag{2.2.2}$$

where by analogy, f is a total kinematic map of the star-shaped manipulator. Loosely speaking, the union of the configuration spaces $\tilde{\mathcal{C}}(p)$ at each point p in W_A gives the configuration space of a star-shaped manipulator:

$$\mathcal{C} = \bigcup_{p \in W_A} \tilde{\mathcal{C}}(p). \tag{2.2.3}$$

Several properties of the configuration spaces $\mathcal{C}_j$ and $\tilde{\mathcal{C}}_j(p)$ are highly relevant and so are reviewed here before analyzing the configuration space of star-shaped manipulators. It is well known that the configuration space of M_j is a product of circles (*i.e.,* $\mathcal{C}_j = (S^1)^{n_j}$) [1]. The workspace W_j contains a critical set Σ_j which is composed of all points p in W_j for which the Jacobian of the kinematic map $Df_j(\Theta_j)$ drops rank for some $\Theta_j \in f_j^{-1}(p)$. These points form concentric circles of radii $|l_{j,1} \pm l_{j,2} \pm \cdots \pm l_{j,n_j}|$, as shown in Fig 2.2.1. When A coincides with a point in Σ_j, the links can be arranged such that they are all colinear, in which case the number of instantaneous degrees of freedom of the endpoint of the leg is reduced from two to one. Now consider the case where the endpoint of leg j is fixed to the point p. In other words, we are interested in the configuration space $\tilde{\mathcal{C}}_j(p)$ of $\tilde{M}_j(p)$, which amounts to calculating the inverse kinematics (IK) $f_j^{-1}(p)$. The structure of $f_j^{-1}(p)$ has been established in [29] for four-link single-loop closed chains, and in [15, 14] for chains with an arbitrary number of links.

Next, we compute $f_j^{-1}(p)$ for a three-link serial chain to explain the basic idea used in [15, 14] for analyzing the IK map of a closed chain with an arbitrary number of links. As shown in Fig. 2.1.2, we begin with the IK of a two-link serial chain. Each point in the workspace could have 0,1,or 2 IK solutions, and the set of points with constant number of IK solutions forms annular regions separated by the critical set of this chain. The IK of a three-link serial chain is then deduced by breaking the chain into a two-link serial chain and a one-link serial chain, and taking the union of the IK solutions of the two-link chain for all points in the workspace of the one-link chain. It is easy to check that for points in the outer most annular region in

[1] Recall the assumption of no joint limits.

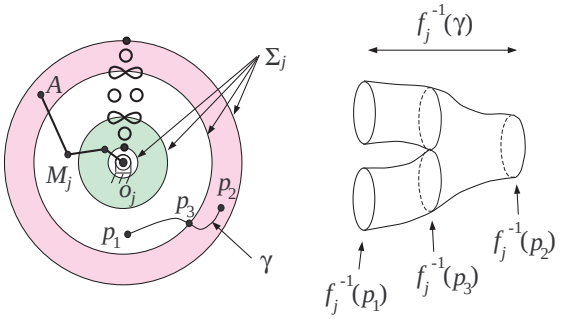

Figure 2.2.1: **Left:** The workspace W_j of a three-link open chain M_j based at o_j. The critical set Σ_j of the kinematic map f_j is four concentric circles. The small circles, figure eights, and points at 12 o'clock show the topology of the configuration space $\tilde{\mathcal{C}}_j(p)$ of the leg when its endpoint is fixed at a point in one of the seven regions delineated by the critical circles (one of the four circles or one of the three open annular regions between them). **Right:** The inverse image of the curve γ - a "pair of pants."

the workspace of the three-link chain, the workspace of the one-link chain (a circle) always intersects with the outer-most critical circle of the two-link chain at two points, indicating that the IK of this point is the union of two curve segments with a pair of endpoints identified, respectively, i.e., a circle. The inverse kinematics for points in other regions can be derived similarly. The results are shown in Fig. 2.2.1. In the 12 o'clock position, points, circles, and figure eights are drawn to represent the global structures of $\tilde{\mathcal{C}}_j(p)$ in the seven regions of W_j. Specifically, when A is fixed to a point p on the outer-most critical circle, $\tilde{\mathcal{C}}_j(p)$ is a single point. For p fixed to any point in the largest open annular region, configuration space is a single circle. Continuing inward, the possible configuration space types are a figure eight (on the second largest critical circle), two disconnected circles, a figure eight again, a single circle, and a single point (on the inner-most critical circle).

First, the connectivity of $\tilde{\mathcal{C}}_j(p)$ is uniquely determined by the number of "long links." Consider the augmented link set composed of the links of M_j and $\overline{o_j p}$, which will be called the fixed base link with length denoted by $l_{j,0}$. Let L_j be the sum of all

the link lengths including the fixed base link (*i.e.*, $L_j = \sum_{i=0}^{n_j} l_{j,i}$). Further, let $\mathcal{L}_j(p)$ be a subset of $\{0, 1, ..., n_j\}$ such that $l_{j,\alpha} + l_{j,\beta} > L_j/2;\ \alpha, \beta \in \mathcal{L}_j(p),\ \alpha \neq \beta$. Over all such sets, let $\mathcal{L}_j^*(p)$ be a set of maximal cardinality. Then the number of long links of $\tilde{M}_j(p)$ is defined as $|\mathcal{L}_j^*(p)|$, where $|\cdot|$ denotes set cardinality.

Lemma 1. **Kapovich and Milson [11], Trinkle and Milgram [15]**
The configuration space $\tilde{\mathcal{C}}_j(p) = f_j^{-1}(p)$ has two components if and only if $|\mathcal{L}_j^*(p)| = 3$, and is connected if and only if $|\mathcal{L}_j^*(p)| = 2$ or 0. No other cardinality is possible.

Let us return to the discussion of Fig. 2.2.1. Viewing W_j as a base manifold and the configuration space corresponding to each end point location as a fibre, it is apparent that the critical set Σ_j partitions W_j into regions over which the configuration spaces $\tilde{\mathcal{C}}_j(p)$ form a trivial fibration. The implications of this observation are useful in determining the configuration space of more complicated mechanisms. Consider a modification to $\tilde{M}_j(p)$ that allows the endpoint to move along a one-dimensional curve segment γ within W_j. Then as long as γ is entirely contained in one of the regions defined by the critical circles, $\tilde{\mathcal{C}}_j(\gamma) = \tilde{\mathcal{C}}_j(p) \times I$, where I is the interval. If γ crosses a critical circle transversally, then $\tilde{\mathcal{C}}_j(\gamma) = (\tilde{\mathcal{C}}_j(p_1) \times I) \bigcup \tilde{\mathcal{C}}_j(p_3) \bigcup (\tilde{\mathcal{C}}_j(p_2) \times I)$, where p_1 is a point in one of the two open annular regions containing γ, p_2 is a point in the other, and p_3 is a point on the critical circle crossed by γ, and $\bigcup$ denotes the standard "gluing" operation. In Fig. 2.2.1, an example γ and the corresponding configuration space $\tilde{\mathcal{C}}_j(\gamma)$ are shown.

2.3 Analysis of Star-Shaped Manipulators

For star-shaped manipulators with one or two legs, the global topological properties of the configuration space $\mathcal{C}$ are fully understood (for one, see [41]; for two, see [15, 14]). The goals of this section are to study the global properties of $\mathcal{C}$ when M has more than two legs and to derive necessary and sufficient conditions for solution existence to the motion planning problem.

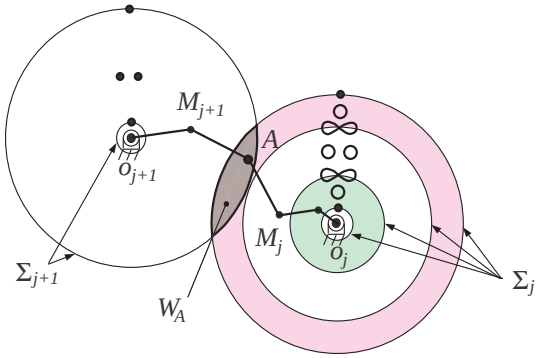

Figure 2.3.1: The workspace W_A of A for a star-shaped manipulator with $k = 2$ is the intersection of the workspaces of A for each leg considered separately. The critical set Σ is composed of the black circular arcs where they bound or intersect the gray area.

Local Analysis

As a direct generalization of the critical set of a single leg, we define the critical set of a star-shaped manipulator as a subset Σ of W_A such that for every $p \in \Sigma$, there exists a configuration c such that at least one of the Jacobians $\{Df_1(c), \cdots, Df_k(c)\}$ drops rank. By definition we have:

$$\Sigma = \left(\bigcup_{i=1}^{k} \Sigma_i \right) \bigcap W_A. \tag{2.3.1}$$

An advantage of this definition is that Σ can be used to stratify W_A such that each stratum is trivially fibred. Figure 2.3.1 shows a star-shaped manipulator with two legs. The critical set Σ is the boundary of the lune formed by the intersection of the outer critical circles of their individual workspaces. For every point interior to the lune, the fibre is two circles (the direct product of two points with one circle). The fibres associated to the vertices of the lune are single points, which correspond to simultaneous full extension of the two legs. Fig. 2.3.2 shows a possible workspace for a star-shaped manipulator with three legs. The critical set defines 65 distinct sets ${}^dU_i$ of varying dimension d, where i is an arbitrarily assigned index that simply counts components. We will refer to these sets as *chambers*. There are 12 two-dimensional,

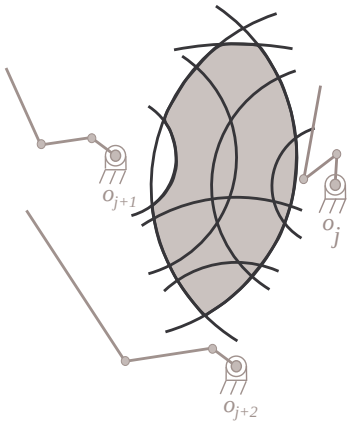

Figure 2.3.2: Workspace (shaded gray) of a star-shaped manipulator with three legs. The critical set partitions W_A into 12 two-dimensional, 32 one-dimensional, and 21 zero-dimensional chambers.

32 one-dimensional, and 21 zero-dimensional chambers, each of which is trivially fibred. Removing the ${}^0U_i$ from Σ partitions it into open one-dimensional chambers ${}^1U_i$, $i = 1, \cdots, {}^1m$. Removing ${}^0U_i$ and ${}^1U_i$ from W_A yields open two-dimensional sets ${}^2U_i$, $i = 1, \cdots, {}^2m$, for which the following relationships hold:

$$\Sigma = \left(\bigcup_{i=1}^{{}^0m} {}^0U_i\right) \bigcup \left(\bigcup_{i=1}^{{}^1m} {}^1U_i\right) \tag{2.3.2}$$

$$W_A - \Sigma = \bigcup_{i=1}^{{}^2m} {}^2U_i. \tag{2.3.3}$$

Proposition. 1. For all $d = 0, 1, 2$ and i, $f^{-1}({}^dU_i) = {}^dU_i \times f^{-1}(p)$, where p is any point in ${}^dU_i$ and the operator $\times$ denotes the direct product. Gluing the $f^{-1}({}^dU_i)$ for all i and d gives the total configuration space $\mathcal{C}$.

Proof: When $d = 0$, ${}^0U_i$ contains a single point, the result follows. When $d = 1$, ${}^1U_i$ belongs to one critical circle of one leg, say $\tilde{M}_j$. Any two points $p_1, p_2 \in {}^1U_i$ are related by a Euclidean rotation $p_2 - o_j = R(p_1 - o_j)$, indicating that $\tilde{\mathcal{C}}_j(p_1)$ and $\tilde{\mathcal{C}}_j(p_2)$

are homotopic. Thus $\tilde{\mathcal{C}}_j(p)$ for all $p \in {}^1U_i$ have equivalent topological structure. For the other legs $\tilde{M}_l$, $l \neq j$, according to [14] (Lemma 6.1 and Corollary 6.5) $\tilde{\mathcal{C}}_l(p)$ for all $p \in {}^1U_i$ have equivalent topological structures as ${}^1U_i$ is free of critical points of $\tilde{M}_l(p)$. Thus $f^{-1}(p) = \tilde{\mathcal{C}}_1(p) \times \cdots \times \tilde{\mathcal{C}}_k(p)$ for all $p \in {}^1U_i$ have equivalent topological structures. The case when $d = 2$ can be proved by applying Lemma 6.1 and Corollary 6.5 of [14] to all legs. ■

Proposition 1 and the fact that ${}^dU_i$ is a simply connected set, reveal that each component of $f^{-1}({}^dU_i)$ is a direct product of one component of $\tilde{\mathcal{C}}_j(p)$, $j = 1, \cdots, k$, with a d-dimensional disk. Using $|\mathcal{L}_j^*(p)|$, $j = 1, \cdots, k$ and Lemma 1, one can show that the number of components of $f^{-1}({}^dU_i)$ is 2^{k_0}, where $k_0 \leq k$ is the number of legs for which $|\mathcal{L}_j^*(p)| = 3$.

Local Path Existence

Before considering the global path existence problem, consider motion planning between two valid configurations $c_{[init]}$ and $c_{[goal]}$ for which the junction A lies in the same chamber. Since the fibre over every point in ${}^dU_i$ is equivalent, path existence amounts to checking the component memberships of the configurations $c_{[init]}$ and $c_{[goal]}$.

For a single leg $\tilde{M}_j(p)$, if the number of long links $|\mathcal{L}_j^*(p)|$ is not three, then any two configurations of $\tilde{M}_j(p)$ are in the same component. When $|\mathcal{L}_j^*(p)| = 3$, choose any two long links and test the sign of the angle between them (with full extension taken as zero). There are two possible signs, one corresponding to *elbow-up* and the other to *elbow-down*. If for two distinct configurations of $\tilde{M}_j$, A lies in the same chamber, there is a continuous motion between them while keeping A in this chamber, if and only if the elbow sign is the same at both configurations (naturally, one must perform the sign test with the same two links and in the same order for both configurations). Considering all the legs together, a continuous motion of A in ${}^dU_i$ exists if and only if a motion exists for each leg individually. The previous discussion serves to prove the following result.

Proposition. 2. Restricted to $f^{-1}({}^d U_i)$, two configurations $c_1, c_2 \in f^{-1}({}^d U_i)$ are path connected if and only if for each leg $\tilde{M}_j$ with $|\mathcal{L}_j^*| = 3$ in ${}^d U_i$, the elbow angle of $\tilde{M}_j$ has the same sign at c_1 and c_2.

Proposition 2 completely solves the path existence problem if W_A consists of a single chamber. However, things become complex when W_A has more than one chamber.

Singular Set and Global configuration space Analysis

Recall that the configuration space $\mathcal{C}$ is a union of $f^{-1}({}^d U_i)$, $d \in \{0, 1, 2\}$, $i = 1, \cdots, {}^d m$ and that $f^{-1}(p)$, $p \in {}^d U_i$ for $d \neq 2$ and all i is a set containing at least a singularity of f. Combining the local configuration space and singular set analysis yields the global structure of configuration space.

Proposition. 3. For all $p \in \Sigma_j$, $f_j^{-1}(p)$ is a singular set containing isolated singularities. If a singularity separates its neighborhood V in $f_j^{-1}(p)$, then it is these singularities which glue the two separated components in $f_j^{-1}(q)$ where $q \in W_A - \Sigma_j$ is a point sufficiently close to p.

Proof: First it is obvious that $f_j^{-1}(p)$ contains isolated singularities for there are finite ways to colinearize all the links of a close chain. Second, let

$$\gamma : (-\varepsilon, \varepsilon) \to W_A,\ \gamma(0) = p$$

be a curve that is transverse to Σ_j. According to Corollary 6.6 of [14], the distance function $s(\gamma(t)) = \int_0^t |\dot{\gamma}| dt$ defines a Morse function on $f_j^{-1}(\gamma)$

$$s \circ f_j : f_j^{-1}(\gamma) \to \mathbb{R}.$$

Note that 0 is a singular value of $s \circ f_j$ and the isolated singularities of $f_j^{-1}(p)$ are also singularities of $s \circ f_j$. The result of Morse theory applying to $s \circ f_j$ yields that $(s \circ f_j)^{-1}(0) = f_j^{-1}(p)$ is given by attaching a handle to $(s \circ f_j)^{-1}(\varepsilon_0) = f_j^{-1}(q)$ for a sufficiently small ε_0 and q a point sufficiently close to p. The Proposition follows. ■

Next, we establish necessary and sufficient conditions for the connectivity of $\mathcal{C}$. Let J be the index set such that for all $j \in J$, $|\mathcal{L}_j^*| = 3$ for at least one chamber ${}^dU_i$. We prove the following theorem.

Theorem 1. Suppose $W_A = \bigcup_{d=0}^{2} \left(\bigcup_{i=1}^{d_m} {}^dU_i \right)$. Then $\mathcal{C} = f^{-1}(W_A)$ is connected if and only if:

1. W_A is connected;

2. $\Sigma_j \bigcap W_A \neq \emptyset$ for all $j \in J$.

Proof: (i) "Necessity:" Since $\mathcal{C}$ is a fibration of the base manifold W_A, it can have one component only when W_A has one component. Thus item 1 of Theorem 1 is required. Second, in order that $\mathcal{C}$ be connected, for each leg M_j restricted to W_A, the configuration space $\tilde{\mathcal{C}}_j(W_A) = f_j^{-1}(W_A)$ must be connected. By definition, for all $j \in J$, there exists a chamber ${}^dU_i$ such that $|\mathcal{L}_j^*| = 3$. The result of Proposition 3 means that $\tilde{\mathcal{C}}_j(W_A)$ is connected only if $W_A \bigcap \Sigma_j \neq \emptyset$.

(ii) "Sufficiency:" Item 1 and 2 imply that $\tilde{\mathcal{C}}_j(W_A)$ are path connected for all j. Moreover, $\mathcal{C}$ is a fibration over W_A. The result follows. ■

Fig. 2.3.3 illustrates the global connectivity for an example W_A corresponding to a star-shaped manipulator with two legs and a workspace for which there are two chambers ${}^2U_1$ and ${}^2U_3$ where leg 1 has three long links and another chamber ${}^2U_4$ where both legs have three long links. Among these chambers, ${}^1U_1$ and ${}^1U_2$ belong to Σ_1, and ${}^1U_3$ belongs to Σ_2. According to Theorem 1, the configuration space is path connected. In this example, the $\mathcal{C}$ is the product of the two structures shown.

Corollary 1. Two configurations c_1 and c_2 of a star-shaped manipulator are in the same component if and only if

1. $f(c_1)$ and $f(c_2)$ are in the same component of W_A;

2. For each leg j with $|\mathcal{L}_j^*| = 3$ for all chambers ${}^dU_i$ in the component of W_A which contains $f(c_1)$ and $f(c_2)$, the elbow sign is same at both c_1 and c_2.

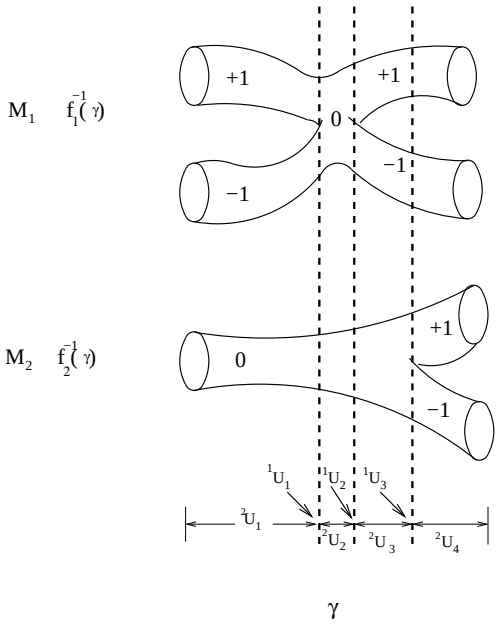

Figure 2.3.3: configuration space of a star-shape manipulator with two legs. For simplicity, only the portion of $f^{-1}(\gamma)$ is shown, where γ is a continuous curve in W_A that visits all chambers.

Remark 1. As a matter of fact, Σ completely determines the connectivity of configuration space. When computing a path between two given configurations, often motions of the junction to points on Σ are incorporated to allow adjustment of leg-angle signs. However, inevitable deviations of the junction from Σ caused by numerical errors, make it impossible to adjust the sign of legs while fixing its end point. For these reasons, points in 2D chambers are preferred for sign adjustment.

2.4 A Polynomial-Time, Exact, Complete Algorithm

Our algorithm consists of two main routines, `PathExists` and `ConstructPath`. `PathExists` solves the path existence problem, i.e., determining if an initial and an goal configuration are path-connected, and `ConstructPath` constructs a path between them if there exists a path.

Notice that the configuration space of a star-shaped manipulator could be very complex. Even the simple planar five-link single-loop closed chain, its configuration space could be as complex as the connected sum of four torii [14]. So determining the path existence without using the configuration space information is difficult. Our strategy is to solve the path existence based on the set of critical circles Σ_j in the workspace, and then construct the path combining our knowledge of the workspace and the structure of the configuration space of single-loop closed chains. We emphasize here that the problem is not just moving the junction point between an initial and a goal position, but moving the manipulator along with all its legs from an initial configuration to a goal configuration. So, the workspace information will be insufficient for path construction. In `ConstructPath`, we employ a move that changes the shape of a leg with its endpoint fixed in the workspace. This move, called the sign-adjust move, uses the knowledge of the configuration space of a single-loop closed chain. Below we will show that the overall complexity of `PathExists` and `ConstructPath` is $O(k^3N^3)$, where N is the maximum number of links in a leg and k is the number of legs. The polynomial complexity is key to the applications like folding of macromolecules, which can can be modeled as a closed chain with large k and N.

The logical flow of `PathExists` is illustrated in Figure 2.4.1. Its input is the topology and link lengths of a star-shaped manipulator and two valid configurations, $c_{[init]}$ and $c_{[goal]}$. The output is the answer to the path existence question. The approach taken is to compute W_A and then, for each leg with its end point constrained to lie in W_A, to determine if its initial and goal configurations are path connected. Notice that W_j is either a disk or an annular region, W_A can be constructed by calculating the intersections between no more than $2n$ circles. So constructing W_A is polynomial-complex. The most difficult issue is to check the path existence. Since the configuration space of a leg is guaranteed to be connected if one of its critical circles Σ_j intersects W_A, the most straight forward way to test connectivity is to explicitly perform the intersections. However, since there are as many as 2^{n_j-1} critical circles, any algorithm based on this approach will have worst-case complexity that is at least

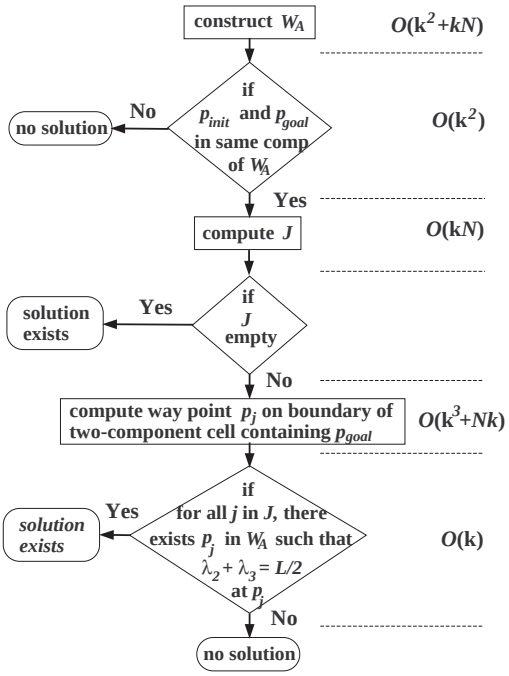

Figure 2.4.1: Logical flow and complexity of the major steps of `PathExists`.

exponential in N. The key contribution of `PathExists` is a polynomial-time algorithm for checking the existence of an intersection between W_A and a critical circles - even though there is an exponential number of these circles. Recall that if a leg has three long links, then it is impossible to move the leg so that the three long links change from an elbow-up configuration to an elbow-down configuration. The following algorithm constructs a novel polynomial-complex method that can determine if there is point in W_A in which the number of long links of a leg is not 3 (see Step 4 in `PathExists`).

1. Construct W_A We compute W_A in three steps.

Step 1: Compute the boundary circles of W_j. In general, W_j is an annulus. The radius of its outer boundary circle is $r_{[max]} = \sum_{i=1}^{n_j} l_{j,i}$, while that of its inner boundary circle, $r_{[min]}$, can be determined by comparing $l_{[max]} := \max_i l_{j,i}$ and $r_{[max]} - l_{[max]}$.

If $l_{[max]} > r_{[max]} - l_{[max]}$, then $r_{[min]} = 2l_{[max]} - r_{[max]}$, else, $r_{[min]} = 0$;

Step 2: Decompose the whole plane into cells using all boundary circles of all legs (e.g., the line sweeping algorithm can do this), and construct the cell adjacency graph;

Step 3: Pick a point from the interior of each cell, compute its distance from each base point, and compare the distance with the radii of the two boundary circles of W_j. The set of cells which can be reached by all legs constitute W_A.
The complexity of this 2-D cell decomposition algorithm is $O(k^2 + kN)$.

2. Are $p_{[init]}$ and $p_{[goal]}$ in same component of W_A? As an immediate consequence of the cell decomposition, this can be answered directly by searching the cell graph.

3. Compute J This step is used to filter out easy solution existence checks, based on the cardinality and members of the sets $\mathcal{L}_j^*(p_{[init]})$ and $\mathcal{L}_j^*(p_{[goal]})$. For each leg $\tilde{M}_j(p_{[init]})$, compute L_j (see Section III) and find the three longest links of the set $\{l_{j,0}, ..., l_{j_{n_j}}\}$. Denote these links by $(p_{[init]}; \lambda_{j,1}, \lambda_{j,2}, \lambda_{j,3})$. Do the same for $(p_{[goal]})$ and define $(p_{[goal]}; \lambda_{j,1}, \lambda_{j,2}, \lambda_{j,3})$. This requires $O(N)$ work. Finally, $|\mathcal{L}_j^*(p_{(\cdot)})| = 3$ if and only if $\lambda_{j,2} + \lambda_{j,3} > L_j/2$. If $\mathcal{L}_j^*(p_{[init]}) = \mathcal{L}_j^*(p_{[goal]})$ and $|\mathcal{L}_j^*(p_{[init]})| = 3$, and if the signs of the long links are different at $c_{[init]}$ and $c_{[goal]}$, then add j into J. Computing J is $O(kN)$.

4. Does the set of long links vary for all $j \in J$? If and only if $q \in W_A$ exists such that $\mathcal{L}_j^*(q) \neq \mathcal{L}_j^*(p_{[init]})$, then it is possible to make the long links colinear and thus change the signs of their relative angles. This can be done by computing a point $q \in W_A$ on the boundary of the cell that contains $p_{[goal]}$ and keeps the same set $\mathcal{L}_j^*(p)$ for all p in this cell. This boundary is characterized by $\lambda_{j,2} + \lambda_{j,3} = L_j/2$. Since $l_{j,0}$ is the only link whose length varies along with p, this boundary must be one or two circles (called inner and outer circles, respectively) whose radii, denoted $d_{[max]}$ and $d_{[min]}$, depend on the link lengths of the leg. Let $L_{j,0} = \sum_{i=1}^{n_j} l_{j,i}$ and suppose the four longest links at $p_{[goal]}$ are $(\lambda_{j,1} > \lambda_{j,2} > \lambda_{j,3} > \lambda_{j,4})$ with $\lambda_{j,2} + \lambda_{j,3} > L_j/2$, we deduce the radii of the boundary circles for four different cases:
Case 1: if $l_{j,0}(p_{[goal]}) = \lambda_{j,1}$, then $d_{[max]} = 2(\lambda_{j,2} + \lambda_{j,3}) - L_{j,0}$, and $d_{[min]} = \max\{L_{j,0} - 2\lambda_{j,3}, 2(\lambda_{j,3} + \lambda_{j,4}) - L_{j,0}\}$.
Case 2: if $l_{j,0}(p_{[goal]}) = \lambda_{j,2}$, $d_{[max]} = 2(\lambda_{j,1} + \lambda_{j,3}) - L_{j,0}$, and $d_{[min]} = \max\{L_{j,0} - 2\lambda_{j,3}, 2(\lambda_{j,3} + \lambda_{j,4}) - L_{j,0}\}$.

Case 3: if $l_{j,0}(p_{[goal]}) = \lambda_{j,3}$, $d_{[max]} = 2(\lambda_{j,1} + \lambda_{j,2}) - L_{j,0}$, and $d_{[min]} = \max\{L_{j,0} - 2\lambda_{j,2}, 2(\lambda_{j,2} + \lambda_{j,4}) - L_{j,0}\}$.
Case 4: Otherwise, $d_{[max]} = \min\{2(\lambda_{j,2} + \lambda_{j,3}) - L_{j,0}, L_{j,0} - 2\lambda_{j,2}\}$, and $d_{[min]} = 0$.
If there is no overlap between the two boundary circles and the component of W_A that contains $p_{[init]}$ and $p_{[goal]}$, then no path exists between $c_{[init]}$ and $c_{[goal]}$. Otherwise, path exists and we obtain way points p_j for all legs $j \in J$. Computing $d_{[max]}$, $d_{[min]}$, and the way points p_j is $O(kN)$.

The basic idea of `ConstructPath` is that when moving from $c_{[init]}$ to $c_{[goal]}$, those legs $j \in J$ may require a change in the signs of relative angles between long links, which is always possible at the way point p_j or other critical points of the corresponding leg. A natural approach then is to use two motion generation primitives: *accordion move* and *sign-adjust move*. The former moves the thorax endpoint (at A) along a specified path segment with all legs moving compliantly so that all loop closures are maintained. The latter keeps the endpoint fixed at a way point $q_j \in \Sigma_j$ (e.g., $q_j = p_j$ or other critical points) while moving leg j into a singular configuration and then to a nearby configuration with the sign of the relative angle between a pair of long links in this leg chosen to match those of $c_{[goal]}$.

Note that though the guard points q_j are in the critical set Σ_j, the configuration at which leg j approaches these points need not to be aligned. Without considering the control issue, a leg can be moved to a colinear configuration with the thorax fixed. Even if control is considered for the sign-adjust move, the thorax can still be maintained to be fixed by keeping all other legs not aligned in the vicinity of q_j.

The input of `ConstructPath` is W_A and its cell graph, $c_{[init]}$, $c_{[goal]}$, and the set of way points $p_j \in W_A$, $j \in J$ computed during the execution of `PathExist`.
1. Construct an initial path `ConstructPath` explores the cell graph of W_A, and constructs a path in W_A connecting $p_{[init]}$ to $p_{[goal]}$ and visiting all of the way points. Since there are at most k way points, this can be done in $O(k^3)$ time (the path has $k+1$ segments each with $O(k^2)$ arcs).

2. Construct *guards* and insert the guards into the path Notice that when one accordion moves a leg in a cell in which the number of long links is not 3 (called one-component cell), neither the signs of concatenating angles, nor the sign between any pair of links in this leg will be kept invariant. Thus even if the desired sign between a pair of long links is adjusted at a way point, it still could change if the leg keeps moving in a one-component cell. For this reason, we set *guards* for legs which have three long links at $p_{[goal]}$. These are the set of points q_j, each of which is the last intersection point between the above constructed path in W_A and the boundary of the two-component cell of leg j containing $p_{[goal]}$. Thus the number of guards (q_j's) may be more than the number of way points since the number of legs that have three long links at $p_{[goal]}$ may be more than the cardinality of J. Next the *guards* are inserted into the path. Later when we construct the path in $\mathcal{C}$, sign-adjust moves are only performed at *guards* q_j (but not p_j) for after that the thorax endpoint gets into the two-component cell and the sign between a pair of long links will not change during accordion moves, i.e., the leg will always remain in the right component of its configuration space. Assuming each arc in the path is approximated by a fixed number of line segments, finding guards is $O(k^3)$.

3. Accordion moves and sign-adjust moves The path in $\mathcal{C}$ then is produced by using accordion moves along the path and sign-adjust moves at the *guards*. At each *guard*, one checks the sign between a pair of long links of the corresponding leg. If it does not match the goal one, then the junction point is fixed while a sign-adjust move is executed, otherwise, the accordion move continues. Once A is coincident with $p_{[goal]}$, one is assured by the previous steps, that with A fixed at $p_{[goal]}$, the configuration of each leg is in the same component of its current configuration space $\tilde{C}_j(p_{[goal]})$ as $c_{[goal]}$. The final move can be accomplished using a special accordion move algorithm found in [14]. At this stage, we remark that finding the set of way points p_j and planning an initial path visiting all p_j is necessary for otherwise, an arbitrary path between $p_{[init]}$ and $p_{[goal]}$ may not intersect the boundary of the two-component cell of a leg that contains $p_{[goal]}$.

The complexity of the accordion move algorithms reported in [15] are $O(N^3)$. Since the path has $O(k^3)$ line segments the complexity of `ConstructPath` is $O(k^3N^3)$. Note that accordion move algorithms with the required behavior can be designed to be $O(N^2)$, so the complexity of `ConstructPath` could be reduced.

Overall, our path planning algorithm is $O(k^3N^3)$.

2.5 Path Optimization and Robustness

If a path between two given configurations exists, it is obvious that in our algorithm the choice of way points, and thus the path between the two configurations, is not unique. So a natural problem is path optimization with respect to meaningful metrics such as path length and singularity avoidance. Basically we say that many possible optimization objectives are potentially useful, but we consider the shortest path in this section. Notice that the way points are necessary for successively constructing a path from $c_{[init]}$ to $c_{[goal]}$ since an arbitrary chosen path of the thorax from $p_{[init]}$ to $p_{[goal]}$ (like the line connecting them) will either go out of W_A, or have no intersection with the critical set Σ_j, in which a sign-adjust move is required for a leg. Thus the optimization problem arises in the choice of way points, the order of the way points, and the path between two consecutive way points.

One may also take into consideration parallel singularities (cf. [43]) and try to avoid them as much as possible by minimizing the number of singularities crossings. More precisely this may be done for example by first clustering singularity regions (see [44]) and then choosing way points with the corresponding path having minimum number of crossings of these regions, finally their connecting path or trajectories (i.e. a path with temporal relations as well as the geometrical ones) should be chosen in the proper way (cf. [45]).

Since $\mathcal{C}$ is a fibration over W_A, a meaningful metric for $\mathcal{C}$ is

$$ds^2 = a_1 dp^T dp + a_2 \sum_{j=1^k} du_j^T V_j^T V_j du_j,\ a_1, a_2 > 0, \tag{2.5.1}$$

where a_1 and a_2 are two weights assigned to $dp^T dp$ and $\sum_{j=1^k} du_j^T V_j^T V_j du_j$, respectively for they are quantities with different physical meaning. The column vectors of $V_j \in \mathbb{R}^{n_j \times (n_j - 2)}$ forms a basis for the null space of the Jacobian $J_j = \frac{\partial f_j}{\partial \Theta_j}$ of leg j, i.e.,

$$J_j V_j = 0.$$

du_j denotes the incremental changes of the local coordinates on $\tilde{\mathcal{C}}_j(p)$. dp and $V_j du_j$ stands for the infinitesimal motion along the base manifold and the fibre, respectively. The shortest path problem is to find a path $(p(t), \Theta_1(t), \cdots, \Theta_k(t))$ such that

$$\int_{t=0}^{1} ds \tag{2.5.2}$$

is minimal. The optimal solution to (2.5.2) satisfies the geodesic equation

$$\ddot{v}_k + \Gamma_{ij}^k \dot{v}_i \dot{v}_j = 0 \tag{2.5.3}$$

where $v = [p^T, u_1^T, \cdots, u_k^T]^T$, and Γ_{ij}^k denotes the Christoffel symbol of the metric (2.5.1). Solving (2.5.3) exactly is difficult. However, an approximation solution can be derived. Since a path from $c_{[init]}$ to $c_{[goal]}$ is globally optimal if and only if this path is also locally optimal, we construct an approximate shortest path in a way so that (i) $p(t)$ connects $p_{[init]}$ and $p_{[goal]}$ and visits all p_i. Moreover, $\int_{t=0}^{1} \sqrt{dp^T dp}$ is minimal; (ii) There is minimal number of accordion moves, and each accordion move is minimal; (iii) Except for the accordion moves, there is no other motions along the fibre.

Remark 2. The path constructed in this way is shortest if no accordion moves are needed for we always achieve minimal $ds = \sqrt{a_1 dp^T dp}$ infinitesimally, while it is only an approximation if there is at least one accordion move.

Mathematically, this problem can be described as

$$\begin{gathered} \min \int_0^1 \|dp\| \\ p(t) \in W_A, \forall t \in [0,1] \\ p_i \in \{p(t)\}, \forall i \\ p_i \in \mathcal{A}_{\delta(i)} \end{gathered}$$

where $\mathcal{A}_j, j \in J$ is the boundary arcs of the two-component cell of leg j that contains $p_{[goal]}$. $\delta(J)$ is a permutation of J with $\delta(J) = J$. Solving this problem exactly is extremely hard, but a random search method (for example, the Controlled Random Search Method [46]) can be used to quickly find a good approximate solution. Using the minimal number of accordion moves has been solved in `ConstructPath`, and the minimal accordion move problem has been solved in [14]. Combining these two, (ii) is solved.

To solve (iii), we notice that for a local motion $dp = [dx, dy]$ of the thorax endpoint, $d\Theta_j^T d\Theta_j$ is minimized if and only if.

$$d\Theta_j = J_j^+ dp$$

where $J_j^+ = J_j^T (J_j J_j^T)^{-1}$.

Another important issue about our planning algorithm is robustness. The sign-adjust move of leg j performed at a guard q_j is only feasible when $\mathcal{C}_j(q_j)$ is connected. Since $q_j \in \Sigma_j$ which is only 1-D, a small perturbation of the junction point in W_A (e.g., due to numerical errors) will violate the condition $p \in \Sigma_j$. When p moves into a two-component cell, then the sign-adjust move may fail. A remedy to this is to modify the path of the thorax in the neighborhood of $q_j \in \Sigma_j$ so that a point q_j' in the interior of a one-component cell is reached. After the sign of leg j is adjusted to the desired one with p fixing at q_j', we apply a constrained accordion move algorithm to ensure that the leg j stays in the right component of $\mathcal{C}_j(p)$ just before its thorax endpoint enters the two-component cell containing $p_{[goal]}$. This resulting algorithm will also be robust to other errors such as the control and sensor errors if they are taken into account.

2.6 Examples

In this section, we demonstrate the correctness and complexity of our algorithm through two examples: a manipulator with three three-link legs, and a manipulator with three five-link legs. Movies of the motion plans are very helpful in understanding

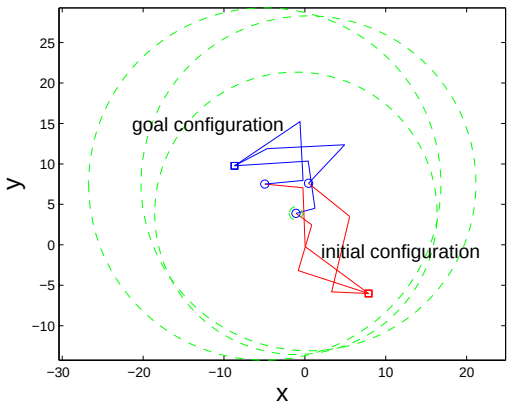

Figure 2.6.1: Manipulator's initial configuration (junction on the right, drawn red) and goal configuration (junction just below the top left, drawn blue.) The boundary circles of W_j are drawn as dashed green lines.

the figures. They can be found at `http://www.cs.rpi.edu/~trink/ccwo.html`.

In the first example, two of the three legs of the manipulator have three long links when A is fixed at $p_{[goal]}$. Figure 2.6.1 shows the manipulator in its starting and goal configurations. Our algorithm predicts $J = \emptyset$.

Then the algorithm constructs a path in W_A from $p_{[init]}$ to $p_{[goal]}$, drawn as the dark solid lines in Fig. 2.6.2. This path intersects

the boundary of the two-component annular region of leg j that contains

$p_{[goal]}$ several times, among which q_j, $j = 1, 2$ are the last ones. These two points are the guards (drawn as diamonds) where sign-adjust moves are performed.

At q_j, $j = 1, 2$, we check the sign of a pair of long links of leg j and see if it matches its sign at the goal. If not, we fix the other two legs and adjust the sign of the chosen long links in leg j. In this particular example, we chose the two longest links as the pair of long links,and we find that at q_1 the sign of leg 1 does not match that at the goal (while at q_2, leg 2 has the same sign as the goal). Before leaving q_j via the next accordion move, the pair of long links of leg j was moved to the elbow-opposite configuration (recall that there are two configurations for these two links,

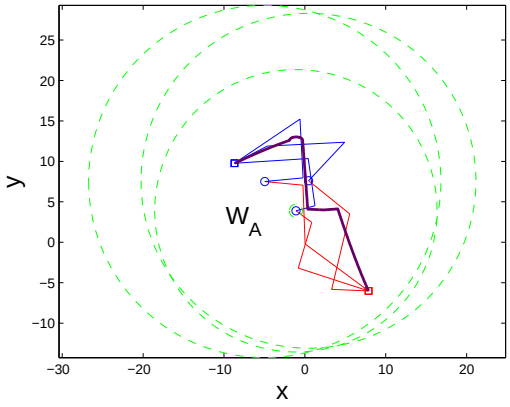

Figure 2.6.2: A path between $p_{[init]}$ and $p_{[goal]}$ that is completely contained in W_A.

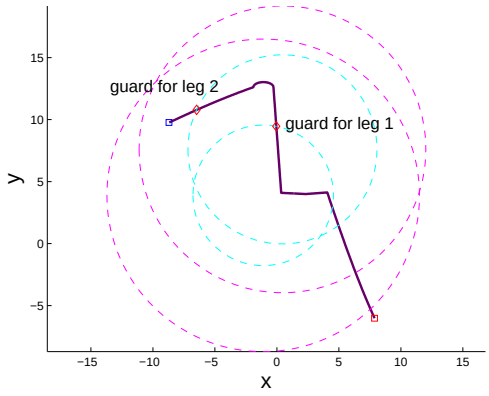

Figure 2.6.3: The two guard points are the last intersection points between the path of A and the boundary circles of two two-component cells.

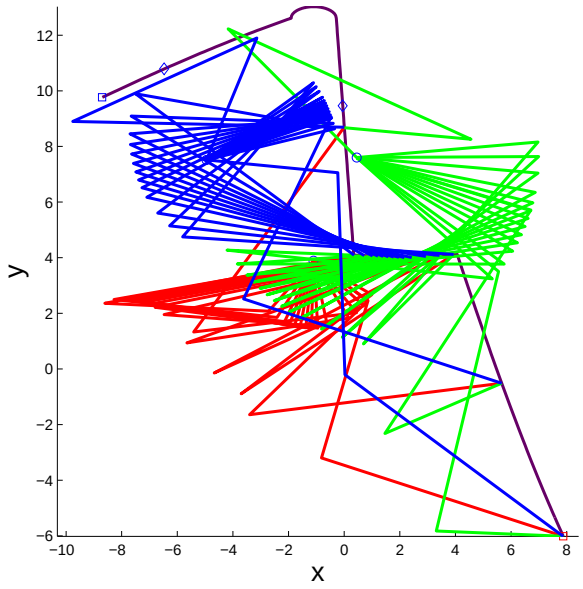

Figure 2.6.4: All legs use an accordion move to move the junction A to the first guard q_1 of leg 1.

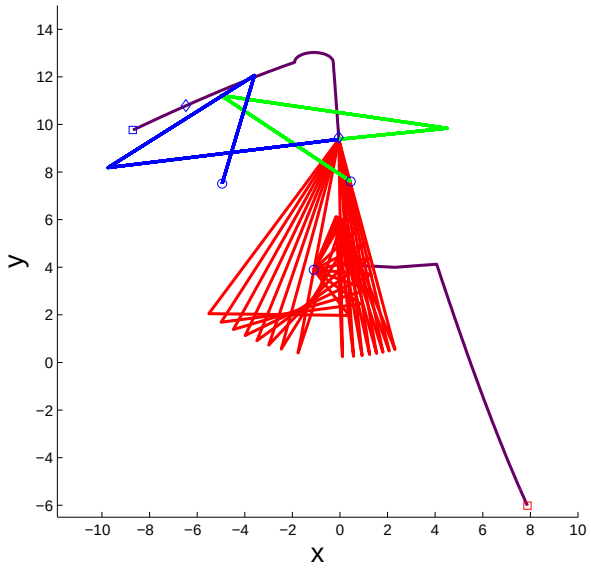

Figure 2.6.5: With the junction A at q_1, the joint angles of leg 1 can be adjusted to achieve the signs required at the goal configuration. All other legs are fixed in place.

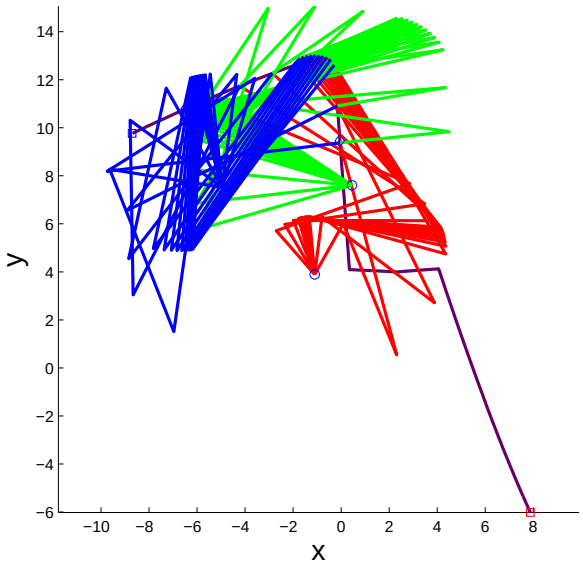

Figure 2.6.6: All legs use an accordion move to move the junction A to the second guard q_2 of leg 2.

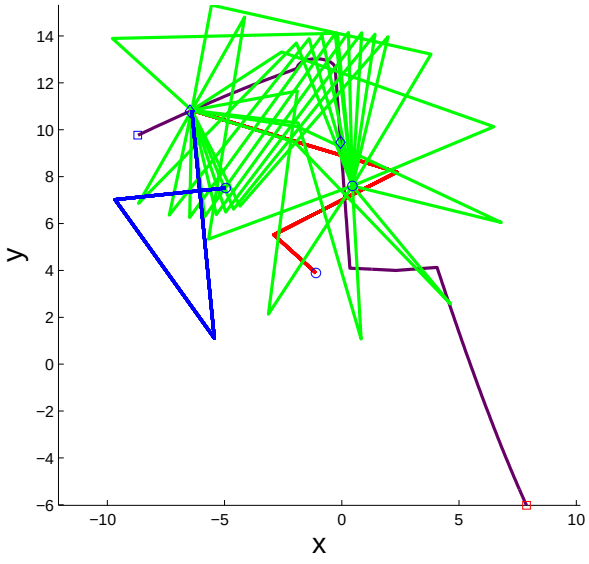

Figure 2.6.7: With the junction A at q_2, the joint angles of leg 2 can be adjusted to achieve the signs required at the goal configuration. All other legs are fixed in place.

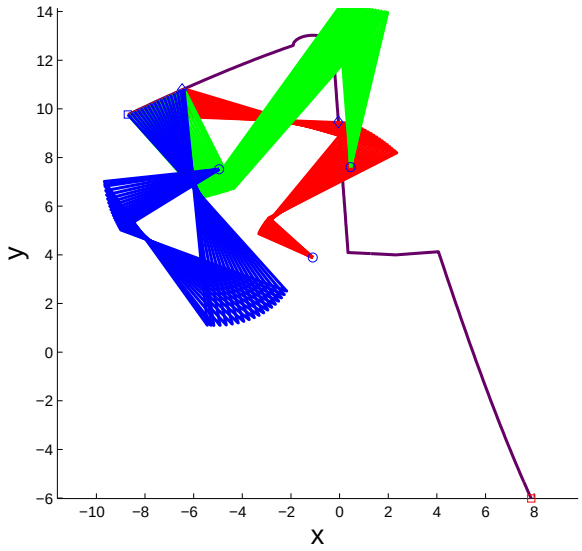

Figure 2.6.8: All legs use an accordion move to move the junction A to its goal location. The signs of the joint angles are preserved guaranteeing that legs 1 and 2 will be in the correct configuration space component once A is fixed at the goal position.

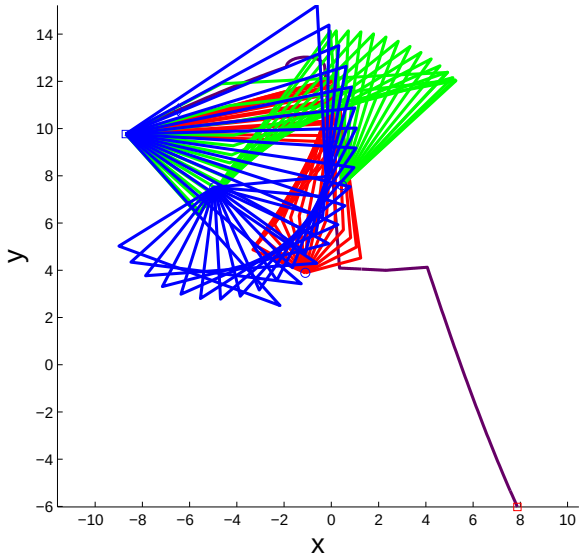

Figure 2.6.9: All legs use the Trinkle-Milgram algorithm to achieve their goal configurations with the junction A fixed.

one is "elbow up", the other is "elbow down"), which has exactly the same sign as the goal configuration. The Trinkle-Milgram algorithm [15] is used to plan such a motion between the two elbow-opposite configurations. Figures 2.6.4 - 2.6.9 show the progress of the manipulation plan as the steps of the complete planning algorithm are carried out.

A bit more complex example in which the star-shaped manipulator has three five-link legs is shown in `http://www.cs.rpi.edu/~trink/ccwo.html`. The computation time for path existence for star-shaped manipulators with less than 10 legs, and legs of less than 10 links is typically from less than 1 second to a few seconds when run in a Matlab, P4, WindowsXP system.

2.7 Discussion

Star-shaped manipulators are closed chain manipulators subject to multiple loop closure constraints. The configuration space of these manipulators is often a lower-dimensional submanifold with high genus [2] embedded in the ambient space. Computing the silhouette of this manifold requires solving the extreme points of the manifold either in the ambient space whose dimension is much higher than that of the manifold itself, or in a set of local neighborhoods (local coordinate charts) whose number grows exponentially along with the genus of the submanifold. Although Canny's algorithm is very efficient in general, there is difficulty in implementation for star-shaped manipulators. Second, the classical cylindrical decomposition of configuration space (e.g. collin's decomposition) is a partition into simple connected subsets of configuration space called cells. However, this algorithm requires a description of the configuration space in terms of a set of polynomials over its ambient space. Again because the dimension of the ambient space could be very high, the computation time of this algorithm could become formidable.

Our algorithm employs the special structural properties (fibration over the workspace)

[2] The genus of a surface is defined as the largest number of nonintersecting simple closed curves that can be drawn on the surface without separating it.

of the configuration space of star-shaped manipulators. It avoids using the coordinates of the ambient space as well as the local coordinate charts that covers the configuration space. In our algorithm the path existence and path construction are solved in polynomial time by combining the cell decomposition of the workspace (which is two dimensional and with simple shape) and the structure of the configuration space of single-loop closed chains. The critical set Σ_j, which marks the change of the topology of the configuration space of each leg, plays a key role in this algorithm.

2.8 Conclusion

In this paper, we studied the global structural properties of planar star-shaped manipulators. Via the analysis of the critical set Σ, we derived the global connectivity of the configuration space, and necessary and sufficient conditions for path existence. Based on these results, we devised a complete polynomial algorithm for motion planning. Simulation examples were used to illustrate the key ideas behind the motion planning problem of planar star-shaped manipulators.

Chapter 3

The configuration space of a parallel polygonal mechanism

Submitted to *Homology Homotopy and Applications*, 2007.
Co-authors: David Blanc and Moshe Shoham.

We study the configuration space $\mathcal{C}$ of a parallel polygonal mechanism, and give necessary conditions for the existence of singularities; this shows that generically $\mathcal{C}$ is a smooth manifold. In the planar case, we construct an explicit Morse function on $\mathcal{C}$, and show how geometric information about the mechanism can be used to identify the critical points.

3.1 Introduction

The mathematical theory of robotics is based on the notion of a mechanism, consisting of links, joints, and rigid parts known as platforms. The *type* of a mechanism is defined by a q-dimensional polyhedral complex, where the parts of dimension ≥ 2 correspond to the platforms, and the complementary one-dimensional graph corresponds to the links and joints. Here we consider only the polygonal case $(q = 2)$. A specific embedding of this complex in the ambient Euclidean space $\mathbb{R}^d$ is called a *configuration*

of the mechanism. The collection of all such embeddings forms a topological space, called the *configuration space* of the mechanism (see [Hal]).

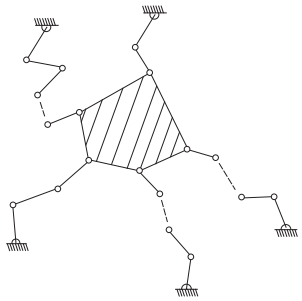

Figure 3.1.1: A pentagonal planar mechanism

The goal of this note is to study the configuration space of a mechanism consisting of a moving polygonal platform, having a flexible leg (consisting of concatenated rods) attached to each vertex, with the other end fixed in $\mathbb{R}^d$. We may think of the latter as forming the *fixed polygon* of the mechanism, "parallel" to the *moving polygon* inside. The spatial version of such a mechanism, consisting of a two-dimensional platform free to move in three dimensions, has been studied extensively, but even the planar version, to which we later specialize, has practical applications – for example, in micro-electro-mechanical systems (MEMS).

Our main results are:

(a) The configuration space of a parallel polygonal mechanism is a smooth manifold, except perhaps in some explicitly described singular cases (Theorem 3.2.2).

(b) The topology of this manifold can be described for a triangular planar mechanism by means of an explicit Morse function (Theorem 3.3.1), whose critical points can be identified geometrically (§3.3.2).

We start with some terminology and notation:

Definition 3.1.1. A *branch* (of *multiplicity* n) is a sequence $L = (\ell_1, \ldots, \ell_n)$ of n positive numbers, which we think of as the lengths of n concatenated rods, having revolute (i.e., rotational) joints at the consecutive meeting points.

Definition 3.1.2. A *configuration* in $\mathbb{R}^d$ for a branch $L = (\ell_1, \ldots, \ell_n)$ consists of n vectors $V = (\mathbf{v}_1, \ldots, \mathbf{v}_n)$ in $\mathbb{R}^d$ with lengths $\|\mathbf{v}_i\| = \ell_i$ $(i = 1, \ldots n)$. We write $\sigma_V := \sum_{i=1}^n \mathbf{v}_i$ for their vector sum.

A branch configuration $V = (\mathbf{v}_1, \ldots, \mathbf{v}_n)$ is *aligned* with a vector $\mathbf{v} \in \mathbb{R}^d$ if all the vectors $\mathbf{v}_i$ are scalar multiples of $\mathbf{v}$, which is called the *direction vector* of V.

The *configuration space* $\mathcal{C}(L)$ of a branch L is the product of n spheres in $\mathbb{R}^d$ of radii $(R_i = \ell_i)_{i=1}^n$. Up to homeomorphism, this is independent of the order on L, so we can (and shall) assume $\ell_1, \ldots, \ell_n$ to be in descending order.

Definition 3.1.3. A *polygonal mechanism* $(\mathcal{L}, \mathcal{X}, \mathcal{P})$ in $\mathbb{R}^d$ consists of:

(a) k branches $\mathcal{L} = \{L^{(i)}\}_{i=1}^k$ of multiplicity $\{n^{(i)}\}_{i=1}^k$, respectively;

(b) k distinct *base points* $\mathcal{X} = \{\mathbf{x}^{(i)}\}_{i=1}^k$ in $\mathbb{R}^d$, to which the initial points of the corresponding branches are attached.

(c) An abstract k-polygon $\mathcal{P}$ in $\mathbb{R}^d$.

Think of this mechanism as a linkage of k branches, starting at the base points (which form a polygon (not necessarily planar) in $\mathbb{R}^d$, called the *fixed platform*), and ending at the vertices of a rigid planar polygon congruent to $\mathcal{P}$, called the *moving platform* of the mechanism. There are revolute joints at both ends of each branch, too.

We use parenthesized superscripts to indicate the branch number, and plain subscripts to indicate the rod number – e.g., $\ell_j^{(i)}$ denotes the length of the j-th rod of the i-th branch.

Remark 3.1.4. Observe that a planar polygon $\mathcal{P}$ in $\mathbb{R}^d$ $(d > 2)$ with vertices $\mathbf{p}^{(1)}, \ldots, \mathbf{p}^{(k)}$ is determined up to isometry by the sequence of triangles $\triangle(\mathbf{p}^{(i)}, \mathbf{p}^{(i+1)}, \mathbf{p}^{(i+2)})$ and $\triangle(\mathbf{p}^{(i)}, \mathbf{p}^{(i+1)}, \mathbf{p}^{(i+3)})$, which are determined in turn by the lengths of their sides $\mathcal{G} := (g^{(i,j)})_{(i,j)\in\mathcal{I}}$. Here $g^{(i,j)} := \|\mathbf{p}^{(i)} - \mathbf{p}^{(j)}\|$, and the index set $\mathcal{I}$ consists of the $3k - 6$ ordered pairs:

$$(1,2), (1,3), (2,3), (1,4), (2,4), (3,4), \ldots, (k-3,k), (k-2,k), (k-1,k)$$

(in this order). Note that these diagonals force $\mathcal{P}$ to be planar, since if we assume that the polygon is contained in the affine plane $\mathcal{E}$ determined by the first three vertices in $\mathbb{R}^d$, then $\mathcal{P}$ is constructed inductively by adding one vertex at a time to an existing edge to form a new triangle.

When $d = 2$, the $2k - 3$ pairs:

$$\mathcal{I} = \{(1,2), (1,3), (2,3), (2,4), (3,4), \ldots, (k-2,k-1), (k-1,k)\}$$

suffice to determine $\mathcal{P}$ completely, if it is convex; otherwise, the only additional data needed is the discrete information as to which half-plane the new vertex is to be placed in.

Definition 3.1.5. A *configuration* for a polygonal mechanism $(\mathcal{L}, \mathcal{X}, \mathcal{P})$ in $\mathbb{R}^d$ consists of a set $\mathcal{V} = (V^{(1)}, \ldots, V^{(k)})$ of k branch configurations for $\mathcal{L}$ (Definition 3.1.2), satisfying the condition that the endpoints $\mathbf{p}^{(i)} := \mathbf{x}^{(i)} + \sigma_{V^{(i)}}$ $(i = 1, \ldots, k)$ of the corresponding branch configurations (attached to the given basepoints) form a planar polygon congruent to $\mathcal{P}$ in $\mathbb{R}^d$. If the branch configuration $V^{(i)}$ is aligned, with direction vector $\mathbf{v}^{(i)}$ (Definition 3.1.2), then the line $\mathrm{Line}^{(i)} := \{\mathbf{x}^{(i)} + t\mathbf{v}^{(i)} \mid t \in \mathbb{R}\}$ is called the *direction line* for $V^{(i)}$ (with $\mathbf{p}^{(i)} \in \mathrm{Line}^{(i)}$).

The set of all configurations for the given mechanism $(\mathcal{L}, \mathcal{X}, \mathcal{P})$ (as a subspace of the product of the appropriate branch configuration spaces), is its *configuration space* $\mathcal{C} = \mathcal{C}(\mathcal{L}, \mathcal{X}, \mathcal{P})$.

Definition 3.1.6. Note that the moving platform $\mathcal{P}$ can be translated and rotated in $\mathbb{R}^d$ (subject to the constraints imposed by the branches and the locations of the fixed

vertices). The space of all allowable positions for $\mathcal{P}$, denoted by $\mathcal{W} = \mathcal{W}(\mathcal{L}, \mathcal{X}, \mathcal{P})$, is called the *work space* for $(\mathcal{L}, \mathcal{X}, \mathcal{P})$. The *work map* $\Phi : \mathcal{C} \to \mathcal{W}$ assigns to each configuration $\mathcal{V}$ the resulting position of $\mathcal{P}$.

3.1.7. Organization. In section 3.2 we show that the configuration spaces $\mathcal{C}$ we consider here, in any ambient dimension, are manifolds (generically). In section 3.3 we describe a Morse function for the configuration space of a generic planar mechanism, analyze its critical points geometrically, and give a simple example showing how this analysis may be used to recover $\mathcal{C}$.

3.2 Generic polygonal mechanisms

We now show that, generically, the configuration space of a polygonal mechanism is a manifold. Of course, it may be smooth even when $(\mathcal{L}, \mathcal{X}, \mathcal{P})$ is not generic, but in such cases singularities can occur (cf. [47] and [12]), and their analysis is of interest in relation to the kinematic singularities.

Definition 3.2.1. A configuration $\mathcal{V} = (V^{(1)}, \ldots, V^{(k)})$ of a polygonal mechanism $(\mathcal{L}, \mathcal{X}, \mathcal{P})$ is called *singular* if:

(a) Two of its branch configurations $V^{(i_1)}$ and $V^{(i_2)}$ are aligned, with coinciding direction lines: $\mathrm{Line}^{(i_1)} = \mathrm{Line}^{(i_2)}$ (see Figure 3.2.1).

(b) Three of its branch configurations are aligned, with direction lines in the same plane meeting in a single point.

(c) Four of its branch configurations are aligned, with direction lines in the same plane.

The mechanism $(\mathcal{L}, \mathcal{X}, \mathcal{P})$ is called *generic* if none of its configurations are singular (compare [49]).

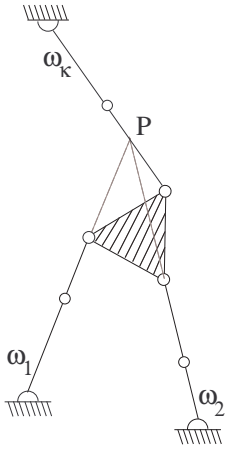

Figure 3.2.1: Singular configuration of type (a)

Theorem 3.2.2. *The configuration space* $\mathcal{C} = \mathcal{C}(\mathcal{L}, \mathcal{X}, \mathcal{P})$ *of a generic polygonal mechanism in* $\mathbb{R}^d$ *is a smooth closed orientable manifold of dimension* $N(d-1)-|\mathcal{I}|$, *where* k *is the number of vertices of* $\mathcal{P}$ *and* $N := \sum_{i=1}^{k} n^{(i)}$.

Proof. For any n, define a map $f_n : (\mathbb{R}^d)^n \to \mathbb{R}^n$ by:

$$f_n(\mathbf{v}_1, \ldots, \mathbf{v}_n) \;:=\; (|\mathbf{v}_1|^2, \ldots, |\mathbf{v}_n|^2) \;.$$

Consider the *constraint map* $F : \mathbb{R}^{dN} \to \mathbb{R}^{N+|\mathcal{I}|}$, defined:

$$F(\mathcal{V}) \;=\; F(V^{(1)}, \ldots, V^{(i)}) \;:=\; (f_{n^{(1)}}(V^{(1)}), \ldots, f_{n^{(k)}}(V^{(k)}), \|\mathbf{a}^{(1,2)}\|^2, \ldots, \|\mathbf{a}^{(k-1,k)}\|^2) \;, \tag{3.2.1}$$

where $\mathbf{p}^{(i)} := \mathbf{x}^{(i)} + \sum_{t=1}^{n^{(i)}} \mathbf{v}_t^{(i)}$ is the endpoint of the i-th branch for the configuration $V^{(i)} = (\mathbf{v}_1^{(i)}, \ldots, \mathbf{v}_{n^{(i)}}^{(i)})$ attached to the basepoint $\mathbf{x}^{(i)} \in \mathbb{R}^d$, and $\mathbf{a}^{(i,j)} := \mathbf{p}^{(i)} - \mathbf{p}^{(j)}$ is the (i,j)-diagonal of the polygon spanned by these endpoints.

Recall from §3.1.4 that $\mathcal{P}$ determines the set of diagonals $\mathcal{G} = (g^{(i,j)})_{(i,j)\in\mathcal{I}}$, where

$$|\mathcal{I}| \;=\; \begin{cases} 3k-6 & \text{if } d > 2 \\ 2k-3 & \text{if } d = 2 \end{cases}$$

Let:

$$Z_{(\mathcal{L},\mathcal{G})} \;:=\; ((\ell_1^{(1)})^2,\ldots,(\ell_{n^{(1)}}^{(1)})^2,\ldots((\ell_1^{(k)})^2,\ldots,(\ell_{n^{(k)}}^{(k)})^2,\; (g^{(1,2)})^2,\ldots,(g^{(k-1,k)})^2)$$

The configuration space $\mathcal{C} = \mathcal{C}(\mathcal{L},\mathcal{X},\mathcal{P})$ is the pre-image of $Z_{(\mathcal{L},\mathcal{G})} \in \mathbb{R}^{N+|\mathcal{I}|}$ under the function F; if $d=2$, $\mathcal{C}$ is one connected component of this pre-image.

$\mathcal{C}$ will be a smooth manifold if $Z_{(\mathcal{L},\mathcal{G})}$ is a regular value of F – i.e., if $\mathrm{dF}_{\mathcal{V}}$ is of rank $N+|\mathcal{I}|$ (see [50, I, Theorem 3.2]). We calculate:

$$\mathrm{dF}_{\mathcal{V}} \;=\; 2\begin{pmatrix} A^{(1)} & 0 & 0 & 0 & \ldots & 0 \\ 0 & A^{(2)} & 0 & 0 & \ldots & 0 \\ 0 & 0 & A^{(3)} & & \ldots & 0 \\ 0 & 0 & 0 & A^{(4)} & \ldots & 0 \\ \vdots & \vdots & \vdots & \vdots & \ddots & \vdots \\ 0 & 0 & 0 & 0 & \ldots & A^{(k)} \\ & & & & & \\ \vec{\mathbf{b}}^{(1,2)} & \vec{\mathbf{b}}^{(2,1)} & 0 & 0 & \ldots & 0 \\ \vec{\mathbf{b}}^{(1,3)} & 0 & \vec{\mathbf{b}}^{(3,1)} & 0 & \ldots & 0 \\ 0 & \vec{\mathbf{b}}^{(2,3)} & \vec{\mathbf{b}}^{(3,2)} & 0 & \ldots & 0 \\ \vdots & \vdots & \vdots & \vdots & \ddots & \vdots \\ 0 & \ldots & 0 & \vec{\mathbf{b}}^{(k-2,k)} & 0 & \vec{\mathbf{b}}^{(k,k-2)} \\ 0 & 0 & \ldots & 0 & \vec{\mathbf{b}}^{(k-1,k)} & \vec{\mathbf{b}}^{(k,k-1)} \end{pmatrix}, \tag{3.2.2}$$

where $A^{(i)}$ is the $n^{(i)} \times dn^{(i)}$ matrix:

$$\begin{pmatrix} \mathbf{v}_1^{(i)} & \ldots & 0 \\ \vdots & \ddots & \vdots \\ 0 & \ldots & \mathbf{v}_{n^{(i)}}^{(i)} \end{pmatrix} \tag{3.2.3}$$

with rows denoted by: $\vec{\mathbf{u}}_1^{(i)},\ldots,\vec{\mathbf{u}}_{n^{(i)}}^{(i)}$.

The $|\mathcal{I}|$ bottom rows $(\vec{\mathbf{w}}_j^{(i)})$ of $\frac{1}{2}\mathrm{dF}$ are indexed by $(i,j)\in\mathcal{I}$, where

$$\vec{\mathbf{w}}_j^{(i)} := (\underbrace{0,\ldots,0}_{d(n^{(1)}+\ldots+n^{(i-1)})},\vec{\mathbf{b}}^{(i,j)},\underbrace{0,\ldots,0}_{d(n^{(i+1)}+\ldots+n^{(j-1)})},\vec{\mathbf{b}}^{(j,i)},\underbrace{0,\ldots,0}_{d(n^{(j+1)}+\ldots+n^{(k)})}),$$

each edge $\mathbf{a}^{(i,j)} \in \mathbb{R}^d$ appearing $n^{(i)}$ times in

$$\vec{\mathbf{b}}^{(i,j)} \;:=\; \underbrace{(\mathbf{a}^{(i,j)}, \mathbf{a}^{(i,j)}, \ldots, \mathbf{a}^{(i,j)})}_{n^{(i)}} \;.$$

If we think of the bottom rows as forming N blocks of $|\mathcal{I}|\times d$ matrices $B_1, \ldots, B_N$, then:

$$\sum_{r=1}^{N} B_r \;=\; 0. \tag{3.2.4}$$

Let $\mathcal{V} \in \mathcal{C} = F^{-1}(Z_{(\mathcal{L},\mathcal{G})})$, and consider a vanishing linear combination of the rows of $\mathrm{dF}_{\mathcal{V}}$:

$$\sum_{i=1}^{k} \left(\sum_{j=1}^{n^{(i)}} \lambda_j^{(i)} \vec{\mathbf{u}}_j^{(i)} \right) \;+\; \sum_{(i,j)\in\mathcal{I}} \gamma^{(i,j)} \vec{\mathbf{w}}_j^{(i)} \;=\; \mathbf{0}\;.$$

For each $1 \le i \le k$, let:

$$\mathbf{v}^{(i)} \;:=\; \sum_{\substack{(s,i)\in\mathcal{I}\\ s<i}} \gamma^{(s,i)} \cdot \mathbf{a}^{(s,i)} \;-\; \sum_{\substack{(i,t)\in\mathcal{I}\\ i<t}} \gamma^{(i,t)} \cdot \mathbf{a}^{(i,t)}\;,$$

and note that if $\lambda_{j'}^{(i)} \neq 0$ for *some* $1 \le j' \le n^{(i)}$, then this holds for all $1 \le j \le n^{(i)}$, so that $\mathbf{v}_j^{(i)} = \frac{1}{\lambda_j^{(i)}} \cdot \mathbf{v}^{(i)}$ (the i-th branch is aligned with direction vector $\mathbf{v}^{(i)}$).

By (3.2.4), $\sum_{i=1}^{k} \mathbf{v}^{(i)} = \mathbf{0}$, so if $\mathbf{v}^{(i)} = \mathbf{0}$ for $i \neq i_0, i_1$, then $\mathbf{v}^{(i_0)} + \mathbf{v}^{(i_1)} = \mathbf{0}$, and thus branches i_0 and i_1 are co-aligned with direction vector $\mathbf{a}^{(i_0,i_1)}$. This cannot happen if $(\mathcal{L}, \mathcal{X}, \mathcal{P})$ is generic (cf. §3.2.1(a)). Similarly, no more than three branches can be aligned (§3.2.1(c)).

Unfortunately, even for generic mechanisms dF need not be of maximal rank. Thus, to complete the proof of the Theorem we need the following:

Proposition 3.2.3. *For a generic polygonal mechanism, any configuration $\mathcal{V}$ having at most three aligned branches is smooth.*

Proof. Without loss of generality we may assume that the three aligned branches are $1, 2$ and k, with direction vectors ω_1, ω_2, and ω_k, respectively.

Let $\hat{\mathcal{C}}$ denote the configuration space of the mechanism obtained from $(\mathcal{L}, \mathcal{X}, \mathcal{P})$ by omitting the last branch, and $\mathcal{C}(k)$ the configuration space for this branch (attached to $\mathbf{x}^{(k)} \in \mathbb{R}^d$).

The *work space* of both mechanisms (i.e., the set of possible locations for the k-th vertex of $\mathcal{P}$) is contained in $\mathbb{R}^d$, and we have *work maps* $\psi : \hat{\mathcal{C}} \to \mathbb{R}^d$ and $\phi : \mathcal{C}(k) \to \mathbb{R}^d$ which associate to each configuration the location of this vertex.

Note that the manifold $\mathcal{C}(k)$ (an n-torus for $n = n^{(k)}$) is the preimage of $Z_{\ell^{(k)}}$ under the map $f = f_n : \mathbb{R}^{nd} \to \mathbb{R}^n$, and we write $i : \mathcal{C}(k) \to \mathbb{R}^{nd}$ for the inclusion. Similarly, $\hat{\mathcal{C}}$ is determined by a smooth constraint map:

$$\hat{F} : \mathbb{R}^M \times \mathcal{S} \to \mathbb{R}^{N-n+|\hat{\mathcal{I}}|}$$

for $M = (N-n)d$, where $\mathcal{S}$ is a point if $k \geq 4$ and $\mathcal{S} = S^{d-2}$ if $k = 3$. Here

$$\begin{aligned} \hat{F}(\hat{\mathcal{V}}) &= \hat{F}(V^{(1)}, \dots, V^{(k-1)}, \mathbf{w}) \\ &:= (f_{n^{(1)}}(V^{(1)}), \dots, f_{n^{(k-1)}}(V^{(k-1)}),\ \|\mathbf{a}^{(1,2)}\|^2,\ \dots,\ \|\mathbf{a}^{(k-2,k-1)}\|^2) \end{aligned} \tag{3.2.5}$$

(with the functions $\|\mathbf{a}^{(i,j)}\|^2$ indexed by $(i,j) \in \hat{\mathcal{I}}$). The vector $\mathbf{w} \in S^\Delta$ is needed for $k = 3$ and $d > 2$, since in that case the location of the first $k-1$ vertices of $\mathcal{P}$ determines the position of the moving platform only up to rotation of $\mathbf{a}^{(1,3)}$ around the given edge $\mathbf{a}^{(1,2)}$ (relative to the plane $\mathcal{E} = \mathcal{E}(\mathbf{v}^{(1)}_{n^{(1)}}, \mathbf{a}^{(1,2)})$ spanned by $\mathbf{v}^{(1)}_{n^{(1)}}$ and $\mathbf{a}^{(1,2)}$).

Thus $\hat{\mathcal{C}}$ is $\hat{F}^{-1}(Z_{(\hat{\mathcal{L}},\hat{\mathcal{G}})})$ for the obvious $(\hat{\mathcal{L}}, \hat{\mathcal{G}})$. Moreover, $(\hat{\mathcal{L}}, \hat{\mathcal{G}})$ is a regular value of $\hat{F}$, as in the proof of Theorem 3.2.2, because $(\mathcal{L}, \mathcal{X}, \mathcal{P})$ is generic, so no branches but $1, 2, k$ are aligned. Thus $\hat{\mathcal{C}}$ is a smooth submanifold, and we write $\hat{\imath} : \hat{\mathcal{C}} \to \mathbb{R}^M$ for the inclusion.

Let $X := \mathcal{C}(k) \times \mathbb{R}^M \times \mathcal{S}$, $Y := \mathbb{R}^d \times \mathbb{R}^M \times \mathcal{S}$, and define $h : X \to Y$ to be the product map $\phi \times \mathrm{Id}_{\mathbb{R}^M} \times \mathrm{Id}_{\mathcal{S}}$ and $g : \hat{\mathcal{C}} \to Y$ to be $(\psi, \hat{\imath})$, so that g is an embedding of $\hat{\mathcal{C}}$ as a submanifold in Y. Since $\mathcal{C} = \mathcal{C}(\mathcal{L}, \mathcal{X}, \mathcal{P})$ is simply the pullback of:

$$\mathcal{C}(k) \xrightarrow{\phi} \mathbb{R}^d \xleftarrow{\psi} \hat{\mathcal{C}}\ ,$$

it may be identified with the preimage of the submanifold $\hat{\mathcal{C}} \subseteq Y$ under h.

Let $\hat{\mathcal{V}} \in \hat{\mathcal{C}}$ be a configuration where the first two branches are aligned (but not co-aligned), with direction vectors in the plane $\mathcal{E}$ determined by the polygon $\mathcal{P}$ – and let $V^{(k)} \in \mathcal{C}(k)$ be an aligned configuration with direction vector $\mathbf{v}^{(k)}$. Assume that $\psi(\hat{\mathcal{V}}) = \phi(V^{(k)})$, and let $\mathbf{x} \in X$ be the configuration $(V^{(k)}, \hat{\imath}(\hat{\mathcal{V}}))$, so that $h(\mathbf{x}) = g(\hat{\mathcal{V}})$. We must therefore show that the point $\mathcal{V} \in \mathcal{C}$ defined by $(\hat{\mathcal{V}}, V^{(k)})$ is smooth:

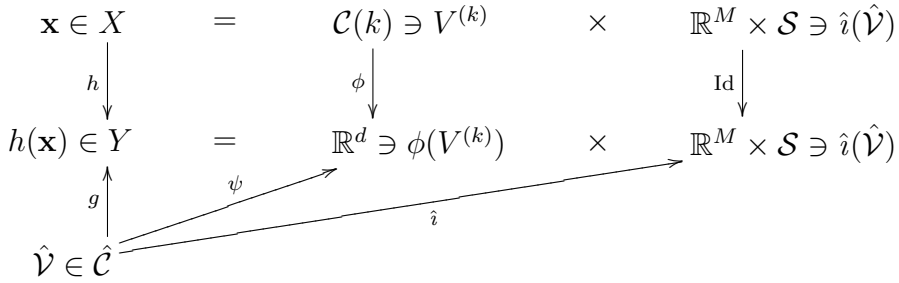

By [50, I, Theorem 3.3]), it suffices to show that $h \pitchfork \hat{\mathcal{C}}$ – i.e., h is locally transverse to $\hat{\mathcal{C}}$ at the points $\mathbf{x} \in X$ and $\hat{\mathcal{V}} \in \hat{\mathcal{C}}$. In other words:

$$\operatorname{Im} \mathrm{d}h_{\mathbf{x}} \; + \; T_{\hat{\mathcal{V}}}(\hat{\mathcal{C}}) \; = \; T_{\hat{\mathcal{V}}}(Y) \; = \; \mathbb{R}^d \times \mathbb{R}^{M+\Delta} \; . \tag{3.2.6}$$

First note that since $\mathcal{C}(k) = f^{-1}(Z_{\ell^{(k)}}) \subseteq \mathbb{R}^{nd}$, the tangent space $T_{V^{(k)}}(\mathcal{C}(k))$ may be identified with the kernel of $\mathrm{d}f_{V^{(k)}} : \mathbb{R}^{nd} \to \mathbb{R}^n$, which is the null space of the matrix $A^{(k)}$ of (4.2.3). Since $V^{(k)}$ is aligned, by assumption, with direction vector ω_k, we see that:

$$\begin{aligned} T_{V^{(k)}}(\mathcal{C}(k)) \; &\cong \; \{(\mathbf{y}_1^{(k)}, \ldots, \mathbf{y}_n^{(k)}) \in \mathbb{R}^{nd} \mid \mathbf{y}_1^{(k)} \cdot \omega_k = 0, \; \ldots, \mathbf{y}_n^{(k)} \cdot \omega_k = 0\} \\ &= \underbrace{\omega_k^{\perp} \times \ldots \times \omega_k^{\perp}}_{n} \end{aligned}$$

Furthermore, $\phi : \mathcal{C}(k) \to \mathbb{R}^d$ extends to $\hat{\phi} : \mathbb{R}^{nd} \to \mathbb{R}^d$ (so that $\hat{\phi} \circ i = \phi$), with

$$\hat{\phi}(\mathbf{v}_1, \ldots, \mathbf{v}_n) \; = \; \mathbf{x}^{(k)} + \mathbf{v}_1 + \cdots + \mathbf{v}_n \; .$$

Since $\hat{\phi}$ is linear, its differential $\mathrm{d}\,\hat{\phi}$ is represented by the $d \times nd$ matrix $(I_d, I_d, \ldots, I_d)$ (n blocks).

Thus:

$$\mathrm{Im}\,\mathrm{dh}_{\mathbf{x}} \;=\; \omega_k^{\perp} \times \mathbb{R}^{M+\Delta}\ ,$$

so that in order for (4.2.5) to hold it suffices to prove that:

$$\omega_k \in T_{\hat{\mathcal{V}}}(\hat{\mathcal{C}}). \tag{3.2.7}$$

Now the tangent space $T_{\hat{\mathcal{V}}}(\hat{\mathcal{C}})$ may be identified with the kernel of:

$$\mathrm{d}\,\hat{F}_{\hat{\mathcal{V}}} : \mathbb{R}^{M+\Delta} \to \mathbb{R}^{N-n+2k-5}\ ,$$

where $\mathrm{d}\,\hat{F}_{\hat{\mathcal{V}}}$ is described as in (4.2.2) by the matrix:

$$\mathrm{d}\,\hat{F}_{\hat{\mathcal{V}}} \;=\; 2\begin{pmatrix} A^{(1)} & 0 & \dots & 0 & 0\dots 0 \\ \vdots & \vdots & \ddots & \vdots & \vdots \\ 0 & 0 & \dots & A^{(k)} & 0\dots 0 \\ & & & & \\ \vec{\mathbf{b}}^{(1,2)} & \vec{\mathbf{b}}^{(2,1)} & \dots & 0 & 0\dots 0 \\ \vdots & \vdots & \ddots & \vdots & 0\dots 0 \\ 0 & 0 & \dots & \vec{\mathbf{b}}^{(k,k-1)} & 0\dots 0 \end{pmatrix} \tag{3.2.8}$$

Since the first two branches are aligned with direction vectors ω_1, ω_2, $T_{\hat{\mathcal{V}}}(\hat{\mathcal{C}})$ may be identified with the set of $N-n$ d-dimensional vectors

$$\mathbf{y}_1^{(1)}, \dots, \mathbf{y}_{n^{(1)}}^{(1)}; \mathbf{y}_1^{(2)}, \dots, \mathbf{y}_{n^{(2)}}^{(2)}; \dots; \mathbf{y}_1^{(k-1)}, \dots, \mathbf{y}_{n^{(k-1)}}^{(k-1)}\ ,$$

together with $\mathbf{z} \in \mathbb{R}^{\Delta}$, where the first $n^{(1)}$ vectors are all in $\omega_1^{\perp}$, the next $n^{(2)}$ are all in $\omega_2^{\perp}$, and the remainder are in individual orthogonal complements:

$$(\mathbf{v}_1^{(3)})^{\perp} \times \dots \times (\mathbf{v}_{n^{(3)}}^{(3)})^{\perp} \times (\mathbf{v}_1^{(k-1)})^{\perp} \times \dots \times (\mathbf{v}_{n^{(k-1)}}^{(k-1)})^{\perp}\ .$$

If we let $\vec{\mathbf{y}}^{(i)} := \sum_{t=1}^{n^{(i)}} \mathbf{y}_t^{(i)}$ $(i = 1, \dots, k-1)$, these must satisfy:

$$\mathbf{a}^{(i,j)} \cdot (\vec{\mathbf{y}}^{(i)} - \vec{\mathbf{y}}^{(j)}) \;=\; 0$$

for each $(i,j) \in \hat{\mathcal{I}}$.

Likewise, $\psi : \hat{\mathcal{C}} \to \mathbb{R}^d$ extends to $\hat{\psi} : \mathbb{R}^M \times \mathcal{S} \to \mathbb{R}^d$, with

$$\hat{\psi}(V^{(1)}, \ldots, V^{(k-1)}, \mathbf{w}) \;=\; \mathbf{x}^{(1)} + \mathbf{v}_1^{(1)} + \cdots + \mathbf{v}_{n^{(1)}}^{(1)} \;+\; R_{\mathbf{w}} \cdot \mathbf{a}^{(1,2)} \;,$$

where $R_{\mathbf{w}}$ is $\lambda \cdot B_{\mathbf{w}} \cdot A_\theta$, for $\lambda := \ell^{(1,k)}/\ell^{(1,2)}$, $B_{\mathbf{w}}$ the rotation matrix about $\mathbf{a}^{(1,2)}$ determined by $\mathbf{w} \in \mathcal{S}$ (if $\mathcal{S} = S^\Delta$), and A_θ rotates $\mathbf{a}^{(1,2)}$ (in the plane $\mathcal{E}$ spanned by $\mathbf{v}_{n^{(1)}}^{(1)}$ and $\mathbf{a}^{(1,2)}$) by the angle θ to the side $\mathbf{a}^{(1,3)}$ in the given polygon $\mathcal{P}$.

Thus $\mathrm{d}\,\hat{\psi}_{(V^{(1)},\ldots,V^{(k-1)},\mathbf{w})}$ is represented by the $(M+\Delta) \times d$ matrix:

$$\left[\; \underbrace{I_d + R_{\mathbf{w}} | \ldots | I_d + R_{\mathbf{w}}}_{n^{(1)}} \;|\; \underbrace{-R_{\mathbf{w}} | \ldots | -R_{\mathbf{w}}}_{n^{(2)}} \;|\; \underbrace{0 \ldots 0}_{dn^{(3)}} \;|\; \ldots \;|\; \underbrace{0 \ldots 0}_{dn^{(k-1)}} \;|\; \frac{\partial R_{\mathbf{w}}}{\partial \mathbf{w}} \;\right] . \tag{3.2.9}$$

Therefore, the image of $\mathrm{d}\,\psi$ is obtained by applying (3.2.9) to $T_{\hat{\mathcal{V}}}(\hat{\mathcal{C}}) \subseteq \mathbb{R}^{M+\Delta}$ described above, and we see that $\mathrm{Im}(\mathrm{d}\,\psi_{\hat{\mathcal{V}}})$ is the sum of

$$\{\vec{\mathbf{y}}^{(1)} + R_{\mathbf{w}}(\vec{\mathbf{y}}^{(1)} - \vec{\mathbf{y}}^{(2)}) \mid \vec{\mathbf{y}}^{(1)} \in \omega_1^\perp,\ \vec{\mathbf{y}}^{(2)} \in \omega_2^\perp,\ (\vec{\mathbf{y}}^{(1)} - \vec{\mathbf{y}}^{(2)}) \in (\mathbf{a}^{(1,2)})^\perp\} \tag{3.2.10}$$

and $\mathrm{Im}\,\frac{\partial R_{\mathbf{w}}}{\partial \mathbf{w}}$.

In the case we are interested in, the two direction vectors ω_1 and ω_2 are in the plane $\mathcal{E}$ spanned by $\mathcal{P}$, so $B_{\mathbf{w}}$ is the identity matrix and thus $R_{\mathbf{w}} = \lambda \cdot A_\theta$ takes $\mathbf{a}^{(1,2)}$ to $\mathbf{a}^{(1,3)}$ in $\mathcal{E}$. Clearly, $\mathrm{Im}(\mathrm{d}\,\psi_{\hat{\mathcal{V}}})$ contains the orthogonal complement $\mathcal{E}^\perp$, so to prove (3.2.7) we may reduce to the case $d = 2$ (all vectors in the plane $\mathcal{E}$), so that in fact (3.2.10) is all of $\mathrm{Im}(\mathrm{d}\,\psi_{\hat{\mathcal{V}}})$.

Now choose unit vectors $\mathbf{c}^{(i)}$ spanning $\omega_i^\perp$ $(i = 1, 2)$ in $\mathcal{E}$, let $\mathbf{d} := A_{\pi/2}(\mathbf{a}^{(1,2)})$ (so that it spans $(\mathbf{a}^{(1,2)})^\perp$), and let $\hat{\mathbf{d}} := R_{\mathbf{w}}\mathbf{d}$. Then $\mathrm{Im}(\mathrm{d}\,\psi_{\hat{\mathcal{V}}})$ is the set of vectors $s\mathbf{c}^{(1)} + t\hat{\mathbf{d}}$ such that $s\mathbf{c}^{(1)} - t\mathbf{d}$ is a multiple of $\mathbf{c}^{(2)}$.

For any three vectors $\mathbf{x}$, $\mathbf{y}$, and $\mathbf{z}$ in $\mathbb{R}^2$ we have:

$$(\mathbf{x} \cdot A_{\pi/2}\mathbf{y})\,\mathbf{z} \;+\; (\mathbf{y} \cdot A_{\pi/2}\mathbf{z})\,\mathbf{x} \;+\; (\mathbf{z} \cdot A_{\pi/2}\mathbf{x})\,\mathbf{y} \;=\; \mathbf{0} \;, \tag{3.2.11}$$

so $\mathbf{c}^{(2)}$ is a multiple of $(\mathbf{a}^{(1,2)} \cdot \mathbf{c}^{(2)})\,\mathbf{c}^{(1)} \;+\; (\omega_1 \cdot \mathbf{c}^{(2)})\,\mathbf{d}$, and thus $\mathrm{Im}(\mathrm{d}\,\psi_{\hat{\mathcal{V}}})$ is spanned by:

$$\mathbf{e} \;:= (\mathbf{a}^{(1,2)} \cdot \mathbf{c}^{(2)})\,\mathbf{c}^{(1)} \;-\; (\omega_1 \cdot \mathbf{c}^{(2)})\,\hat{\mathbf{d}} \;.$$

Therefore, (3.2.7) fails only if ω_k is perpendicular to $\mathbf{e}$ – in other words, if ω_k is proportional to:

$$(\mathbf{a}^{(1,2)} \cdot \mathbf{c}^{(2)})\,\omega_1 \;-\; (\omega_1 \cdot \mathbf{c}^{(2)})\,\mathbf{a}^{(1,3)}$$

or equivalently, to:

$$\mathbf{w} \;:=\; \frac{(\mathbf{d} \cdot \omega_2)}{(\omega_1 \cdot \mathbf{c}^{(2)})}\,\omega_1 \;-\; \mathbf{a}^{(1,3)} \;,$$

which by (3.2.11) is precisely the vector connecting the meeting point $P := \mathbf{p}^{(1)} + \frac{(\mathbf{d}\cdot\omega_2)}{(\omega_1\cdot\mathbf{c}^{(2)})}\,\omega_1$ of $\mathrm{Line}^{(1)}$ and $\mathrm{Line}^{(2)}$ with the end point $\mathbf{p}^{(3)} = \mathbf{p}^{(1)} + \mathbf{a}^{(1,3)}$ of $V^{(k)}$, so that ω_k is proportional to $\mathbf{w}$ if and only if the direction line $\mathrm{Line}^{(3)}$ passes through P – which cannot happen in a generic mechanism (see Figure 3.2.1 and Definition 3.2.1(b)).

This completes the proof of Proposition 3.2.3, and thus of Theorem 3.2.2. □

3.3 Morse functions for planar mechanisms

From now on we shall concentrate on the simplest type of polygonal mechanism – namely, planar mechanisms $(d = 2)$ having triangular platforms $(k = 3)$ and exactly two links per branch $(n^{(1)} = n^{(2)} = n^{(3)} = 2)$. These mechanism are known in the robotics literature as 3-*RRR* (rotational) mechanisms.

Recall that a smooth real-valued function on a manifold is called a *Morse function* if all its critical points are non-degenerate (cf. [51, I, §2]). Such functions may be used to deduce the cellular structure of the manifold, and thus recover its homotopy type (see [51, I, §3]). Our goal is to describe a Morse function for the configuration space of a 3-RRR mechanism.

Theorem 3.3.1. *The function* $f(\mathcal{V}) := \sum_{j=1}^{3} \|\mathbf{v}^{(j)}\|^2$ *is generically a Morse function on* $C(\mathcal{L}, \mathcal{X}, \mathcal{P})$, *where* $\mathbf{v}^{(j)} := \mathbf{v}_1^{(j)} + \mathbf{v}_2^{(j)} = \mathbf{p}^{(j)} - \mathbf{x}^{(j)}$.

Proof. In order to show that the critical points of f are non-degenerate, we must choose a local coordinate system near each such point.

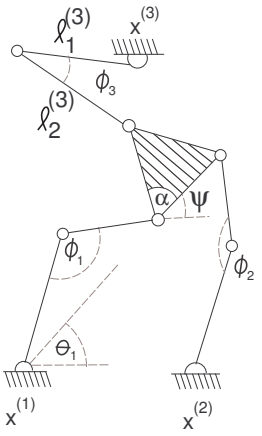

Figure 3.3.1: Local coordinates

Unfortunately, there is no uniform choice of such a system, so we must distinguish three cases:

Case I: Let $\Phi := (\phi_1, \phi_2, \phi_3)$, where ϕ_j denotes the angle between the vectors $-\mathbf{v}_1^{(j)}$ and $\mathbf{v}_2^{(j)}$ for $j = 1, 2, 3$. Then:

$$h^{(j)}(\phi_j) \;:=\; \|\mathbf{v}^{(j)}\| \;=\; \|\mathbf{v}_1^{(j)} + \mathbf{v}_2^{(j)}\| \;=\; \sqrt{(\ell_1^{(j)})^2 + (\ell_2^{(j)})^2 - 2\ell_1^{(j)}\,\ell_2^{(j)}\cos\phi_1} \tag{3.3.1}$$

and thus $f(\Phi) \;=\; \sum_{j=1}^{3} h^{(j)}(\phi_j)^2$, so that:

$$\begin{aligned} \nabla f \;=\; \nabla_\Phi\, f \;&= 2\left(\ell_1^{(1)}\ell_2^{(1)}\,\sin(\phi_1),\; \ell_1^{(2)}\ell_2^{(2)}\,\sin(\phi_2),\; \ell_1^{(3)}\ell_2^{(3)}\,\sin(\phi_3)\right) \\ &= 2\left((\mathbf{v}_1^{(1)})^\perp \cdot \mathbf{v}_2^{(1)},\; (\mathbf{v}_1^{(2)})^\perp \cdot \mathbf{v}_2^{(2)},\; (\mathbf{v}_1^{(3)})^\perp \cdot \mathbf{v}_2^{(3)}\right) \end{aligned} \tag{3.3.2}$$

where $\vec{\mathbf{w}}^\perp := (b, -a)$ for $\vec{\mathbf{w}} = (a, b)$.

Thus Φ is a critical point if and only if:

$$\Phi \;=\; \frac{\pi}{2}\,(1+\sigma_1,\, 1+\sigma_2,\, 1+\sigma_3) \qquad \text{for } \; \sigma_1, \sigma_2, \sigma_3 \in \{\pm 1\}\;. \tag{3.3.3}$$

Computing the Hessian at a critical point Φ yields:

$$H_\Phi \;=\; \begin{pmatrix} \sigma_1\,\ell_1^{(1)}\ell_2^{(1)} & 0 & 0 \\ 0 & \sigma_2\,\ell_1^{(2)}\ell_2^{(2)} & 0 \\ 0 & 0 & \sigma_3\,\ell_1^{(3)}\ell_2^{(3)} \end{pmatrix}\;,$$

which is non-degenerate, with index Ind_Φ equal to the number of negative values in $\{\sigma_1, \sigma_2, \sigma_3\}$. Such critical points will be refered to as *type I*.

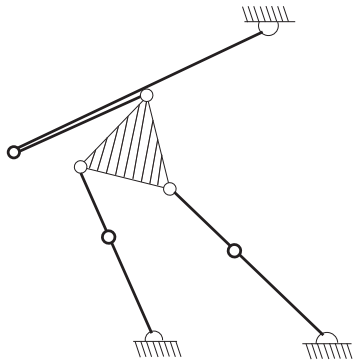

Figure 3.3.2: Type I critical point

Case II: As we saw, critical points of f appear when all three branches are aligned. However, for some mechanisms this will never happen, because one or two branches can never fully stretch or fold – that is, ϕ_3 (say) takes values in a proper subset $[a_1, a_2] \cup [-a_2, -a_1]$ of $[-\pi, \pi]$ (see Example 3.3.3). Clearly, ϕ_3 cannot then serve as a local coordinate at a point $(\phi_1, \phi_2, \pm a_k)$.

However, if the first two branches can both be aligned, then in the vicinity of doubly aligned configurations we take $\hat{\Phi} := (\phi_1, \phi_2, \theta_1)$, where ϕ_j $(j = 1, 2)$ as in Case I, and θ_j is the angle between $\mathbf{v}^{(j)} := \mathbf{v}_1^{(j)} + \mathbf{v}_2^{(j)}$ and the vector $\mathbf{x}^{(2)}$ (we assume for simplicity that $\mathbf{x}^{(1)}$ is at the origin).

Since

$$\mathbf{v}^{(j)} = h^{(j)}(\cos\theta_j, \sin\theta_j) \ , \tag{3.3.4}$$

using (3.3.1) we have:

$$(\partial_{\phi_j}\mathbf{v}^{(j)},\ \partial_{\phi_{j'}}\mathbf{v}^{(j)},\ \partial_{\theta_j}\mathbf{v}^{(j)}) \ = \ (\frac{(\mathbf{v}_1^{(j)})^\perp \cdot \mathbf{v}_2^{(j)}}{h^{(j)}(\phi_j)^2}\,\mathbf{v}^{(j)},\ 0,\ -(\mathbf{v}^{(j)})^\perp)) \ , \tag{3.3.5}$$

for $\{j, j'\} = \{1, 2\}$.

However, since θ_2 is a dependent variable, we may differentiate the norms in:

$$\mathbf{v}^{(1)} + \mathbf{a}^{(1,2)} - \mathbf{v}^{(2)} \ = \ \mathbf{x}^{(2)} \tag{3.3.6}$$

implicitly and deduce that:

$$\partial_{\theta_1}\,\mathbf{v}^{(2)} \;=\; -\,\partial_{\theta_1}\,\theta_2\,(\mathbf{v}^{(2)})^{\perp} \;=\; -\,\frac{\mathbf{a}^{(1,2)}\cdot(\mathbf{v}^{(1)})^{\perp}}{\mathbf{a}^{(1,2)}\cdot(\mathbf{v}^{(2)})^{\perp}}\,(\mathbf{v}^{(2)})^{\perp}\;. \tag{3.3.7}$$

Differentiating (3.3.6) itself and using (3.3.5), (3.3.7) and (3.2.11) yields:

$$\nabla_{\hat{\Phi}}\mathbf{a}^{(1,2)} \;=\; (-\frac{(\mathbf{v}_1^{(1)})^{\perp}\cdot\mathbf{v}_2^{(1)}}{h^{(1)}(\phi_1)^2}\,\mathbf{v}^{(1)},\;\; -\,\frac{(\mathbf{v}_1^{(2)})^{\perp}\cdot\mathbf{v}_2^{(2)}}{h^{(2)}(\phi_2)^2}\,\mathbf{v}^{(2)},\;\; \frac{\mathbf{v}^{(1)}\cdot(\mathbf{v}^{(2)})^{\perp}}{\mathbf{a}^{(1,2)}\cdot(\mathbf{v}^{(2)})^{\perp}}\,(\mathbf{a}^{(1,2)})^{\perp}\,) \tag{3.3.8}$$

Since $\mathbf{x}^{(1)}=\mathbf{0}$, we see $\mathbf{v}^{(3)} \;=\; \mathbf{v}^{(1)}+\mathbf{a}^{(1,3)}-\mathbf{x}^{(3)}$, so:

$$\begin{cases} \partial_{\phi_1} f \;=\; 2\,(\mathbf{v}_1^{(1)})^{\perp}\cdot\mathbf{v}_2^{(1)}\;\frac{2h^{(1)}(\phi_1)^2+\mathbf{v}^{(1)}\cdot(\mathbf{a}^{(1,3)}-\mathbf{x}^{(3)})+(\mathbf{x}^{(3)}-\mathbf{v}^{(1)})\cdot(B_\alpha\mathbf{v}^{(1)})}{h^{(1)}(\phi_1)^2} \\ \partial_{\phi_2} f \;=\; 2\,(\mathbf{v}_1^{(2)})^{\perp}\cdot\mathbf{v}_2^{(2)}\;\frac{h^{(2)}(\phi_2)^2\;+(\mathbf{x}^{(3)}-\mathbf{v}^{(1)})\cdot(B_\alpha\mathbf{v}^{(2)})}{h^{(2)}(\phi_2)^2} \\ \partial_{\theta_1} f \;=\; 2\,(\mathbf{x}^{(3)}-\mathbf{a}^{(1,3)})\cdot(\mathbf{v}^{(1)})^{\perp}\;+\;2\,\frac{[\mathbf{v}^{(1)}\cdot(\mathbf{v}^{(2)})^{\perp}]\,[(\mathbf{v}^{(1)}-\mathbf{x}^{(3)})\cdot(\mathbf{a}^{(1,3)})^{\perp}]}{\mathbf{a}^{(1,2)}\cdot(\mathbf{v}^{(2)})^{\perp}} \end{cases} \tag{3.3.9}$$

where B_α is the rotation-and-dilitation matrix taking $\mathbf{a}^{(1,2)}$ to $\mathbf{a}^{(1,3)}$.

Note that we use the coordinates $\hat{\Phi}$ only at points where the first two branches are aligned, so that $\mathbf{v}_2^{(j)}\cdot(\mathbf{v}_1^{(j)})^{\perp}=0$ for $j=1,2$, and thus the first two entries of $\nabla_{\hat{\Phi}}(f)$ vanish at these points. The vanishing of $\frac{\partial f}{\partial\theta_1}$ is equivalent to the condition:

$$\begin{aligned} &[\mathbf{x}^{(3)}\cdot(\mathbf{v}^{(1)})^{\perp}]\,[\mathbf{a}^{(1,2)}\cdot(\mathbf{v}^{(2)})^{\perp}] \;-\; [\mathbf{a}^{(1,3)})\cdot(\mathbf{v}^{(1)})^{\perp}]\,[\mathbf{a}^{(1,2)}\cdot(\mathbf{v}^{(2)})^{\perp}] \\ &+\;[\mathbf{v}^{(1)}\cdot(\mathbf{v}^{(2)})^{\perp}]\,[\mathbf{v}^{(1)}\cdot(\mathbf{a}^{(1,3)})^{\perp}] \;-\; [\mathbf{v}^{(1)}\cdot(\mathbf{v}^{(2)})^{\perp}]\,[\mathbf{x}^{(3)}\cdot(\mathbf{a}^{(1,3)})^{\perp}] \;=\; 0 \end{aligned} \tag{3.3.10}$$

Note that by (3.2.11) again, the intersection of $\mathrm{Line}^{(1)}$ with $\mathrm{Line}^{(2)}$ is at the point:

$$P := \mathbf{x}^{(3)}+\mathbf{v}^{(1)}+\frac{\mathbf{a}^{(1,2)}\cdot(\mathbf{v}^{(2)})^{\perp}}{\mathbf{v}^{(1)}\cdot(\mathbf{v}^{(2)})^{\perp}}\,\mathbf{v}^{(1)}\;,$$

and (3.3.10) is equivalent to the colinearity of $\mathbf{x}^{(3)}$, P, and $\mathbf{v}^{(1)}+\mathbf{a}^{(1,3)}$. Such critical points will be refered to as *type II*.

Calculating the Hessian matrix H_f of f at a critical point, we find that it is

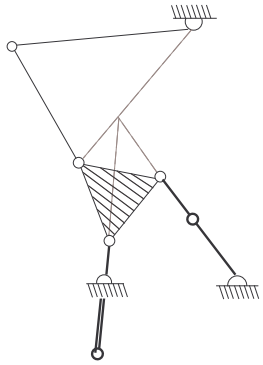

Figure 3.3.3: Type II critical point

diagonal, with:

$$\begin{aligned}
\partial_{\phi_1\phi_1} f &= -2\,\mathbf{v}_1^{(1)}\cdot\mathbf{v}_2^{(1)}\;\frac{2h^{(1)}(\phi_1)^2+\mathbf{v}^{(1)}\cdot(\mathbf{a}^{(1,3)}-\mathbf{x}^{(3)})+(\mathbf{x}^{(3)}-\mathbf{v}^{(1)})\cdot(B_\alpha\mathbf{v}^{(1)})}{h^{(1)}(\phi_1)^2}\\
\partial_{\phi_2\phi_2} f &= -2\,\mathbf{v}_1^{(2)}\cdot\mathbf{v}_2^{(2)}\;\frac{h^{(2)}(\phi_2)^2\;+(\mathbf{x}^{(3)}-\mathbf{v}^{(1)})\cdot(B_\alpha\mathbf{v}^{(2)})}{h^{(2)}(\phi_2)^2}\\
\partial_{\theta_1\theta_1} f &= \frac{2}{[\mathbf{a}^{(1,2)}\cdot(\mathbf{v}^{(2)})^\perp]^2}\;(\;-\;2\,[\mathbf{v}^{(1)}\cdot(\mathbf{v}^{(2)})^\perp]\,[\mathbf{a}^{(1,3)}\cdot\mathbf{v}^{(1)}]\,[\mathbf{a}^{(1,2)}\cdot(\mathbf{v}^{(2)})^\perp]\\
&\quad+\;[(\mathbf{x}^{(3)}-\mathbf{a}^{(1,3)})\cdot\mathbf{v}^{(1)}]\,[\mathbf{a}^{(1,2)}\cdot(\mathbf{v}^{(2)})^\perp]^2\\
&\quad+\;[\mathbf{v}^{(1)}\cdot\mathbf{v}^{(2)}]\,[\mathbf{a}^{(1,2)}\cdot(\mathbf{v}^{(1)}-\mathbf{v}^{(2)})^\perp]\,[(\mathbf{v}^{(1)}-\mathbf{x}^{(3)})\cdot(\mathbf{a}^{(1,3)})^\perp]\\
&\quad+\;[\mathbf{v}^{(1)}\cdot(\mathbf{v}^{(2)})^\perp]^2\,[(\mathbf{v}^{(1)}-\mathbf{x}^{(3)})\cdot(\mathbf{a}^{(1,3)})]\\
&\quad+\;[\mathbf{a}^{(1,2)}\cdot\mathbf{v}^{(2)}]\,[(\mathbf{v}^{(2)}-\mathbf{a}^{(1,2)})\cdot(\mathbf{v}^{(1)})^\perp]\,[(\mathbf{x}^{(3)}-\mathbf{a}^{(1,3)})\cdot(\mathbf{v}^{(1)})^\perp]\;)
\end{aligned}$$

If we solve (3.3.9) to find explicitly the critical points of f in the coordinates $\hat{\Phi}$, and then substitute into the expression we have found for H_f at these points, we obtain a polynomial expression of degree 6 in the parameters $(\mathcal{L},\mathcal{X},\mathcal{G})$ for the mechanism. Thus the critical point we identified is degenerate only when this polynomial vanishes, so generically f is indeed a Morse function.

Case III: Note that the work space $\mathcal{W}$ for each vertex of $\mathcal{P}$ is the intersection of three annuli (so it is compact), and thus the boundary of $\mathcal{W}$ must intersect at least one of the bounding circles of the annuli. Therefore, at least one of the three branches

(say, the first) *can* be aligned.

Thus, at critical points of f where neither Φ nor $\hat{\Phi}$ can be used as local coordinates, the first branch is aligned, and we take $\Psi := (\theta_1, \phi_1, \psi)$ as our local coordinates, where θ_1 and ϕ_1 are as in Case II above, and ψ denotes the angle between $\mathbf{a}^{(1,2)}$ and $\mathbf{x}^{(2)}$ (see Figure 3.3.1). Note that this will not work when the second branch is also aligned, since these coordinates only determine the length of $\mathbf{v}^{(2)}$, and not "elbow up/down" near $\phi_2 = \frac{\pi}{2}(1 + \sigma_2)$.

Here:

$$f(\Psi) \;=\; \|\mathbf{v}_1^{(1)} + \mathbf{v}_2^{(1)}\|^2 \;+\; \|\mathbf{v}^{(1)} + \mathbf{a}^{(1,2)} - \mathbf{x}^{(2)}\|^2 \;+\; \|\mathbf{v}^{(1)} + \mathbf{a}^{(1,3)} - \mathbf{x}^{(3)}\|^2 \;.$$

and since $\mathbf{a}^{(1,2)} = g^{(1,2)}(\cos\psi, \sin\psi)$, we have $\nabla_\Psi(\mathbf{v}^{(1)}) = (-(\mathbf{v}^{(1)})^\perp,\ \frac{(\mathbf{v}_1^{(1)})^\perp \cdot \mathbf{v}_2^{(1)}}{h^{(1)}(\phi_1)^2}\,\mathbf{v}^{(1)},\ 0)$ and $\nabla_\Psi(\mathbf{a}^{(1,j)}) = (0,\ 0,\ -(\mathbf{a}^{(1,j)})^\perp$ for $j = 2, 3$, so:

$$\begin{aligned}
\partial_{\theta_1} f \;&= 2(\mathbf{v}^{(1)})^\perp \cdot ((\mathbf{x}^{(2)} + \mathbf{x}^{(3)}) - (\mathbf{a}^{(1,2)} + \mathbf{a}^{(1,3)})) \\
\partial_{\phi_1} f \;&= -\,(\mathbf{v}_1^{(1)})^\perp \cdot \mathbf{v}_2^{(1)}\; \frac{\mathbf{v}^{(1)} \cdot (4\,\mathbf{v}^{(1)} + \mathbf{a}^{(1,2)} + \mathbf{a}^{(1,3)} - \mathbf{x}^{(2)} - \mathbf{x}^{(3)})}{\|\mathbf{v}^{(1)}\|^2} \\
\partial_{\psi} f \;&= (\mathbf{a}^{(1,2)})^\perp \cdot (\mathbf{x}^{(2)} - \mathbf{v}^{(1)}) \;+\; (\mathbf{a}^{(1,3)})^\perp \cdot (\mathbf{x}^{(3)} - \mathbf{v}^{(1)})
\end{aligned} \tag{3.3.11}$$

We are using the coordinates Ψ because the first leg is aligned, so indeed $\partial_{\phi_1} f = 0$. In order for this to be a critical point, we have two additional geometric conditions: the vanishing of $\partial_{\theta_1} f$ implies that the vector connecting the midpoints of sides of the fixed and moving platforms opposite the first vertex – that is, $A := (\mathbf{x}^{(2)} + \mathbf{x}^{(3)})/2$ and $B := (\mathbf{a}^{(2)} + \mathbf{a}^{(3)})/2$ – is aligned with $\mathbf{v}^{(1)}$ (see Figure 3.3.4). On the other hand, the vanishing (in addition) of $\partial_\psi f$ is equivalent to:

$$(\mathbf{v}^{(2)})^\perp \cdot \mathbf{x}^{(2)} \;+\; (\mathbf{v}^{(3)})^\perp \cdot \mathbf{x}^{(3)} \;=\; 0\;, \tag{3.3.12}$$

which means that the areas of the triangles spanned by $\mathbf{v}^{(j)}$ and $\mathbf{x}^{(j)}$ $(j = 2, 3)$ are equal. Such critical points will be refered to as *type III*.

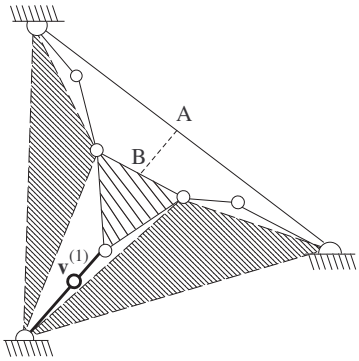

Figure 3.3.4: Type III critical point

Now, calculating the Hessian of f at the critical points we have:

$$\begin{aligned}
\partial_{\theta_1\theta_1} f &= -\ 2\mathbf{v}^{(1)} \cdot ((\mathbf{x}^{(2)} + \mathbf{x}^{(3)}) - (\mathbf{a}^{(1,2)} + \mathbf{a}^{(1,3)})) \\
\partial_{\phi_1\theta_1} f &= \partial_{\phi_1\psi} f \ = \ 0 \\
\partial_{\psi\theta_1} f &= 2\mathbf{v}^{(1)} \cdot (\mathbf{a}^{(1,2)} + \mathbf{a}^{(1,3)}) \\
\partial_{\phi_1\phi_1} f &= \mathbf{v}_1^{(1)} \cdot \mathbf{v}_2^{(1)} \ \frac{\mathbf{v}^{(1)} \cdot (4\,\mathbf{v}^{(1)} + \mathbf{a}^{(1,2)} + \mathbf{a}^{(1,3)} - \mathbf{x}^{(2)} - \mathbf{x}^{(3)})}{\|\mathbf{v}^{(1)}\|^2} \\
\partial_{\psi\psi} f &= \mathbf{a}^{(1,2)} \cdot (\mathbf{x}^{(2)} - \mathbf{v}^{(1)}) \ + \ \mathbf{a}^{(1,3)} \cdot (\mathbf{x}^{(3)} - \mathbf{v}^{(1)})
\end{aligned}$$

Again, generically the critical point is non-degenerate. □

3.3.2. Identifying the critical points.

Since we usually have no explicit description of the configuration space $\mathcal{C}$ as a manifold, it is hard to calculate the Morse function $f : \mathcal{C} \to \mathbb{R}$ directly. However, in the course of proving Theorem 3.2.2 we gave a geometric description of each of the possible critical points of f – which are the main ingredient needed for analyzing the topology of $\mathcal{C}$ – in terms of the work space $\mathcal{W}$. We can use this geometric information in order to identify all possible candidates for critical points, and then we need only calculate df in local coordinates at these points (also provided in the proof above) to check if they are indeed critical, and find their indices.

Recall that $\mathcal{W}$ (Definition 3.1.6) is the space of all possible locations of the moving platform $\mathcal{P}$, whose vertices must be situated in the respective work spaces $\mathcal{W}_i$ $(i = 1, 2, 3)$ of (the end points of) the three branches. Each $\mathcal{W}_i$ is an annulus centered at the i-the vertex $\mathbf{x}^{(i)}$ of the fixed triangle.

Also recall the concept of the *coupler curve* γ of a planar four-bar linkage - that is, a degenerate polygonal mechanism with $k = 2$ linear branches $(n^{(1)} = n^{(2)} = 1)$, but having a triangular platform $\mathcal{P}$: the coupler curve is the work space for the third (unattached) vertex of $\mathcal{P}$. See [Hal, Ch. 4]. We consider the coupler curves for two vertices $\mathbf{x}^{(i)}$ (say $i = 1, 2$) of a triangular mechanism $(\mathcal{L}, \mathcal{X}, \mathcal{P})$ as above, in which the two corresponding branches are aligned, so that each can be replaced by a single linear branch of length $\ell^{(i)} := \ell_1^{(i)} + \ell_2^{(i)}$ or $\ell_1^{(i)} - \ell_2^{(i)}$, as the case may be.

(1) The critical points of type I (all three branches aligned) correspond to placements of $\mathcal{P}$ with all three vertices on the (inner or outer) boundary circles of these annuli. Determining these is a straightforward geometric problem, which can be described as intersecting the coupler curve for the first two vertices, say, with the two boundary circles of $\mathcal{W}_3$.

(2) For critical points of type II, we need also a line field V along the coupler curve γ, where $V(\gamma(t))$ is the line from $\gamma(t)$ to the intersection point $P(t)$ of $\text{Line}^{(1)}$ with $\text{Line}^{(2)}$. This line field is readily calculated from γ. The critical points are then those configurations for which $V(\gamma(t))$ passes through $\mathbf{x}^{(3)}$.

(3) For critical points of type III, the first vertex $\mathbf{v}^{(1)}$ of $\mathcal{P}$ must lie on one of the two boundary circles of $\mathcal{W}_1$. Given $\mathbf{v}^{(1)}$, the possible positions of $\mathcal{P}$ are determined by its rotation angle θ around its first vertex, and at most two values θ', θ'' of θ satisfy condition (3.3.12). Thus we can define on $\partial\mathcal{W}_1$ two line fields V', V'' which associate to $\mathbf{v}^{(1)}$ the line between the midpoints of the $(2, 3)$-side of the fixed and moving triangles in the positions corresponding to θ', θ'' respectively. The critical points are those for which the vector $\mathbf{v}^{(1)}$ lies on one of these two lines.

Example 3.3.3. In general, the critical points of a manifold do not determine its topology, though they impose certain restrictions on its homology, and thus on its homotopy type, via the Morse inequalities. However, in the simplest cases the geometric considerations described above limit the possible critical points so severely that the configuration space $\mathcal{C}$ can be recovered in full. Note that there are two connected components in $\mathcal{C}$, determined by the orientation of the moving platform.

For example, consider a triangular mechanism with one branch (say, $k = 3$) having one very large link, so that the work space for the vertex $\mathbf{p}^{(3)}$ contains those for all points of the moving platform, and thus imposes no restriction on the allowed configurations. We assume the moving platform is a small triangle, and that the work space for (the vertex of) the first branch is a small annulus, intersecting that of the second branch in a crescent-shaped lune, which is the approximate "work space" for the moving platform (i.e., for its barycenter). Finally, assume that the fixed vertex $\mathbf{x}^{(3)}$ is far to the left (see Figure 3.3.5).

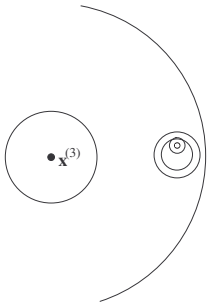

Figure 3.3.5: Work spaces for the three moving vertices

Now we may analyze the possible critical points as follows:

(1) Since the two small annuli above are wholly contained in the large one, and the moving platform is small, there are no critical points of type I.

(2) Note that since the linkage is not Grashof (cf. [11]), there are exactly two cases where $\text{Line}^{(1)}$ meets $\text{Line}^{(2)}$ on the inner boundary circle of the work space

for vertex 2. Since $g^{(23)}$ is very small, any critical points of type II must occur nearby, so that the edges $\mathbf{a}^{(12)}$ and $\mathbf{a}^{(13)}$ (which nearly coincide) are aligned with $\mathbf{v}^{(1)}$ (see Figure 3.3.6).

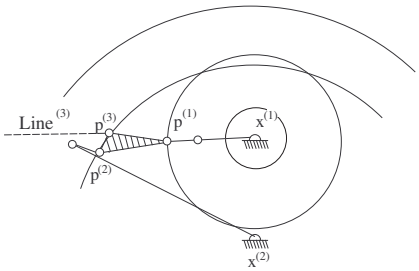

Figure 3.3.6: A critical point of type II

By choosing appropriate generic values for the parameters, we can ensure that there are exactly two critical of type II in each component of $\mathcal{C}$.

(3) Consider the three dashed lines $L^{(k)}$ in Figure 3.3.7, each connecting $\mathbf{x}^{(k)}$ with the midpoint of opposite (fixed) edge (for $k = 1, 2, 3$). Because the moving triangle is so small, the vector $\mathbf{v}^{(k)}$ must approximate the direction of $L^{(k)}$ in order to obtain a critical point of type III – but since these lines do not pass near the approximate work space for the moving platform, no such critical points can occur.

Thus each component of the configuration space $\mathcal{C}(\mathcal{L}, \mathcal{X}, \mathcal{P})$ has exactly two critical points in this case (both of type II), so it is homeomorphic to S^3.

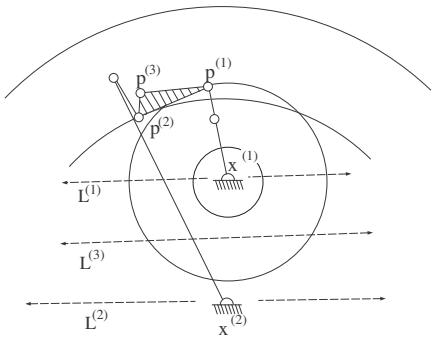

Figure 3.3.7: Potential critical points of type III

Chapter 4

Uncertainty singularities in parallel mechanisms

Submitted to *IEEE Transactions on Robotics*, 2006.
Co-authors: David Blanc and Moshe Shoham.

We study singularities for a parallel mechanism with spherical joints and moving planar platform, giving a necessary condition for an uncertainty singularity (defined topologically, in terms of the configuration space) to occur, and describe the corresponding instantaneous kinematic singularity. An explicit example is provided.

4.1 Introduction

Kinematic singularities of parallel mechanisms have been studied extensively in the literature (cf. [52], and [53, 54] for the example of open kinematic chains). On the other hand, many authors have investigated *topological* singularities of the configuration spaces of such mechanisms (see, e.g., [11, 12, 14, 27]).

In this note, we study parallel mechanisms with rotational joints and planar moving platform, and give a necessary geometric condition for uncertainty singularities in

such mechanisms (Theorem 4.2.3). We then explain how such topological singularities give rise to instantaneous kinematic singularities (Proposition 4.3.1). Finally, the occurence of an uncertainty singularity is illustrated visually in an explicit example (Section 4.4).

4.1.1 Topological singularities

By choosing appropriate local coordinates for a given mechanism Γ, we can think of the set of all its configurations as a topological space $\mathcal{C}$, called its *configuration space*, and try to endow it with the structure of a differentiable manifold. The points of $\mathcal{C}$ where this cannot be done constitute the *topological singularities* of Γ. See Section 4.2 below for further details.

These are refered to in the robotics literature as *uncertainty singularities*: they occur when the *instantaneous* mobility is greater than the *full cycle* mobility (cf. [52]). In such a position the mechanism as a whole gains an additional degree of freedom. At times, such singularities are the only point where two disjoint regions of $\mathcal{C}$ meet, allowing transition between different operating modes. See [55] for an examination of such transitions in the case of a constraint singularity for a 3-URU 3-DOF parallel mechanism.

4.1.2 Kinematic singularities

In general, a configuration $\mathcal{V}$ is naturally described by the vector $\mathbf{x} = (x_1, \ldots, x_N)$ whose coordinates x_i correspond to the positions of the various joints and links of the mechanism. In practice, we choose a subset $\mathbf{x}_{\text{in}}$ of *input* coordinates (corresponding to the actuated joints), which can serve as local coordinates for $\mathcal{C}$ around $\mathcal{V}$. In addition, we often focus on a subset $\mathbf{x}_{\text{out}}$ of *output* coordinates of interest (which may describe the position of the end effector). The structure of the mechanism imposes relations which must hold among the coordinate x_i; in particular, we may assume that:

$$F(\mathbf{x}_{\text{in}}, \mathbf{x}_{\text{out}}) = 0 \tag{4.1.1}$$

identically in a neighborhood of $\mathcal{V}$ in $\mathcal{C}$. The Jacobian $J := \frac{\partial F}{\partial \mathbf{x}}$ consists of two blocs $\frac{\partial F}{\partial \mathbf{x}_{\text{in}}}$ and $J_{\text{out}} := \frac{\partial F}{\partial \mathbf{x}_{\text{out}}}$, where J_{out} must be nonsingular if the $\mathbf{x}_{\text{in}}$ are to serve as local coordinates near $\mathcal{V}$.

The kinematics of the mechanism are described by a path $\mathbf{x}(t)$ $(t \in \mathbb{R})$ in the configuration space. Differentiating (4.1.1) with respect to t we get $\frac{\partial F}{\partial \mathbf{x}} \dot{\mathbf{x}} = 0$, which can be written in the form:

$$J_{\text{in}} \, \dot{\mathbf{x}}_{\text{in}} \;=\; J_{\text{out}} \, \dot{\mathbf{x}}_{\text{out}} \tag{4.1.2}$$

where $J_{\text{in}} := -\frac{\partial F}{\partial \mathbf{x}_{\text{in}}}$. If J_{out} is of maximal rank and J_{in} is not, $\mathcal{V}$ is called a kinematic singularity *of type I*: this means that we cannot obtain every (infinitesimal) change in output we may want by an appropriate change in the actuated joints. On the other hand, if J_{in} is of maximal rank and J_{out} is not, $\mathcal{V}$ is called singular of *of type II*: in this case the actuated joints do not determine uniquely the behavior of the outputs. Finally, if neither J_{out} nor J_{in} is of maximal rank, $\mathcal{V}$ is called singular *of type III* (cf. [5]). Gosselin and Angeles give examples of all three types of singularities for a parallel 3-RRR planar mechanism.

However, as Zlatanov, Fenton and Benhabib observe, the choice of $\mathbf{x}_{\text{in}}$ and $\mathbf{x}_{\text{out}}$ is arbitrary; moreover, in general it need not fully determine the mechanism, which may have additional "passive coordinates" of interest. They therefore provide a different approach to the singularity analysis of an arbitrary kinematic chain (see [56]).

4.2 Topological singularities

We consider *polygonal* mechanism Γ in $\mathbb{R}^d$ $(d = 2, 3)$, consisting of a moving platform $\mathcal{P}$ (planar k-polygonal), with k branches attached to its vertices. The i-th branch is a sequence of $n^{(i)}$ concatenated links of lengths $\ell_j^{(i)}$ $(j = 1, \dots n^{(i)})$, connected by spherical joints. One end of the branch is attached to a vertex of the moving platform, and the other is fixed at $\mathbf{x}^{(i)} \in \mathbb{R}^d$.

Definition 4.2.1. A *configuration* for an n-link branch consists of n vectors $(\mathbf{v}_1, \dots, \mathbf{v}_n)$ in $\mathbb{R}^d$ of specified lengths $\|\mathbf{v}_j\| = \ell_j$ $(j = 1, \dots n)$.

A branch configuration is said to be *aligned* if all the vectors $\mathbf{v}_i$ are scalar multiples of $\mathbf{v}$, which is called the *direction vector* of V. The *direction line* for V is $\text{Line} := \{\mathbf{x} + t\mathbf{v} \mid t \in \mathbb{R}\}$.

A configuration for Γ consists of a set $\mathcal{V} = (V^{(1)}, \ldots, V^{(k)})$ of configurations for each of the k branches, such that the k endpoints

$$\mathbf{p}^{(i)} := \mathbf{x}^{(i)} + \sum_{i=1}^{n} \mathbf{v}_i \quad (i = 1, \ldots, k)$$

of the corresponding branch configurations form a polygon congruent to the given moving platform $\mathcal{P}$. The set $\mathcal{C} = \mathcal{C}_\Gamma$ of all such configurations, topologized in the obvious way, is the *configuration space* of Γ.

Convention: Parenthesized superscripts indicate the branch number, and subscripts indicate the link number. For example, $\ell_j^{(i)}$ denotes the length of the j-th link of the i-th branch.

Definition 4.2.2. A configuration $\mathcal{V}$ for Γ is called *singular of type (a)* if two of its branch configurations $V^{(i_1)}$ and $V^{(i_2)}$ are aligned, with coinciding direction lines: $\text{Line}^{(i_1)} = \text{Line}^{(i_2)}$. See Fig. 4.2.1.

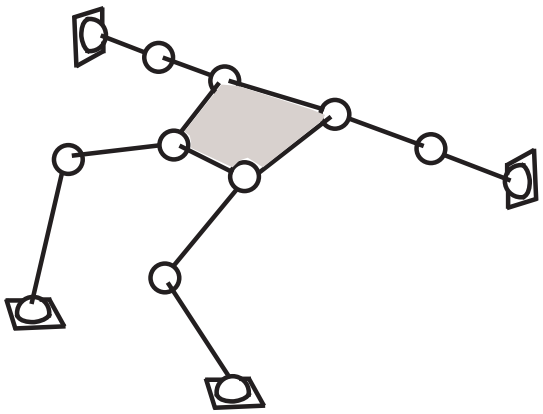

Figure 4.2.1: A singular configuration of type (a)

It is *singular of type (b)* if three of its branch configurations are aligned, with direction lines in the same plane meeting in a single point (this is referred to in literature as a *flat pencil*). See Fig. 4.2.2.

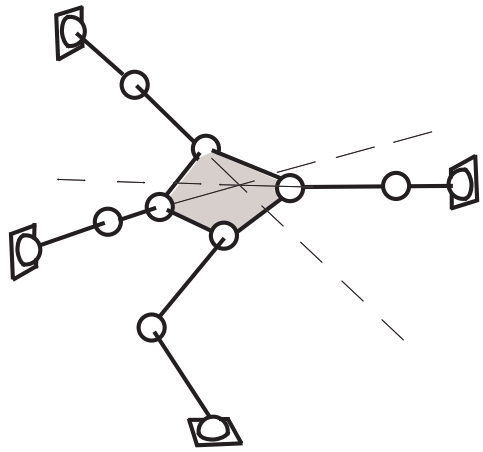

Figure 4.2.2: A singular configuration of type (b)

It is *singular of type (c)* if four of its branch configurations are aligned, with direction lines in the same plane.

We can now formulate our main result:

Theorem 4.2.3. *A necessary condition for a configuration* $\mathcal{V} = (V^{(1)}, \ldots, V^{(k)})$ *of a polygonal mechanism* Γ *to be an uncertainty singularity is that it be singular of type (a), (b) or (c).*

Examples 4.2.4. Before sketching the proof, consider the following two examples:

(1) If $\mathcal{V}$ is singular of type (a), as in Fig. 4.2.1, we can construct an open neighborhood $U \subset \mathcal{C}$ of $\mathcal{V}$ as a product $U_{\text{aligned}} \times U_{\text{rest}}$. Here U_{aligned} may be identified with an neighborhood of $\mathcal{V}$ in the configuration space of a closed chain mechanism Γ', consisting of the aligned branches of Γ. In the case where the aligned branches have one and two links respectively, U_{aligned} is a one-point union of two 2-discs (see [57, Proposition 4.1]), so it is singular.

On the other hand, U_{rest} is a neighborhood of $\mathcal{V}$ in the configuration space of the mechanism obtained from Γ by omitting the aligned branches, which is non-singular (generically).

(2) Consider a mechanism with a triangular platform, and two branches with one

link each. In this case, the workspace for the third vertex of the platform is the coupler curve γ for the corresponding 4-chain mechanism (see [Hal, Ch. 4]), while the workspace for the third branch is an annulus A.

For suitable parameters, the boundary ∂A (where the third branch is aligned) will be tangent to γ. The corresponding configuration $\mathcal{V}$ for Γ will be singular of type (b), as in Fig. 4.2.3.

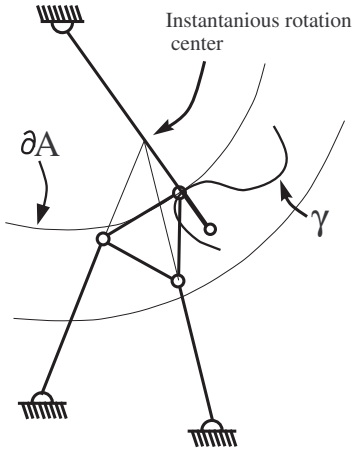

Figure 4.2.3: Coupler curve tangent to branch workspace boundary

Note that near $\mathcal{V}$ each point in γ has two corresponding configurations, associated to "elbow up/down" positions of the third branch, which coalesce at $\mathcal{V}$ itself; thus $\mathcal{V}$ has a singular neighborhood consisting of two transverse intervals.

Sketch of proof of Theorem 4.2.3:

A configuration $\mathcal{V}$ for the polygonal mechanism Γ in $\mathbb{R}^d$ $(d = 2, 3)$ is determined by the Nd Cartesian coordinates of the endpoints of the $N = \sum_{i=1}^{k} n^{(i)}$ links of Γ. However, there are $M := N + dk - 3(d-1)$ relations among these imposed by the lengths of the links and a certain minimal collection $\mathcal{I}$ of edges and diagonals of the polygonal platform $\mathcal{P}$. Thus the configuration space $\mathcal{C}$ is the preimage of a certain

vector $Z \in \mathbb{R}^M$ under the *constraint map* $F : \mathbb{R}^{dN} \to \mathbb{R}^M$, defined:

$$\begin{aligned} F(\mathcal{V}) \ :=& (f_{n^{(1)}}(V^{(1)}), \ldots, f_{n^{(k)}}(V^{(k)}), \\ & \|\mathbf{a}^{(1,2)}\|^2, \ldots, \|\mathbf{a}^{(k-1,k)}\|^2) \ , \end{aligned} \tag{4.2.1}$$

where $f_n(\mathbf{v}_1, \ldots, \mathbf{v}_n) := (|\mathbf{v}_1|^2, \ldots, |\mathbf{v}_n|^2)$ and $\mathbf{a}^{(i,j)}$ is the (i,j)-diagonal (or edge) of $\mathcal{P}$ spanned by the endpoints of branches i and j.

Step I. By the Regular Value Theorem, $\mathcal{C}$ will be a smooth manifold if $\mathrm{dF}_{\mathcal{V}}$ is of rank M, where $\mathrm{dF}_{\mathcal{V}}/2$ is:

$$\begin{pmatrix} A^{(1)} & 0 & 0 & \ldots & 0 \\ 0 & A^{(2)} & 0 & \ldots & 0 \\ \vdots & \vdots & \vdots & \ddots & \vdots \\ 0 & 0 & 0 & \ldots & A^{(k)} \\ \vec{\mathbf{b}}^{(1,2)} & \vec{\mathbf{b}}^{(2,1)} & 0 & \ldots & 0 \\ \vec{\mathbf{b}}^{(1,3)} & 0 & \vec{\mathbf{b}}^{(3,1)} & \ldots & 0 \\ 0 & \vec{\mathbf{b}}^{(2,3)} & \vec{\mathbf{b}}^{(3,2)} & \ldots & 0 \\ \vdots & \vdots & \vdots & \ddots & \vdots \\ 0 & \ldots & 0 & \ldots & \vec{\mathbf{b}}^{(k,k-1)} \end{pmatrix} \tag{4.2.2}$$

and $A^{(i)}$ is the $n^{(i)} \times dn^{(i)}$ matrix:

$$\begin{pmatrix} \mathbf{v}_1^{(i)} & \ldots & 0 \\ \vdots & \ddots & \vdots \\ 0 & \ldots & \mathbf{v}_{n^{(i)}}^{(i)} \end{pmatrix} \ . \tag{4.2.3}$$

Each edge $\mathbf{a}^{(i,j)} \in \mathbb{R}^d$ appears $n^{(i)}$ times in the vector

$$\vec{\mathbf{b}}^{(i,j)} \ := \ \underbrace{(\mathbf{a}^{(i,j)}, \mathbf{a}^{(i,j)}, \ldots, \mathbf{a}^{(i,j)})}_{n^{(i)}} . \tag{4.2.4}$$

Step II. Let $\mathcal{V} \in \mathcal{C} = F^{-1}(Z)$, and consider a vanishing linear combination of the rows of $\mathrm{dF}_{\mathcal{V}}$. If some row of $A^{(i)}$ has a non-zero coefficient, so does at least one

of the $M-N$ bottom rows; but since these are all repeated, as in (4.2.4), we see that all the direction vectors $\mathbf{v}_j^{(i)}$ for the i-th branch must be equal – that is, this branch is aligned, with the direction vector $\mathbf{v}^{(i)}$ a linear combination of appropriate diagonals $\mathbf{a}^{(k,\ell)}$ of $\mathcal{P}$, and thus lying in the plane $\mathcal{E}$ determined by $\mathcal{P}$.

Moreover, from (4.2.2) we see that $\sum_{i=1}^{k} \mathbf{v}^{(i)} = \mathbf{0}$. Therefore, if $\mathbf{v}^{(i)} = \mathbf{0}$ for $i \neq i_0, i_1$, then $\mathbf{v}^{(i_0)} + \mathbf{v}^{(i_1)} = \mathbf{0}$, and thus branches i_0 and i_1 are co-aligned with direction vector $\mathbf{a}^{(i_0,i_1)}$, yielding a singularity of type (a).

On the other hand, if at least four branches are aligned (with direction vectors in E), we obtain a singularity of type (c).

Step III. Now assume we have exactly three aligned branches, say $1, 2$ and k. Let $\hat{\mathcal{C}}$ denote the configuration space of the mechanism obtained by omitting the last (k-th) branch – again given as the fiber of an appropriate constraint map $\hat{F} : \mathbb{R}^{(N-n^{(k)})d} \times \mathcal{S} \to \mathbb{R}^K$ (where $\mathcal{S} = S^{d-2}$ if $k = 3$, and a point otherwise), with $\hat{\imath} : \hat{\mathcal{C}} \to \mathbb{R}^{(N-n^{(k)})d}$ the inclusion. Similarly, let $\mathcal{C}(k)$ be the configuration space for the k-th branch (an $n^{(k)}$-torus, with the obvious embedding $i : \mathcal{C}(k) \to \mathbb{R}^{n^{(k)}d}$).

The *workspace* of both mechanisms – that is, the possible locations for the k-th vertex of the moving platform – are in $\mathbb{R}^d$, and we denote the *work maps* by $\psi : \hat{\mathcal{C}} \to \mathbb{R}^d$ and $\phi : \mathcal{C}(k) \to \mathbb{R}^d$.

Let $X := \mathcal{C}(k) \times \mathbb{R}^{(N-n^{(k)})d} \times \mathcal{S}$, $Y := \mathbb{R}^d \times \mathbb{R}^{(N-n^{(k)})d} \times \mathcal{S}$, and define $h : X \to Y$ to be the product map $\phi \times \mathrm{Id}$, and $g : \hat{\mathcal{C}} \to Y$ to be $(\psi, \hat{\imath})$. Thus $\mathcal{C}$ (the configuration space for Γ) is the preimage of the submanifold $\hat{\mathcal{C}} \subseteq Y$ under h.

Let $\hat{\mathcal{V}} \in \hat{\mathcal{C}}$ be a configuration where branches 1 and 2 are aligned, with distinct direction vectors ω_1, ω_2 in $\mathcal{E}$ (the plane of $\mathcal{P}$), and let $V^{(k)} \in \mathcal{C}(k)$ be an aligned configuration with direction vector $\omega_k \in \mathcal{E}$. Assume that $\psi(\hat{\mathcal{V}}) = \phi(V^{(k)})$, and let $\mathbf{x} \in X$ be the configuration $(V^{(k)}, \hat{\imath}(\hat{\mathcal{V}}))$.

To prove Theorem 4.2.3, we must show that if the point $\mathcal{V} \in \mathcal{C}$ defined by $(\hat{\mathcal{V}}, V^{(k)})$ is not singular of type (b), then it is smooth. This would follow if h is locally transverse to $\hat{\mathcal{C}}$ at the points $\mathbf{x} \in X$ and $\hat{\mathcal{V}} \in \hat{\mathcal{C}}$, in other words:

$$\mathrm{Im}\, \mathrm{d}h_{\mathbf{x}} \; + \; T_{\hat{\mathcal{V}}}(\hat{\mathcal{C}}) \; = \; T_{\hat{\mathcal{V}}}(Y) \; . \tag{4.2.5}$$

But $T_{V^{(k)}}(\mathcal{C}(k))$ is just the null space of $A^{(k)}$ of (4.2.3), namely: $(\omega_k^{\perp})^n$, so it suffices to prove that $\omega_k \in T_{\hat{\mathcal{V}}}(\hat{\mathcal{C}})$. Choose unit vectors $\mathbf{c}^{(i)}$ spanning $\omega_i^{\perp}$ $(i = 1, 2)$ in $\mathcal{E}$; then $\omega_k \notin T_{\hat{\mathcal{V}}}(\hat{\mathcal{C}})$ only if ω_k is proportional to: $(\mathbf{a}^{(1,2)} \cdot \mathbf{c}^{(2)})\, \omega_1 - (\omega_1 \cdot \mathbf{c}^{(2)})\, \mathbf{a}^{(1,3)}$, which is the vector connecting the meeting point of $\mathrm{Line}^{(1)}$ and $\mathrm{Line}^{(2)}$ with the end point of $V^{(k)}$. See [57] for the details. □

4.3 Kinematic singularities

Theorem 4.2.3 gives a *necessary* condition for a configuration to be singular (topologically): namely, that some subset $\{i_1, \ldots, i_m\}$ of its branches be aligned, with direction lines $(\mathrm{Line}^{(i_j)})_{j=1}^m$. Moreover, the Plücker line coordinates of these lines must span certain types of *varieties*, of positive codimension in $\mathbb{R}^6$ (see [58, §5]).

We now show how uncertainty singularities give rise to kinematic singularities, for the polygonal mechanism discussed in Section 4.2.

4.3.1 Mechanism architectures

Recall from §4.1.2 that the latter require an *actuation input choice* – that is, a choice of input coordinates $\mathbf{x}_{\mathrm{in}}$ (corresponding to the actuated joints), and output coordinates $\mathbf{x}_{\mathrm{out}}$ (corresponding to the end effector of the mechanism: in our case, the position and orientation of the moving platform).

For the spatial case (i.e., Γ embedded in $\mathbb{R}^3$, and having spherical joints), there are three architectures to consider as a result of platform mobility considerations:

(a) Six branches $\{i_1, \ldots, i_6\} \subseteq \{1, \ldots, k\}$, where the j-th branch has $n^{(i_j)} - 1$ spherical actuators (say, at all joints but the last two).

(b) One branch i_1 having a total of $n^{(i_1)}$ spherical actuators (at each joint but the last); and three more branches i_2, i_3, and i_4, with $n^{(i_j)} - 1$ spherical actuators in the j-th branch $(j = 2, 3, 4)$.

(c) Two branches i_1, i_2 with actuators at each joint but the last; and one more branch i_3 with $n^{(i_3)} - 1$ spherical actuators.

4.3.2 Kinematic analysis through screw theory

We use screw theory (see [62]) to describe the forces operating at each joint of our mechanism:

A *screw* \$ is a Plücker vector in $\mathbb{R}P^5$, describing a line – or equivalently, the position and direction of vector – in $\mathbb{R}^3$ (cf. [58, §5]). Thus Fig. 4.3.1 depicts the equivalent kinematic chain of an arbitrary branch i of a mechanism, where the movement of each spherical joint j is described by three unit screws $\$_{j,1}^{(i)}$, $\$_{j,2}^{(i)}$, and $\$_{j,3}^{(i)}$ attached to its center. Note that just before a passive joint, we can make do with two screws.

Considering the i-th branch as an open chain, we can express the instantaneous twist of the end-effector as:

$$\$_p \;=\; \sum_{j=0}^{n^{(i)}} \sum_{k=1}^{3} \$_{j,k}^{(i)} \cdot \dot{\theta}_{j,k}^{(i)} \tag{4.3.1}$$

where $\theta_{j,k}^{(i)}$ is the input coordinate for the $\$_{j,k}^{(i)}$ screw (cf. [59, §5.6]).

In order to rid (4.3.1) of the passive joints, for the i-th branch, we must multiply both sides by appropriate reciprocal screws. More precisely, choose a basis $\{\$_t^{(i)\perp}\}_{t=1}^{\lambda^{(i)}}$ for the space $V^{(i)}$ of common reciprocals of the screws of all passive joints for this branch:

(a) If the branch has $n^{(i)} - 1$ spherical actuators, at all joints but the last two, the reciprocal screw for these two joints corresponds to the line passing through them (i.e., $V^{(i)}$ is one-dimensional).

(b) If the branch has $n^{(i)}$ spherical actuators, at all but the last joint, $V^{(i)}$ is 3-dimensional, with the corresponding lines all passing through the last joint (see [59, Ch. 5]).

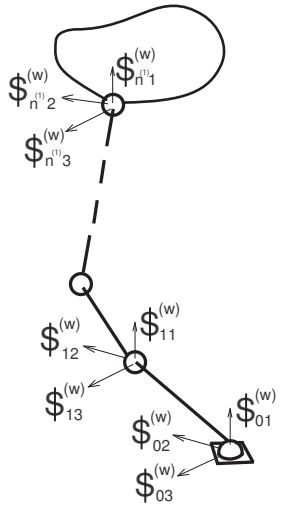

Figure 4.3.1: Equivalent kinematic structure of a branch

For the i-th branch we obtain a system of $\lambda^{(i)}$ linear equations for $\$_p$:

$$\$_t^{(i)\perp} \cdot \$_p \;=\; \sum_{j=0}^{n^{(i)}} \sum_{k=1}^{3} \$_t^{(i)\perp} \cdot \$_{j,k}^{(i)} \cdot \dot{\theta}_{j,k}^{(i)} \tag{4.3.2}$$

$(t = 1, \ldots, \ell^{(i)})$, in which of course the unactuated inputs $\dot{\theta}_{j,k}^{(i)}$ have zero coefficient.

Combining the $\lambda = \sum_{i=1}^{k} \lambda^{(i)}$ equations (4.3.2) for all k branches, we obtain equation (4.1.2) for the chosen architecture ($\lambda = 6$ for the first two, and $\lambda = 7$ for the third).

The $\lambda \times 6$ matrix J_{out} will take the form:

$$J_{\text{out}} = \begin{pmatrix} \$_1^{(1)\perp} \\ \vdots \\ \$_{\lambda^{(1)}}^{(1)\perp} \\ \vdots \\ \$_{\lambda^{(k)}}^{(k)\perp} \end{pmatrix} \tag{4.3.3}$$

whose rows are the reciprocal screws of all actuated branches.

The matrix J_{in} is bloc-diagonal:

$$J_{\text{in}} = \begin{pmatrix} A^{(i_1)} & \dots & 0 \\ \vdots & \ddots & \vdots \\ 0 & \dots & A^{(i_k)} \end{pmatrix},$$

with the i-th bloc (for the i-th actuated branch, with d passive joints) a $\lambda^{(i)} \times (n^{(i)} - d)$ matrix of the form:

$$A^{(i)} := \begin{pmatrix} \$_1^{(i)\perp} \cdot \$_{0,1}^{(i)} & \dots & \$_1^{(i)\perp} \cdot \$_{n^{(i)}-d,3}^{(i)} \\ \vdots & & \vdots \\ \$_{\lambda^{(i)}}^{(i)\perp} \cdot \$_{0,1}^{(i)} & \dots & \$_{\lambda^{(i)}}^{(i)\perp} \cdot \$_{n^{(i)}-d,3}^{(i)} \end{pmatrix}.$$

Proposition 4.3.1. *For a polygonal mechanism Γ (with no unactuated branches), there is an instantaneous kinematic singularity of type I or III at any uncertainty singularity.*

Proof. At an uncertainty singularity at least two branches are aligned, so the reciprocals to the passive joint(s) are reciprocal to all screws of these branches, and thus $A^{(i)} = 0$ for these branches. Since $\lambda \leq 7$, J_{in} is singular.

Now by Theorem 4.2.3, an uncertainty singularity can have:

1. Two coaligned branches, each with a pair of unactuated joints: they have a common reciprocal (and $\lambda = 6$), so J_{out} has rank ≤ 5. The same holds in the second architecture whenever two branches are coaligned.

2. Three aligned branches whose lines lie in a planar pencil, each with a pair of unactuated joints: in this case the corresponding screws are linearly dependent, so again J_{out} has rank ≤ 5.

3. Four aligned branches whose lines are in one plane: the lines of those with a pair of unactuated joints each lie in a planar pencil (rank 3). In the first architecture, the last two lines each add at most 1 to the rank; in the second, adding the last line form a degenerate congruence (total rank 4). Thus in any case J_{out} has rank ≤ 5.

□

4.4 An illustrative example

We now give an visual presentation of an uncertainty singularity in an explicit 3-URU 3-DOF mechanism Γ, introduced in [17].

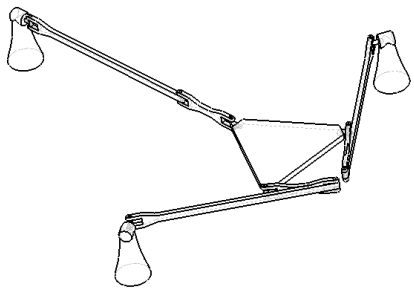

Figure 4.4.1: Singular config. for a 3-DOF 3-URU mechanism

The centers of the three U-joints at the base (platform) form an equilateral triangle. The three R-joint axes fixed in the base (platform) meet (not at the center of the base(platform) triangle) in a "Y" shape. The three intermediate R joints in each branch are all parallel.

Remark 4.4.1. To enable visualization near the singular configuration $\mathcal{V} \in \mathcal{C}$, we need a mechanism with instantaneous mobility near $\mathcal{V}$ equal to 3. We therefore make sure that the intersection point of the three R-joint axes avoids the center of the base platform (otherwise mobility would be increased by the additional spin dexterity of the extended branch).

In the region in $\mathcal{C}$ where Γ acts as a planar mechanism (see [61]), the pose of the moving platform $\mathcal{P}$ (an equilateral triangle) is determined by two coordinates (say, x and y) of its barycenter $\mathbf{p}$, and its planar rotation ϕ. Denote by r the common distance $d(\mathbf{p}, \mathbf{p}^{(i)})$ $(i = 1, 2, 3)$.

The work space for each vertex $\mathbf{p}^{(i)}$ of $\mathcal{P}$ is an annulus $\mathcal{A}^{(i)}$ centered at the fixed endpoint $\mathbf{x}^{(i)}$ of the i-th branch, with radii $\ell_1^{(i)} \pm \ell_2^{(i)}$ respectively. Thus if

we fix the orientation ϕ of $\mathcal{P}$, the resulting constrained work space $\mathcal{W}_\phi$ for $\mathbf{p}$ (the shaded area in Fig. 4.4.2) is the intersection of three annuli (with centers at $T^{(i)}$): namely, the displacements $\hat{\mathcal{A}}^{(i)}$ $(i = 1, 2, 3)$ of $\mathcal{A}^{(i)}$ by a vector $\mathbf{p}^{(i)}\mathbf{p} = \mathbf{x}^{(i)}T^{(i)}$ of length r.

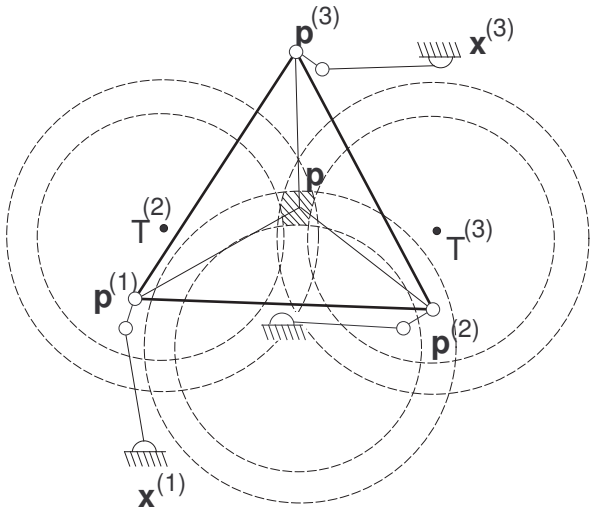

Figure 4.4.2: constrained work space $\mathcal{W}_\phi$ for $\mathbf{p}$ with fixed ϕ

Thus $\mathcal{C}$ is described in the vicinity of $\mathcal{V}$ by the location of $\mathbf{p}$ in $\mathcal{W}_\phi$ and the orientation $\phi \in I$. Generically, the work spaces $\mathcal{W}_\phi$ will all be homeomorphic to a fixed space $\mathcal{W}'$ for nearby values of ϕ, so that a neighborhood of $\mathcal{V}$ will be a topological product $I \times \mathcal{W}'$. However, for some values of ϕ, $\mathcal{W}_\phi$ may vanish, so a larger neighborhood U of $\mathcal{V}$ need not be connected (see Fig. 4.4.3).

In addition, we need discrete data on the elbow up/down position of each branch at $\mathcal{V}$, so the relevant region of $\mathcal{C}$ will actually contain eight identical copies of U, each consisting of one or more product "boxes" as above. Since the boundaries of $\mathcal{W}_\phi$ are at the boundaries of the annuli $\hat{\mathcal{A}}^{(i)}$, where the links of the i-th branch are aligned, the faces of each box are identified with a corresponding face in another box. The aligned poses can be calculated analytically using the algorithm in Gosselin and Merlet (cf. [60]), since each of the extreme situations can be treated as an equivalent 3-RPR robot, whose link lengths are fixed and known.

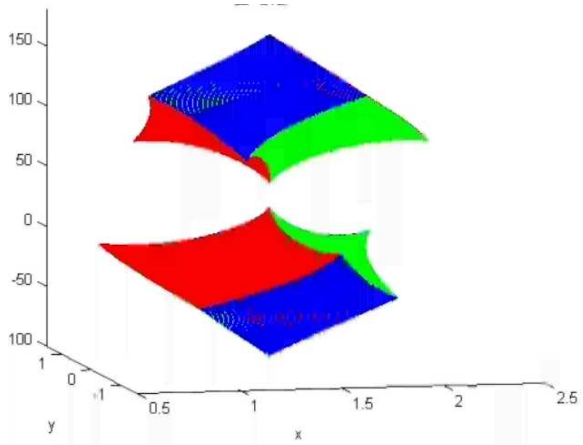

Figure 4.4.3: configuration space for 3-RRR mechanism

For example, gluing faces for the situation depicted in Fig. 4.4.3 yields two 3-tori. (Of course, this is only true in the region where the mechanism platform motion is planar – see Remark 4.4.1; so all we can conclude about $\mathcal{C}$ near $\mathcal{V}$ is that it has two connected components, locally isomorphic to $\mathbb{R}^3$.)

As the parameters vary, we find that the two connected components of U approach each other, and for an appropriate value they touch at one point (see Fig. 4.4.4). As a result, $\mathcal{C}$ is now locally homeomorphic to $\mathbb{R}^3 \vee_{\mathcal{V}} \mathbb{R}^3$ that is a singular point where two regions meet.

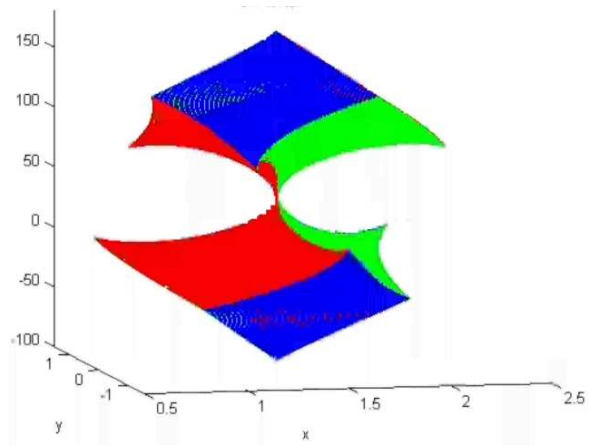

Figure 4.4.4: configuration space is locally $\mathbf{T}^3 \vee_c \mathbf{T}^3$

4.5 Conclusions

In this paper we derive necessary conditions for the existence of topological (uncertainty) singularities in a class of spatial and planar robots having arbitrary number of legs and arbitrary number of spherical joints in each leg, all attached to a moving planar platform. We conclude that a topological singularity emerges when one of the following holds: two legs are aligned and have common direction, three legs are aligned and form a flat pencil or when four legs are aligned and lie in the same plane.

We then relate these topological singular points with the well known kinematics ones.

Lastly, these results are used in an illustrative example for a topological singular point, where intrinsically the robot actuation is not sufficient - regardless of the actuators placements.

Chapter 5

Discussion

Recently a growing interest has arise applying toplogy theory to Robotics in general and to parallel robots configuration spaces in particular. To this end, main focus had been set on the configuration spaces of a type of robot called *polygonal linkage*, which is simply a concatenation of links and hinged joints forming a closed chain, obviously these are of limited practical use. Generally speaking for a given robot the configuration space dimension equals its mobility, thus for most robots in use the configuration space is of dimension three or more. Furthermore since investigation focuses usually on global properties of the configuration space, common mathematical tools are useless.

In what follows we discuss our investigation generally without getting into detailed mathematics and formal defintions. In order to keep things simple we have started our investigation studying a robot we named *arachnoid mechanism* which admits a two dimensional configuration space if as depicted in Figure 1.1.1. The robot is constructed of k branches fixed at their one end and a common other end for all branches,(the figure depicts a planar robot with branches having only two links while our discussion holds also for the spatial case where each branch may have an arbitrary number of links). Note that this type of mechanism resembles some parallel robots which are in practical use. Our first task was to examine if its configuration space is

a manifold, this could be easily done by applying the regular value theorem (see [50, I, Thm. 3.2]): By identifying the configuration space as the pre-image of a certain map $G : \mathbb{R}^{d(N-k+1)} \to R^N$, that sends each two successive joint loci to their distance and finding the conditions for the jacobian dG to have full rank amounts to Theorem 1.2.1. Thus configuration space of an arachnoid mechanism is generically a closed orientable manifold of dimension $d(N-k+1)-N$, where N is the total number of links in the given mechanism and $d = 2, 3$ for the planar and spatial cases respectively. Furthermore the cases in which this is not true (i.e. the configuration space possess at least one topological singularity) are when two branches (or more) are co-aligned (see Definition 1.1.3,1) or when $d+1$ branches are aligned (Definition 1.1.3,2).

We continue our investigation by explicitly characterizing the topology of a certain kind of arachnoid mechanism: The configuration space for any branch and base-point x is an n-torus T^n, with $\phi : T^n \to W$ which maps into the associated work space. Note that the fiber $\phi^{-1}(z)$ over any point $z \in \operatorname{Int} W$ is the configuration space for the closed chain with links lengths $\ell_0, \ell_1, \cdots, \ell_n$, where $\ell_0 := z - x$. If z is on the boundary of the work space, then $\phi^{-1}(z)$ is evidently discrete. Thus the configuration space is the pullback:

$$\mathcal{C} \;=\; \{(\tau_1, \ldots, \tau_k) \in \prod_{i=1}^{k} \mathbf{T}^{n^{(i)}} \mid \phi_1(\tau_1) = \ldots = \phi_k(\tau_k) \in \mathcal{W}\}. \tag{5.0.1}$$

For the special planar case where all branches have exactly two links each point within the work space $\operatorname{Int}(W)$ corresponds (within the configuration space) to a discrete number of copies (see Figure 1.3.1), thus

$$\operatorname{Int}(W) \times \{0, 1, 2, \cdots, k\} \in \mathcal{C}$$

while a point within the work space boundary ∂W corresponds to certain suitable gluing of the $\operatorname{Int}(W)$ replicas, this way we can explicitly calculate the Euler characteristics from the work space as stated in Theorem 1.3.5. In the non-generic case we can carefully follow the singularities emerging by "traveling" through the *moduli*

space: the latter is the space of geometric characterization of the mechanism in hand, i.e. lengths of rods and platforms geometry. This space is divided by *walls* into *cells* where all points (mechanisms) within a given cell are associated to the same configuration space. Hence in order to understand the topological singularities within a wall (non-generic mechanisms) we simply travel from cell to cell and track changes. We have found that the singularities emerging are *pinch points* of a discrete number of 2-discs which is given as a theorem in 1.4.1.

In order to take advantage of the results discussed above we continued our study with the problem of motion planning for a *star-shaped mechanisms* (see Figure 2.1.1)which are simply planar arachnoid mechanisms. Since we consider only a point end-effector, the direct kinematics is straightforward while the inverse kinematics is more complex. Thus, while for most parallel mechanisms using configuration spaceas a mean for path planning should be carefully considered, here our approach is natural. Actually (a slightly modified) motion planing strategy taken below can be applied to any planar robot with a simple graph topology, though we will not consider such here. In view of equation 5.0.1 and the question of motion planning physibility we would like to inquire if a fiber contains a given configuration - which later on we think of as the goal configuration:
We first follow some topological properties of the configuration spaces (the number of components and the structures of the components) of single-loop closed chains with spherical joints (see Figure 2.2.1). These properties drove (see Theorem 2 in [15]) the design of a complete, polynomial-time motion planning algorithm, which we shall use here. "Adding up" more branches (see Figure 2.3.1) we can define the work space *critical* parts $\Sigma = \left(\bigcup_{i=1}^{k} \Sigma_i\right) \bigcap W_A$ as the regions where at least one of the branches is aligned (see Figure 2.3.2).
We proceed by introducing the conditions (Theorem 2 and Corollary 1) in which two given configurations are in the same connected component of the configuration space which simply put is true iff each branch **that cannot be aligned in any way** need

not change its *Elbow UP/Down* signs (of a set of links called *large links*) in order to move from initial configuration to goal (see Figure 2.3.3).

Our strategy is to solve the path existence based on the set of critical regions in the workspace, and then construct the path combining our knowledge of the workspace and the structure of the configuration space of single-loop closed chains. Note that the problem is not just moving the junction point between an initial and a goal position, but moving the manipulator along with all its legs from an initial configuration to a goal configuration. So, the workspace information will be insufficient for path construction. We employ a move that changes the shape of a leg with its endpoint fixed in the workspace. This move, called the *sign-adjust move*, uses the knowledge of the configuration space of a single-loop closed chain. We then showed that the overall complexity of the motion planning algorithm is $O(k^3N^3)$, where N is the maximum number of links in a leg and k is the number of branches. The polynomial complexity is key to the applications like folding of macro- molecules, which can be modeled as a closed chain with large k and N.

Our next goal was to study the configuration space of mechanism we call a *polygonal mechanism* which consists of a moving polygonal platform, having branches attached to each vertex, with the other end fixed in $\mathbb{R}^d$, while each branch is a concatenation of rods with revolute (i.e., rotational) joints at the consecutive meeting points.(see Figure 3.1.1). As done before, we use the regular value theorem to find the conditions in which a polygonal mechanism configuration space is a manifold. Proving the above involves a careful examination of the geometry that uniquely determines the mechanism (see Remark 3.1.4). Furthermore by *generic* we mean that there is a zero-measure of non-generic cases, formally we define generic in Definition 3.2.1.

The map we consider $F : \mathbb{R}^{dN} \to \mathbb{R}^{N+|\mathcal{I}|}$, (see proof of Theorem 3.2.2) is defined

as:

$$F(\mathcal{V}) \;=\; F(V^{(1)},\ldots,V^{(i)}) \;:=\; (f_{n^{(1)}}(V^{(1)}),\ldots,f_{n^{(k)}}(V^{(k)}),\|\mathbf{a}^{(1,2)}\|^2,\ldots,\|\mathbf{a}^{(k-1,k)}\|^2)\ , \tag{5.0.2}$$

Which admits a full ranked jacobian iff all participant branches are aligned and $\sum_{i=1}^{k}\mathbf{v}^{(i)}$, on the moving platform. Concluding these results:

1. Two participants vectors is not a generic case (Figure 4.2.1).
2. Four or more participants vectors is not a generic case and we disallow it.
3. Three participants vectors is a generic case - (coupler curve intersection with a circle)

So we need the finer *Transversality theorem* handling the three aligned legs case to find that for a generic polygonal mechanism, any configuration having at most three aligned branches is smooth (Proposition 3.2.3). Finally by redefining the "three aligned branches case" as one where the three branches are aligned, with direction lines in the same plane meeting in a single point as depicted in Figure **??** (which is referred to in literature as a flat pencil) we complete Theorem 3.2.2 proof.

Thus we gave a necessary condition for an uncertainty singularity to occur in a polygonal spatial/planar mechanism with arbitrary number of branches and arbitrary number of links in each branch. Naturally one can inquired about the corresponding instantaneous kinematic singularities:
First (Section 4.3.1) we numerate all edundant/non-redundant architecture possibilities for statically defining the moving platform, then we use screw theory to describe (Proposition 4.3.1) the kinematic singularities emerging due to the topological ones. Finally we give a visual presentation (Figure 4.4.4) of an uncertainty singularity in an explicit 3-URU 3-DOF mechanism.

We Conclude our study by constructing a morse function for the simplest type of polygonal mechanism – namely, planar mechanisms $(d = 2)$ having triangular

platforms $(k = 3)$ and exactly two links per branch $(n^{(1)} = n^{(2)} = n^{(3)} = 2)$. We propose a morse function 3.3.1, prove it is Morse and find its critical points (Figures 3.3.2,3.3.3,3.3.4), and give a computation for a mechanism having S^3 configuration space(Figure 3.3.5).

5.1 conclusions

Configuration space is hard thing to follow. Nevertheless for the two dimensional case (see chapter 2 - the *Arachnoid mechanism*) were actual visualization is possible one can "find his way". Configuration space had been found explicitly: we devised an easy way to "build up" this space as a handle body, which if followed can be used as a guide for further bigger dimensioned configuration space investigations. Singularities results in this regard can be easily applicable either in design stage or for motion planning and control in cases were the robot configuration space is intentionally designed to contain topology singularities. Thus a further investigation of topological singularities may naturally begin with these results. We have found that said singularities in the two dimensional case, are simply a wedge of discs. Clearly, generally this is not the case, and apart of presentations of 3-dimensional configuration space singularities for given mechanisms, we haven't found any characterization, but it seems like a good subject to deal with in the future.

The question of the manifold character of configuration space which arose at the beginning of our research had popped again once we had begun thinking of the *polygonal mechanisms*, except in this case, solution was not an easy task. We had found that polygonal mechanisms have generically a manifold configuration space. Moreover we introduced three necessary conditions for a polygonal mechanism to have a topological singularity. We underline here that these are not sufficient, for example consider a triangular mechanism having $2, 1, 1$ links in its associated first, second and third branches. If we (virtually) disconnect the first branch from the rest of the mechanism we end with an open 2-chain and a coupler mechanism. Consequently

the work space of the 2-open chain is an annulus, while the coupler's work space is a coupler curve. Note that for the situation depicted below where the coupler curve is tangent to the annulus, while the annulus intersects the coupler curve into two segments, all branches are aligned and their lines of alignment intersect in one point (the tangency point). Still the configuration where both curves are tangent does not induces a topological singular configuration. Thus there is a need to continue the research, and come up with a sufficient condition for topological singularities. The

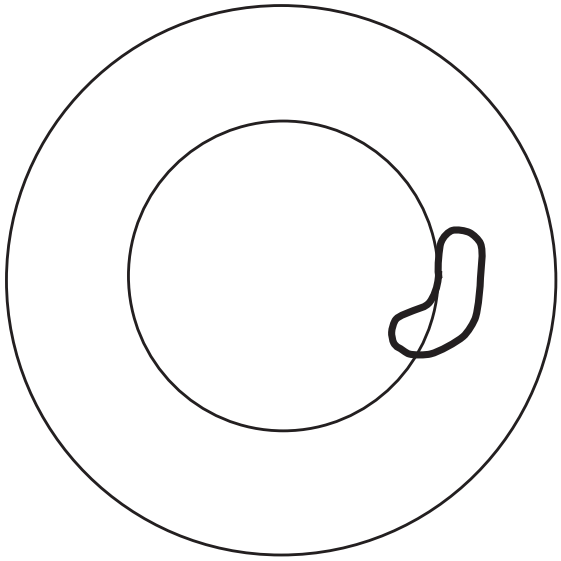

Figure 5.1.1: A counter example for singular criterion presented in last chapter.

manifold character of the generic star-shaped mechanism, generic arachnoid mechanism, generic polygonal mechanisms is herein proved, while the manifold character for simple closed chain mechanism (link loops) had been proven in literature.

On the other hand Kempe [Kem] proved in 1876 that given an arbitrary real algebraic curve there exist a linkage such that one of its vertices will trace the curve. Jordan and Steiner [JS] construct an homeomorphism between any given algebraic variety and some components of a mechanical linkage configuration space.

The above may indicate a more general truth. Thus we conclude this dissertation

with the conjecture:

Conjecture 5.1.1. All planar (spatial) graph mechanisms comprised of rigid rods and rotational (spherical) joints have a smooth orientable manifold configuration spaces for a generic set of lengths

By the term *generic* we mean "almost every set of lengths".

Thats all folks...

Chapter 6

Appendix - The configuration space as a fibred product.

Configuration space can be defined as *the set of all possible embeddings of a mechanism into the ambient space*. While this is sufficient for most discussions one should distinguish between two possible definitions, one in which transformation of the mechanism as a hole is "permitted" and one where those are "forbidden". This two does not always endow equivalent results:

Let a *graph mechanism*, be a graph $(G(v,e),\mathcal{L})$ having edge and vertex sets such that $e(G)\subseteq v(g)\times v(g)$ and a set of fixed lengths $\mathcal{L}=\{\ell_{(i,j)}|(i,j)\in e(G)\}$. Also denote by $\mathbf{x}_i$ the location of the i-th vertex. Under these notations the configuration space we describe in this dissertation is the quotient $\mathcal{C}=\mathcal{R}(G)/\Lambda$ where

$$\mathcal{R}(G)=\{\mathbf{x}_i\in\mathbb{R}^{v(G)}|i\in v(G),\|\mathbf{x}_i-\mathbf{x}_j\|=\ell_{(i,j)}\}$$

and Λ the group of isometries of translations and rotations in $\mathbb{R}^2$, or in $\mathbb{R}^3$. Thus Λ "fixes" the the mechanism to a fixed frame. The difference between these two definitions for the configuration space can be realized in the following. A subgraph H of graph G is a graph such that $v(H)\subset v(G)$ and $e(H)\subset e(G)$. Which leads to the definition:

Definition 6.0.2. A *sub-mechanism* $(H,\mathcal{L}|_H)\subset(G,\mathcal{L})$ is a subgraph H of G

together with the restricted length subset $\mathcal{L}|_H$, and we denote such a sub-mechanism simply by H. A *leg* is a sub-mechanism such that all vertices in H has valence 1 or 2.

In light of these definitions one can define a feasible configuration of a parallel mechanism as such that all of its branches "agree" upon one (or more) leg configuration. One could naively claim that for a arachnoid mechanisms the configuration space is simply the fibered product of the configuration spaceof its legs, but this is not true. Alternatively we know that:

Theorem 6.0.3. *Given a mechanism $(G, \mathcal{L})$ with a set $H_1, H_2, H \subset G$ of its sub-mechanisms such that $H_1 \cap H_2 = H$ then $\mathcal{R}(\mathcal{L})$ is the pullback of the the natural projections:*

$$\mathcal{R}(H_1) \xrightarrow{\pi_{H_1}} \mathcal{R}(H) \xleftarrow{\pi_{H_2}} \mathcal{R}(H_2).$$

Note that this does not extend to a the configuration space $\mathcal{C}$ since the induced projections $\{\mathcal{R}(H_i)/\Lambda \to \mathcal{R}(H)/\Lambda\}$ are determined up to isometry Λ and thus do not determine a unique point.
for example take the mechanism depicted in figure 6 and denote the two rods H_1, H_2 then $\mathcal{C}(H_i) = pt$ (for we should fix one link) and $\mathcal{C}(H_1 \cap H_2) = pt$. $\mathcal{C}$ of the entire mechanism is obviously S^1.

For convenience we restrict the proof to the case where there are only 2 sub-mechanisms, but this can be trivially extended to any number of sub-mechanisms:

Proof. Let $H := H_1 \cap H_2$ as before. in order to show that

$$\mathcal{R}(G) = \mathcal{R}(H_1) \times_H \mathcal{R}(H_2)$$

we should show that for every space $\mathcal{R}$ and maps $\tilde{P}_{H_i} : \mathcal{R} \to \mathcal{R}(H_i)$ $(i = 1, 2)$ such that $\tilde{P}_{H_1} \circ \pi_{H_1} = \tilde{P}_{H_2} \circ \pi_{H_2}$ then there exist a unique map $\mu : \mathcal{R} \to \mathcal{R}(G)$, such that

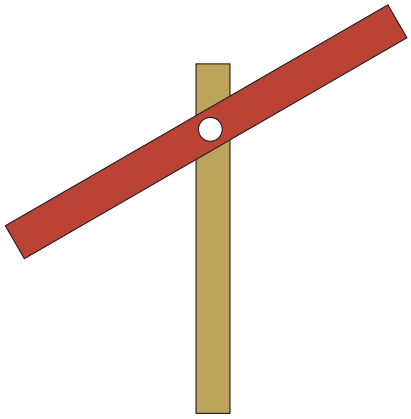

Figure 6.0.1: Example mechanism

the following diagram commutes (that is for $i = 1, 2$ the identity $P_{H_i} \circ \mu = \tilde{P}_{H_i}$ holds)

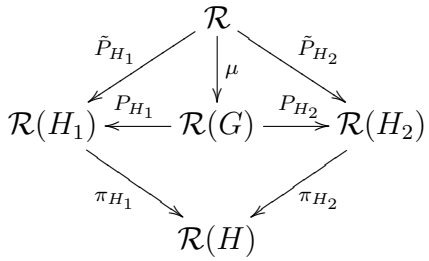

So we assume the existence of such $\mathcal{R}$ and maps $\tilde{P}_{H_i}$ such that the diagram commutes and use the known fact that *the configuration space of a cloud of points is a direct product* to prove the uniqueness of μ.

Denote the configuration space of $v(K)$ *free* points in $\mathbb{R}^2$ by $\mathcal{C}_f(K)$ for some submechanism K. (here "free" means that we require no distance constraints).

The configuration space of the cloud of points $v(G)$ is a direct product of $\mathcal{C}_f(H_1)$ and $\mathcal{C}_f(H_2)$:

$$\mathcal{C}_f(H_1) \xleftarrow{P_1} \mathcal{C}_f(G) \xrightarrow{P_2} \mathcal{C}_f(H_2)$$

where P_i are projections. If there is an $\mathcal{R}$ with the corresponding maps

$$\mathcal{C}(H_1) \xleftarrow{\tilde{P}_1} \mathcal{R} \xrightarrow{\tilde{P}_2} \mathcal{C}(H_2)$$

such that its pullback diagram commutes, then there is a unique map $\mu : \mathcal{R} \to \mathcal{C}_f(G)$. Note there are inclusion maps $j_K : \mathcal{R}(K) \hookrightarrow \mathcal{C}_f(K)$ for all submechanisms K.

Now, if we set $\tilde{P}_i = j_{H_i} \circ \tilde{P}_{H_i}$ then there is a unique map μ such that $P_i \circ \mu = j_{H_i} \circ \tilde{P}_i$ (and keeps the diagram commutative). But since $j_{H_i} \circ \tilde{P}_i$ "keeps distances" so is $P_i \circ \mu$ lastly since P_i is just a projection we have proven that μ "keeps" distances so we can deduce that $\mu(\mathcal{R}) \subset \mathcal{R}(G)$ which completes the proof (and wonderful 3.5 years) (since in the $\mathcal{C}_f$-diagram μ is unique). $\square$

Bibliography

[1] G. Liu, Y. Lou & Z. Li, *SSingularities of Parallel Manipulators: A Geometric Treatment*, *IEEE Trans. on Robotics And Automation* **19,4** (2003), 579-594.

[C] D. R. J. chillingworth, "Differential Topology with a view to Applications", *Research Notes in Mathematics, π Vol. 9*, 2001.

[2] D. Eldar, *Maps and Machines*, Hebrew Univ. M.Sc. project, in preparation, `http://www.math.toronto.edu/ drobn/People/Eldar`.

[3] M. Farber, *Instabilities of Robot Motion*, preprint, 2002 `cs.RO/0205015`.

[4] S. Goldberger, M. Shoham and O. Ben-Porat, *Robots in Surgery - Reality or Vision*, *Ob. Gyn. Update* **22** (1997), 4-8.

[5] C. Gosselin & J. Angeles, *Singularity analysis of Closed Loop Kinematic Chains*, *IEEE Trans. on Robotics And Automation* **6** (1990), 281-290.

[6] J.C. Hausman & A. Knutson, *The Cohomology Ring of Polygon Spaces*, *Ann. Inst. Fourier (Grenoble)* **48** (1998), 281-321.

[7] M.W. Hirsch, *Differential Topology*, Springer-Verlag, Berlin-New York, 1976.

[8] M. Holcomb, *On the Moduli Spaces of Multipolygonal Linkages in the Plane*, preprint, 2003, `math.GT/0307001`.

[9] J.C. Hausman & E. Rodriguez, *The Space of Clouds in an Euclidan Space*, preprint, 2002.

[10] Y. Kamiyama, *Topology of equilateral polygon linkages in the (Euclidean) plane modulo isometry group*, *Oska J. Math.* **36** (1999), 731-745.

[11] M. Kapovich & J. Millson, *On the moduli space of polygons in the Euclidean plane*, *J. Differential Geom.* **42** (1995), 430-464.

[12] Y. Kamiyama & M. Tezuka, *Topology and Geometry of Equilateral Polygon linkages in the Euclidean plane*, *Quart. J. Math. (Oxford)* **50**, 1999, 463-470.

[13] Y. Kamiyama, M. Tezuka & T. Toma, *Homology Of the Configuration spaces of Quasi-equilateral Polygonal Linkages*, *Trans. Am. Math. Soc.* **350** (1998), 4869-4896.

[14] R.J. Milgram & J. Trinkle, *The Geometry of Configuration spaces of Closed Chains in Two and Three Dimensions*, to appear in *Homology, Homotopy & Applications*.

[15] R.J. Milgram & J. Trinkle, *Motion Planning for Planar n-Bar Mechanisms with Revolute Joints*, in *IEEE Int. Conf. on Intelligent Robots and Systems* , IEEE, 2001, 1602-1608.

[16] N. Simaan & M. Shoham, *Singularity analysis of a class of Composite serial In-Parallel Robots*, *IEEE Transactions On Robotics and Automation* **17** (2001), 301-311.

[17] D.S. Zlatanov, R.G. Felton & B. Benhabib, *Classification and Interpretation of Singularities of Redundant Mechanisms*, *Proceedings of the ASME 24th Annual Design Automation Conference, Atlanta, GA*, Sept. 1998, Paper #DETC98/MECH-5896.

[18] M. Cherif and K.K. Gupta, *Planning Quasi-Static Fingertip Manipulation For Reconfiguring Objects*. IEEE Transactions on Robotics and Automation, Vol. 15, No. 5, PP. 837-848, 1999.

[19] D. E. Koditschek, *Exact Robot Navigation by Means of Potential Functions: Some Topological Considerations.* IEEE International Conference on Robotics and Automation, PP. 1-6, 1987.

[20] Lozano-Perez83, *Spatial Planning: A Configuration Space Approach.* IEEE Transactions on Computers, Vol. C-32, No. 2, PP. 108-119, 1983.

[21] D.J. Jacobs, A.J. Reider, L.A. Kuhn, and M.F. Thorpe, *Protein Flexibility Predictions Using Graph Theory.* PROTEINS: Structure, Function, and Genetics, 44:150-165.

[22] J. Cortés, T. Siméon, and J.P. Laumond, *A Random Loop Generator for Planning the Motions of Closed Kinematic Chains using PRM Methods.* In Proceedings of the 2002 IEEE International Conference on Robotics and Automation, pages 2141-2146, 2002.

[23] J. Cortes and T. Siméon, *Probabilistic Motion Planning for Parallel Mechanisms.* In Proceedings of the 2003 IEEE International Conference on Robotics and Automation, pages 4354-4359, 2003.

[24] E. Rimon and D. E. Koditschek, *Exact Robot Navigation Using Cost Functions: The Case of Distinct Spherical Boundaries in E^n.* IEEE International Conference on Robotics and Automation, PP. 1791-1796, 1988.

[25] D. Hsu, J.C. Latombe, and R. Motwani, *Path Planning in Expansive Configuration Spaces.* IEEE International Conference on Robotics and Automation, 1997.

[26] E. Rimon and D. E. Koditschek, *The Construction of Analytic Diffeomorphisms for Exact Robot Navigation on Star Worlds.* IEEE International Conference on Robotics and Automation, PP. 21-26, 1989.

[27] N. Shvalb, M. Shoham, D. Blanc *The Configuration Space of an Arachnoid Mechanism.* To appear in Forum Mathemaicum 2005.

[28] J. Barraquand and J.-C. Latombe, *Nonholonomic Multibody Mobile Robots: Controllability and motion planning in the presence of obstacles.* IEEE Interantional Conference on Robotics and Automation, PP. 2328-2335, 1991.

[29] J.W. Burdick. On the inverse kinematics of redundant manipulators: characterization of the self-motion manifolds. *IEEE Int. Conf. on Robotics and Automation* (ICRA), pages 264−270, May 1989.

[30] J. Schwartz, J. Hopcroft, and M. Sharir, *Planning, Geometry, and Complexity of Robot Motion.* Ablex, 1987.

[31] S. M. LaValle and J. J. Kuffner, *Rapidly-exploring random trees: Progress and prospects.* In B. R. Donald, K. M. Lynch, and D. Rus, editors, Algorithmic and Computational Robotics: New Directions, pages 293-308, A K Peters, Wellesley, MA, 2001.

[32] J.T. Schwartz and M. Sharir, *On the piano movers II. General techniques for computing topological properties on real algebraic manifolds.* Adv. Appl. Math., vol.4, PP. 298-351, 1983.

[33] L. Han and N.M. Amato, *A kinematics-based probabilistic roadmap method for closed chain systems.* in Algorithmic and Computational Robotics: New Directions, B.R. Donald, K.M. Lynch, and D. Rus, Eds. AK Peters, Wellesley, PP. 233-246, 2001.

[34] N. Amato, B. Bayazit, L. Dale, C. Jones, and D. Vallejo, *OBPRM: An obstacle-based PRM for 3d workspaces.* in Robotics: The Algorithmic Perspective, P. Agarwal, L. Kavraki, and M. Mason, Eds. Natick, MA: A.K. Peters, 1998, PP. 156-168.

[35] V. Boor, M. Overmas, and A.F. van der Stappen, *The Gaussian sampling strategy for probabilistic roadmap planners.* IEEE International Conference on Robotics and Automation, 1999.

[36] R. Bohlin and L. Kavraki, *Path planning using lazy PRM.* IEEE International Conference on Robotics and Automation, PP. 521-528, 2000.

[37] J.J. Kuffner and S.M. LaValle, *RRT-Connect: An Efficient Approach to Single-Query Path Planning.* IEEE International Conference on Robotics and Automation, PP. 995-1001, 2000.

[38] S.M. LaValle and J.J. Kuffner, *Randomized kinodynamic planning.* IEEE International Conference on Robotics and Automation, 1999.

[39] J.F. Canny, *The Complexity of Robot Motion Planning.* Cambridge, MA: MIT Press, 1988.

[40] L.E. Kavraki, P. Švestka, J.C. Latombe, and M.H. Overmars, *Probablistic Roadmaps for path planning in high-dimensional configuration space.* IEEE Transactions on Robotics and Automation, 12(4):566-580, 1996.

[41] J.C. Latombe, *Robot Motion PLanning.* Kluwer Academic Publishers, 1992.

[42] J. Yakey, S. M. LaValle, and L. E. Kavraki, *Randomized path planning for linkages with closed kinematic chains.* IEEE Transactions on Robotics and Automation, 17(6):951–958, December 2001.

[43] J. Sefrioui and C.M. Gosselin, *On the quadratic nature of the singularity curves of planar three-degree-of-freedom parallel manipulators.* Mechanism and Machine Theory, 30(4):533–551, May 1995.

[44] A.K. Dash, C. I-Ming, Y. Song-Huat and Y. Guilin, *Singularity-free path planning of parallel manipulators using clustering algorithm and line geometry.* Robotics and Automation, 1:761- 766, September 2003.

[45] D.N. Nenchev ,Y. Tsumaki and M. Uchiyama *Singularity-Consistent Parameterization of Robot Motion and Control* The International Journal of Robotics Research, 19(2):159-182, 2000.

[46] J.R. Banga and W.D. Seider, *Global Optimization of Chemical Processes Using Stachastic Algorithms*, State of the Art in Global Optimization: Computational Methods and Applications, C.A. Floudas and P.M. Pardalos (Eds.), Kluwer Academic Publishers, pages 563-583, 1996.

[47] M.Š. Farber & D. Schütz, *Homology of planar polygon spaces*, preprint, 2006, `math.AT/0609140`.

[48] A.S. Hall, Jr., *Kinematics and Linkage Design*, Prentice-Hall, Englewood Cliffs, NJ, 1961.

[49] J.-C. Hausmann, *Sur la topologie des bras articulés*, in S. Jackowski, R. Oliver, & K. Pawałowski, eds., *Algebraic Topology - Poznán 1989*, Springer Lec. Notes Math. **1474**, Berlin-New York, 1991, 146-159.

[50] M.W. Hirsch, *Differential Topology*, Springer-Verlag, Berlin-New York, 1976.

[51] J. Milnor, *Morse Theory*, Princeton University Press, Princeton, NJ, 1963.

[52] K.H. Hunt, "Kinematic Geometry of Mechanisms", Oxford Universty Press, Oxford, UK, 1978.

[53] K.H. Hunt, "Special configurations of robot-arms via screw theory, Part 1", *Robotica* **4** (1986), 171-179.

[54] K.J. Waldron, S.L. Wang & S.J. Bolin, "A study of the Jacobian matrix of serial manipulator", *Trans. of ASME, J. Mech. Trans. Aut. in Des.* **107** (1985), 230-238.

[55] D.S. Zlatanov, I. Bonev & C. Gosselin, "Constraint Singularities as Configuration Space Singularities", *Advances in Robot Kinematics: Theory and Applications*, Kluwer Academic Press, 2002, 183-192.

[56] D.S. Zlatanov, R.G. Felton & B. Benhabib, "Singularity analysis of Mechanisms and Robots via a Motion–Space Model of the Instantaneous Kenmatics", *Proceedings IEEE Conf. in Robotics & Automation*, 1994, 980-985.

[Hal] A.S. Hall, Jr., *Kinematics and Linkage Design*, Prentice-Hall, Englewood Cliffs, NJ, 1961.

[57] N. Shvalb, M. Shoham & D. Blanc, "The Conifguration space of parallel mechanisms", preprint, 2006.

[58] J.P. Merlet, *Parallel Robots*, Kluwer Academic Publishers, Dordrecht, 2000.

[59] L.W. Tsai, *Robot Analysis - The mechanics of serial and parallel manipulators*, Wiley interscience Publication - John Wiley & Sons, New York, 1999.

[60] C.M. Gosselin & J.P. Merlet, "The Direct Kinematics of Planar Parallel Manipulators: Special Architectures and Number of Solutions", *Mechanism & Machine Theory* **29** (1994), 1083-1097.

[61] D.S. Zlatanov, R.G. Fenton & B. Benhabib, "Classification and Interpertation of Singularities of Redundant Mechanisms", *ASME Design Engineering Technical Conference*, 1998, 1-10.

[62] J.K. Davidson & K.H. Hunt *Robots and Screw Theory - Applications of kinematics and robotics*, Oxford University Press, Oxford, UK, 2004.

[63] V.I. Arnold, S.M. Gusein-Zade & A.N. Varchencko, *Singularities of Differentiable Maps*, Vol. I, Monographs in Mathematics, Academic Press, New York, 1985.

[Kem] A. B. Kempe, "On a General Method of Describing Plane Curves of the n–th Degree by Linkwork", *Proc. London Math. Soc., Vol. 7*, 1875.

[JS] D. Jordan and M. Steiner, "Configuration Spaces of Mechanical Linkages" *Descrete and Computational Geometry Vol. 22* 1999, 297–315.

Chapter 7

Hebrew introduction

1

1